THESIS REPORT
Master's Degree
Institute for Systems Research

Modeling and Simulation of Effects of Material Microstructure on Machining Processes

by R. Ratnakar
Advisor: G.M. Zhang

The Institute for Systems Research is supported by the National Science Foundation Engineering Research Center Program (NSFD CD 8803012), Industry and the University

M.S. 93-10

Abstract

Title of Thesis:	Modeling and Simulation of Effects of Material Microstructure on Machining Processes
Name of degree candidate:	Rajesh Ratnakar
Degree and Year:	Master of Science, 1993
Thesis directed by:	Dr. Guangming Zhang, Assistant Professor, Department of Mechanical Engineering, and Institute for Systems Research

The concept of computer integrated manufacturing has been the primary focus of research in the manufacturing community, to achieve high product quality and productivity. The need to continually improve on manufacturing processes necessitates the identification and modeling of all factors that affect product quality in the manufacturing process. The sources of machine tool vibration during the machining process is one such set of significant factors that is of interest.

This thesis work attempts to explain the effect of the non-homogeneous distribution of workpiece material microstructure on machining quality. The main contributions of this thesis are (1) that two stochastic models, using the concepts of sample variance and Markov chains, are used to simulate the microhardness distribution, (2) that an algorithm is developed for the calculation of the sample shape function, critical to the sample variance model, and (3) that a computer simulator has been built to simulate the turning process, which takes the cutting conditions and the microstructural image of the material as its inputs, and

evaluates the machining performance. The validity of the models in describing random excitation has been confirmed by comparison of dynamic force values obtained from experiments and from simulation.

This integrated approach of analyzing the machining process provides the production engineer with a tool for estimating the optimal cutting conditions for a given material. It also provides the design engineer a method of selection of materials based on their ability to be machined to a required surface finish.

Modeling and Simulation of Effects of Material Microstructure on Machining Processes

by

Rajesh Ratnakar

Thesis submitted to the Faculty of the Graduate School
of The University of Maryland in partial fulfillment
of the requirements for the degree of
Master of Science
1993

Advisory Committee:

Assistant Professor Guangming Zhang, Chairman/Advisor
Professor William L. Fourney
Assistant Professor Ioannis E. Minis

Dedication

To my dear parents

Acknowledgements

I would like to sincerely thank my advisor and guide, Dr. Guangming Zhang, for his guidance during the course of my thesis. I would also like to thank him and the Institute for Systems Research for supporting me and my research work. I would also like to thank Prof. W.L. Fourney and Prof. I. Minis for consenting to be members of my committee and for their constructive criticism of my work. I wish to thank Dr. Bigio and Dr. Sallet for all their help and guidance.

I would also like to thank the other members of my team for helping me at various stages of my thesis. In particular, I appreciate all the help offered by Shuvankar who spent a lot of time working with me on numerous occasions. I would also like to thank Satish for helping me on the computer programs and Goutam and Tsuwei for their suggestions and help.

Finally, I am really grateful to my parents for all that they have done for me. And, of course, Vinu and Anu, ... thank you!!!

Table of Contents

List of Tables

List of Figures

Chapter 1

Introduction

1.1 Background

The use of machining in the manufacturing cycle of both metallic and non-metallic parts has always been wide. Different machining processes have been used efficiently for many years and the quality of the parts made has always improved. The high surface finish requirement of machined surfaces necessitates a better understanding of the machining process.

A lot of research has been done to develop models to describe different machining operations in the past years and significant progress been made in developing controls to improve the machining performance. The results have been very encouraging and have almost always kept machining process abilities in hand with the product requirements. The surface finish requirements of the industry are always tied up with the cutting dynamics of the machining process. Thus this

has often been the topic of study for many researchers. Most of the research has always been to address the problems in machining in a macroscale. Mathematical models for cutting processes have existed for a long time. Merchant [1] after extensive research on cutting forces formulated the composite cutting force diagram which explains the relationship between cutting force components in orthogonal cutting. Kronenberg [3] established numerous relationships between different cutting parameters and the cutting force with the help of results from his experimental research. It was, in fact, Kronenberg who first established a concrete relationship between the material hardness and the cutting force. It is this relationship that forms the basis for the establishment of cutting force variation based on microhardness distribution, explored in this thesis.

The main apparent factors that affect surface finish in machining are the tool geometry and the dynamic characteristics of the cutting process. It is fairly easy to predict the nature of the finished surface with the knowledge of these factors. But in practical machining, it is observed that the surface finish obtained is very different from that predicted by such a model. This nature of the machined surface is because of many other factors like tool vibration, chip formation and flow, material properties, tool wear, etc. Some of these factors can be controlled during the machining operation, but others like tool vibration require proper mathematical models to describe them, before any effective controls can be built in.

Tool vibration was one of the greatest concerns of machine tool researchers

in the fifties and the sixties. The desire to characterize the tool vibration and control it resulted in a lot of significant work during that period. The machine tool structure was often modeled as a single or two degree of freedom spring - mass - damper system. Arnold [4] used the popular Van der Pol model, to relate the cutting velocity variation to the vibration in the cutting tool structure. The effect of regeneration was characterized by Tobias and his co-workers [5]. Regeneration arises when successive cuts overlap in a machining process. He introduced the concept of the overlap factor to account for this effect. The formulation of the stability chart by the use of such models was also done by Tobias [6]. He later refined the model by the incorporation of the coupling coefficient and the penetration rate factor to explain the effects of regenerative feedback in a more accurate way. Tlusty [7], first by himself and later with Polacek [8], used the mode coupling theory for exploring the stability limits in machining processes. Merritt [2] modeled the cutting process by both, a single and a two degree of freedom model, and was able to explain the cause of self-excited chatter that occurs during machining. He employed the classical control system approach to model the regenerative effect as a feedback loop with a time lag. He was able to simplify the formulation of the lobed borderlines on the stability charts.

Tool vibration is caused by factors which can be categorized into deterministic and random factors. The dynamic response of the tool as a result of the load due to the nominal cutting area of the workpiece can be accurately predicted and

hence is called the deterministic tool vibration. All the work by the researchers mentioned earlier in characterizing vibrations helps explain only this deterministic part. It is seen in practical machining that this does not completely account for the vibration present. This is because of the other component - the random vibration. The attempts in the building of a complete and accurate model to characterize the random tool vibration have only resulted in limited success. It is very important to identify the cause of the random vibration and model its nature, before it can be controlled.

The main cause of the random vibration in machining is due to the variation in the cutting force caused by the non-homogeneous distribution of the microhardness in the workpiece material. Zhang and Kapoor [12], [13] proposed the relationship between the material microstructure and the random vibration occuring in machining. A model to describe the material microstructural distribution in the longitudinal direction was also proposed by Zhang and Hwang [15]. The prediction of cutting forces during machining, its dynamic nature and its effects on the structural dynamics of the machine tool has always been an important field of research for scientists in the field of machining. A study of the nature of the microstructure of the workpiece material can help describe the nature of the random excitation of the tool cutting it. If the random excitation is accurately modeled, it can be effectively used to design controls for minimizing them and hence improve surface finish of machined surfaces.

This thesis work aims at addressing this problem of characterizing random

vibration and relating it to surface finish. The work can be divided in terms of the various functional models used to address this issue. They are the following:

- Material Description Models
    - a) Sample Variance Model
    - b) Markov Models
        - Single Distribution
        - Multiple Distribution
- Tool Vibration Evaluation Model
- Surface Evaluation and Surface Topography Generation Model

The material description model explains a statistical way of describing and quantifying the nature of the material microhardness distribution. This model is then used to describe the nature of the force variation in the turning process. Since the focus of this research is in the characterization of random vibration caused due to material micro-nonhomogeneity, the accuracy of this model is critical. The model essentially has two approaches to describe the material distribution. The first approach, referred to as the "sample variance theory", describes the nature of the microstructural variation within a revolution of the workpiece, while another stochastic model which applies the "Markov chains" principle, describes the same along the feed direction. Together, they very effectively describe the random excitation that occurs during machining.

1.2 Presentation Outline

This thesis is organized into six chapters. This first chapter was an introduction to the topic describing briefly some earlier work done in related fields. It also represents an attempt in highlighting the need for work in this field and the significance of this research.

The second chapter explains the models employed for the description of the microstructure of the material. This lays the most important foundation for this thesis. The two important models - the sample variance model and the Markov models form the basis on which the random excitation to the cutting tool structure is characterized. Since these models are used to recreate different materials for use in the simulation of the cutting process, it is explained in detail. This also forms one of the most important contributions of this thesis work. The sample variance model describes the material microstructure in the cross section of a cylindrical bar. The Markov models, on the other hand, augments the sample variance model, to account for longitudinal trends commonly present in rolled materials.

The third chapter is an adaptation of the popular dynamical description of a typical machine tool structure to the turning process, as used here. The nature of the cutting force, its dynamical nature due to random hardness variation and the resultant nature of the tool vibration are covered in this chapter. The model to recreate the surface produced for visual analysis on a computer and for surface

analysis for the different surface finish parameters is also described.

The fourth chapter explains the way these models were implemented for computer simulation of the cutting process. The simulation program essentially consists of three modules. The first module explains the way pictures of the microstructure are analyzed to arrive at the different parameters that are used for the excitation of the tool structure. The second module explains the method of evaluating the tool response to the excitation from the material. Finally, the surface evaluation module describes the method of evaluation of the workpiece surface obtained as a result of the tool response.

The fifth chapter presents the results obtained by the use of the different models and the attempts at validating them experimentally. The results of the computer simulation runs for different cutting conditions are presented. These results are then compared with the results obtained from cutting tests that were performed. The chapter also explains the results of the experiments performed using different grades of steel having different microstructures. An analysis of the cutting forces generated during machining is also made. The forces measured during the cutting experiments are compared with the forces generated from the simulation package and the effectiveness of the different models evaluated. Thus the capacity of the model to describe the nature of the random vibration for materials of different microstructures is demonstrated.

The sixth chapter is a brief presentation of the conclusions from the work done. The significance of the results and the ways these results can be used for

improvements in the cutting process are also presented. Recommendations for improvement of the simulation package and possible directions for future work are also presented in this chapter.

Chapter 2

Material Microstructure Modeling

Mathematical modeling of a machining process to describe random vibration includes modeling of the material which forms the source of the random excitation and modeling of the tool structure to describe the nature of vibration and its effect on the nature of the surface generated. In order to model the material effectively two important concepts of stochastic processes of sample variance and Markov chains have been used. A typical material of cylindrical rolled metal bars exhibits two different distributions, one along its cross section and another along the longitudinal (rolled) direction. The sample variance approach models the material distribution along the cross section while the Markov chain approach models the nature of any longitudinal trends in the microstructure present in rolled materials that exhibit elongated grain structure.

2.1 Sample Variance Model

The workpiece material has a distinct nature of its microstructure. The microstructure is dependent on the material composition, purity and the method of fabrication. These factors cause the microstructure to differ from material to material and from grade to grade. The hardness of these microconstituents often differ resulting in a non-homogeneity in the local microhardness of the material. It is this non-homogeneity of the distribution of the material's microstructure that is almost always the primary cause of random vibration in the cutting process. It is, thus, critical to develop a statistically sound mathematical model that can very accurately describe the material's microstructure distribution. It is for this reason that the sample variance theory is used.

The sample variance theory was originally proposed by Dankwerts [9] in 1952 to describe the distribution of the constituents of mixtures. The theory has since been improved and used by other researchers like Scott [10] and Tucker [11] in the field of polymer processing. Since the nature of a nonhomogeneous mixture is similar to the microstructure of steel, such a model was used as a basis for the description of the material microstructure of the workpiece material for a boring process, by Zhang and Kapoor [12]. The nature of the tool vibration during the boring operation was accurately modeled by them, with the help of this model. This model has been improvised and used in this thesis. An algorithm has been developed for the calculation of the sample shape function, a geometrical

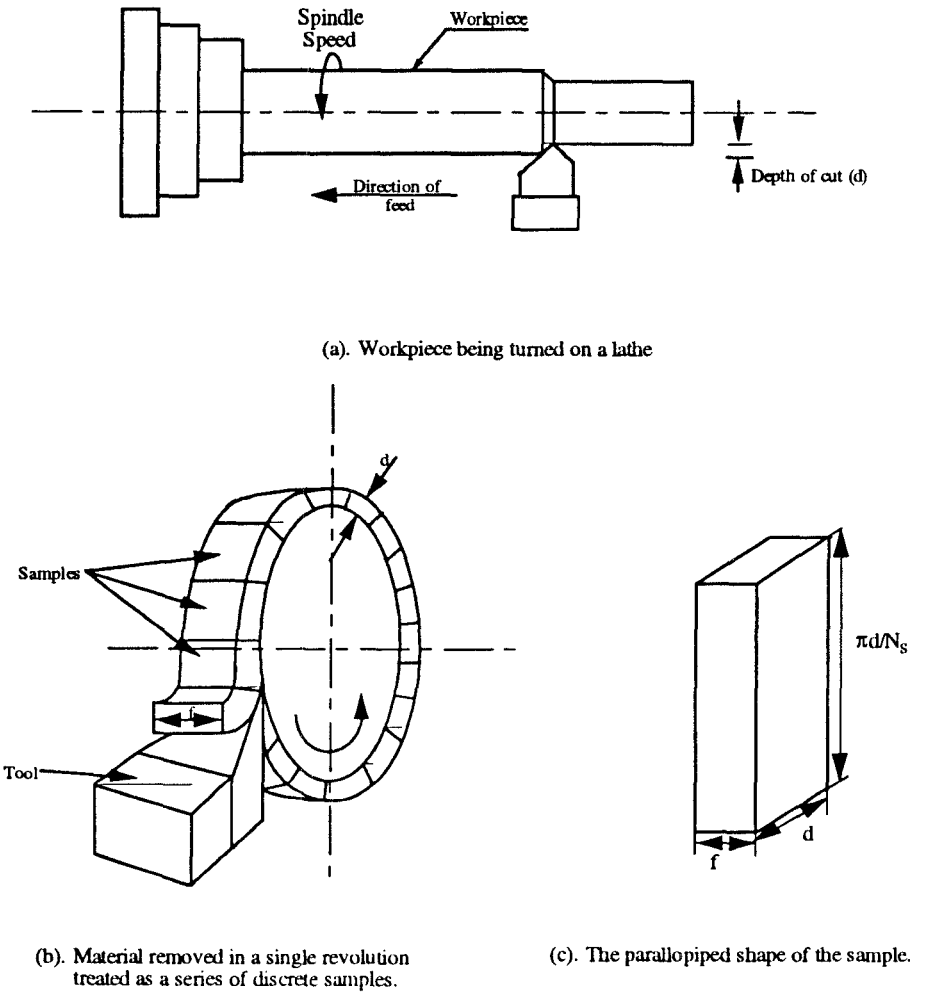

Figure 2.1: Nature of the material removed

parameter used by this model, given any set of cutting conditions. It is for this reason that the model developed by them, has been described here.

The sample variance model treats the metal being cut as a series of discrete blocks, referred to as samples, that together comprise the material removed by the cutting operation. This concept is illustrated in Figure 2.1 which shows a cylindrical bar being turned on a lathe.

As the tool comes into contact with the different samples which contain vary-

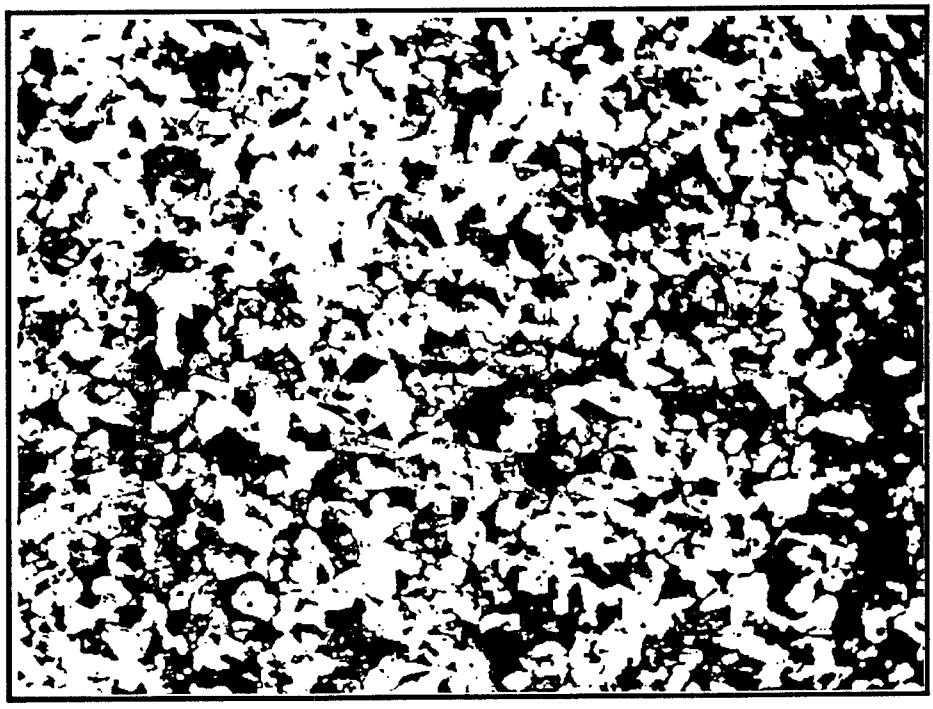

Figure 2.2: Digitized image of cross section of 4340 steel bar

ing ratios of the phases of the material having different hardness, the cutting force varies resulting in vibration in the tool. Figure 2.2 shows a cross section of a 4340 alloy steel bar. The photograph is taken from a microscope and digitized. The dark regions represent the pearlite structure, while the bright regions are the ferrite structures. Similar analyses along the longitudinal direction can give a complete picture of the distribution of the microstructure in steel, as seen from Figure 2.3. It is very important here to again emphasize that the model's application is not limited to just carbon steels, but can be applied to any metal or nonmetal that exhibits nonhomogeneous microstructure. Carbon steel, which has just two phases - pearlite and ferrite, has been taken as an example for the study and hence, the model is described with reference to this material.

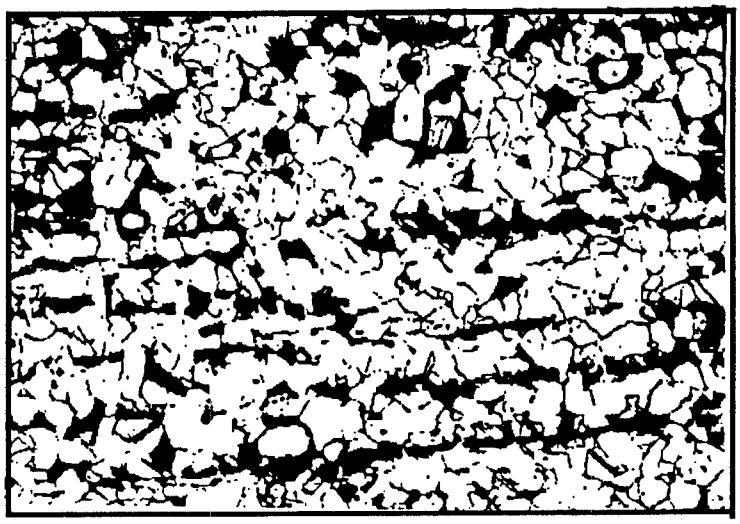

Figure 2.3: Digitized image of longitudinal section of steel

The distribution of the microstructure in steel is dependent on the composition, manufacturing process and type of heat treatment. These factors can change the nature of the microstructure yielding different sizes and shapes of different phases present. Hence for any mathematical model, to accurately represent the structure, it should describe the size, shape and the distribution of the microstructure.

2.1.1 Nature of Samples

The force variation due to the microhardness is considered to be a result of only the samples passing through the shearing zone. It is therefore, necessary to characterize the size and nature of the hardness distribution of these samples.

The shape of the sample has a direct bearing on the sample variance and this

is demonstrated later in this thesis. The shape of the sample is a function of the cutting parameters. Figure 2.1(c) shows the material removed from one revolution of the workpiece during turning. The material removed is a parallelepiped, with the depth of cut and feed as the dimensions describing its cross-section, and the length being the circumference of the cylinder. This length is divided into a number of sections, each representing a smaller parallelepiped, referred to as the sample. Since the feed in turning is almost always the smallest dimension the parallelepiped may be approximated to a cuboid without loss in accuracy. The number of sections into which the material removed is divided into, i.e. the number of samples, determines the size of the sample. The model has to accurately describe the nature of the random tool vibration. The frequency of this random excitation is directly related to the number of samples. The sample number should, therefore, be such that the frequency of excitation is greater than, and a multiple of the frequency of tool response. Hence, for the most accurate description of the excitation, the number of samples is based on the frequency of tool vibration determined experimentally. The most significant frequency obtained from the power series expansion is used for the calculation of the frequency of excitation. The relationship between the frequency of excitation and the number sample is expressed as [12]

$$N_s = F_{max} * 2 * 60/N \tag{2.1}$$

where N_s is the number of samples, F_{max} the maximum value of the significant frequencies of vibration obtained from the power series expansion of the cutting

force data, and N is the spindle speed in revolutions per minute.

2.1.2 Microhardness Distribution

The hardness of an individual sample is the compositional weighted average of its microconstituents. Such a linear relationship has been established empirically. In a two phase material like low carbon steel (pearlite and ferrite), the mean hardness of the i'th sample is given by

$$\mu_{si} = \frac{\sum_{j=1}^{N}(volume_j * hardness_j)}{totalvolume}, \tag{2.2}$$

where the summation is made over the different pixels that comprise the cross section. The distribution of the microstructure in the material is a random variable, as this microstructure is a result of the variations in the manufacturing process of steel. Thus, depending on the nature of the microstructural distribution, the sample has different mean hardness. In order to find the mean hardness of the sample, it is necessary to know the microstructural distribution and the hardness values of the different phases. The distribution of the microstructure can be obtained by microscopic analyses of the samples. The samples are sectioned, the sections polished and etched to expose the true nature of the microstructure. This surface is then analyzed under a microscope, and the picture digitized and stored in a computer. The hardness of the different phases present in the material is found by the use of the Vickers microhardness tester. The distribution, together with the hardness values of the phases, is sufficient to describe the mean hardness of the sample.

The mean hardness varies from sample to sample. This is because the different samples exhibit different microstructural distribution. As described earlier, this sample mean hardness is a random variable. The variation of the means of the sample mean hardness follow a normal distribution, according to the central limit theorem. Thus, it can be described statistically by a mean and a standard deviation for the normal distribution.

It is easy to see that the mean of the sample mean hardness is the same as the mean of the population distribution. However, the sample mean variance (and hence the standard deviation) varies from that of the population. It is therefore necessary to determine this variance. It is also important to note that the value of the sample mean variance is a function of the sample shape. Every time the cutting parameters of feed, depth of cut and speed are changed, the sample size and shape change and hence the change in the sample variance. This relationship between the cutting parameters and their effect on the sample mean hardness distribution, and thus on the random vibration is one of the contributions of this thesis work.

2.1.3 Sample Variance

The sample variance can be calculated by the conventional method, wherein the mean of the samples is individually calculated over an entire range of samples to evaluate the variance. However, this method is not very practical. Analyzing the microstructure of the samples individually, for each of the samples and using that

for sample variance calculations involves a tremendous amount of time. Another serious drawback is that the sample variance cannot be calculated on-line for variations in the cutting parameters during a machining process. As mentioned earlier, any change in the cutting parameters affects the sample shape and hence the sample variance. The distribution of the mean hardness is thus affected. Although the mean remains the same, the sample variance does change.

The sample mean variance theory is used here to facilitate the calculation of the sample variance as the sample shape and size vary. This theory [11], originally used to describe the nature of mixtures, relates the distribution of the components of a mixture and the size of samples to arrive at the sample concentration variance. This situation is analogous to the present study of the microhardness distribution.

There are two important functions that are involved in the sample variance calculation. They are the correlation coefficient function, which describes the nature of the distribution of the microconstituent distribution, and the sample shape function, which relates the shape of the sample to the sample variance. It is, therefore, imperative that the meaning of these two functions be understood before any relationship between these functions and the sample mean hardness variance is presented.

2.1.4 Correlation Coefficient Function

In statistics, the correlation coefficient function measures the strength of the linear relationship between two variables [19]. In the case of microstructural distribution, it can be used to describe the segregation of the different phases of the material in the workpiece, each of these phases being a random variable. In other words, it explains the probability of the hardness of different points at different distances being the same or different. This can account for a meaningful description of the size and spatial distribution of the pearlite and ferrite structures in steel.

A fairly good description of the nature of the microstructure can be obtained by making an analysis of the variance of the microconstituents of a large number of the samples, each being of the same size. In such an analysis the coordinates of the location from which the sample is taken is often ignored, even if known. Had the spatial distribution of the microstructure been known to be completely random or perfectly segregated, this would not matter. But as is evident from the nature of the microstructure from the Figure 2.2, this is not the case. Hence the limitation on the information of the microstructure, that can be provided by the sample variance. Moreover, the process is incapable of estimating sample variance of the samples of other different sizes. The correlation coefficient function is used widely in statistics to explain such relationships.

The following description makes the use of this correlation coefficient function clearer. Suppose an element is selected at random from the material. It can have

a 100% composition of one of the phases with a certain probability 'P' associated with it, the number 'P' being the volumetric composition of that particular phase in the overall material. If another element were to be chosen in the vicinity of the first element, the probability of this element having the same composition would almost always vary and would be a function of the distribution of the microstructure. The probability of this being the same composition would be given by

$$P(c(q+r)=1 \| c(q)=1) = p + (1-p)\rho(r) \tag{2.3}$$

where P is the probability that component 'c' is 100% or 1 at a position 'q + r' given the composition is 100% or 1 at position 'q' [10]. The term 'q' is the vector position with respect to an origin, while 'r' is the vector position with reference to the first element. $\rho(r)$ is the correlation coefficient function that characterizes the distribution of the components and is determined empirically from image analysis of the digitized pictures of the microstructure. It can be seen that $\rho(r)$ approaches 1 as r approaches 0 and for microstructures of the form of steel, where there is no long range segregation, $\rho(r)$ becomes 0 as r approaches infinity. When $\rho(r)$ has a value 1 there is said to be perfect correlation, while a $\rho(r)$ value of 0 implies absence of correlation.

The concept of correlation coefficient function can be better understood with the help of Figure 2.4. Figure 2.4(a) shows the correlation coefficient function of a set of spheroidal particles. Figure 2.4(b) is the correlation coefficient function of elongated strips. The difference between the two functions is obvious. Also

Figure 2.4(c) shows another set of spheroidal particles, but of a much larger size. The correlation coefficient function approaches zero much slower than that for the smaller particles in Figure 2.4(a).

Mathematically, the correlation coefficient function, $\rho(r)$, between points '1' and '2' at a distance 'r' between them is given by

$$\rho(r) = \frac{E[(H_1 - \mu_a)(H_2 - \mu_a)]}{\sigma_a^2} \tag{2.4}$$

where μ_a is the mean hardness of elements in a population, H_1,H_2, the hardness at the different elements of the population and σ_a^2, the variance of the population distribution.

2.1.5 Sample Shape Function

In order to introduce a spatial relationship of the microstructure distribution, the concept of a sample shape function is used. The use and the meaning of this function becomes clearer as the equation for the sample variance is derived [12].

The population variance σ_a^2 is given by the standard statistical equation

$$\sigma_a^2 = E[(H_i - \mu_a)^2] \tag{2.5}$$

where H_i is the hardness of the i'th element of the material (pixel in a digitized picture) and μ_a is the mean hardness of all such elements of the population.

The sample variance σ_s^2 is given by

$$\sigma_s^2 = E[(\mu_{sj} - \bar{\mu}_s)^2] \tag{2.6}$$

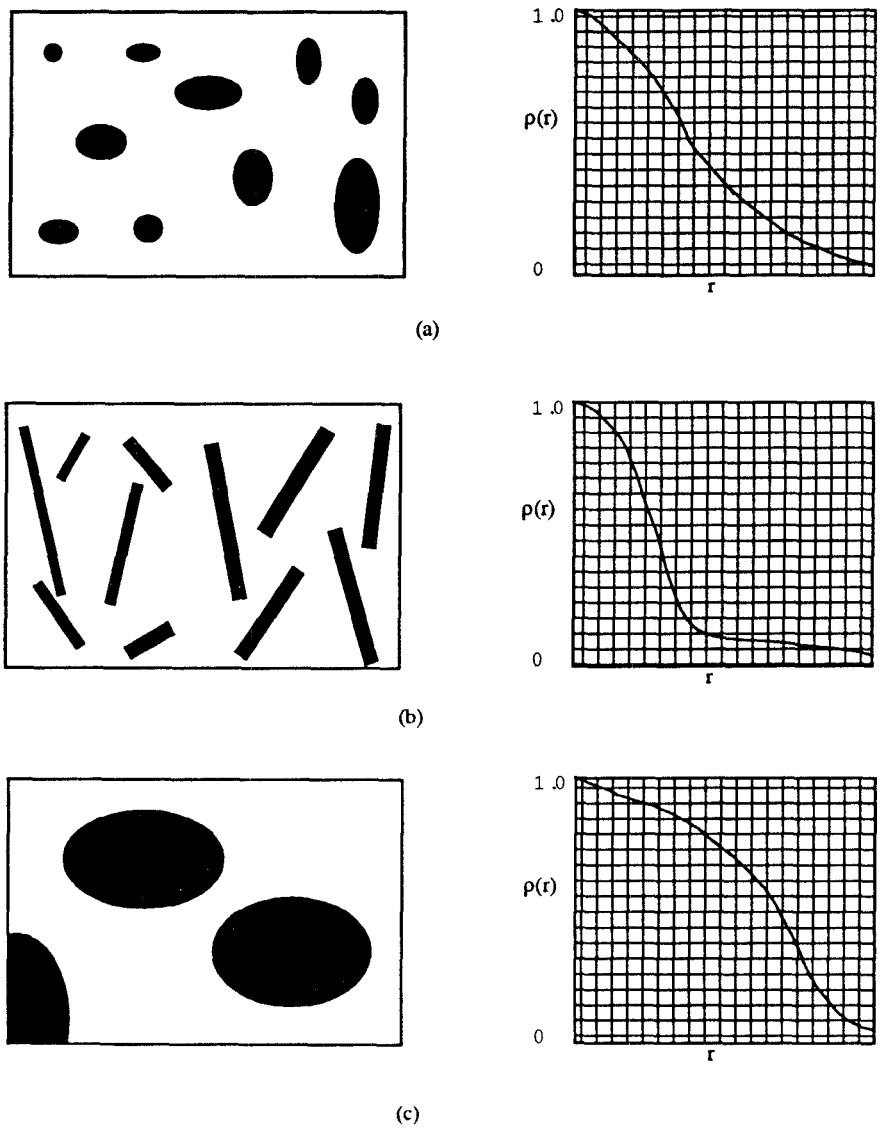

Figure 2.4: Nature of the correlation coefficient functions for different distributions

where μ_{sj} is the mean hardness of the j'th sample, and $\bar{\mu}_s$ is the mean of the means of these samples.

But according to the central limit theorem in statistics, $\bar{\mu}_s = \mu_a$ Therefore,

$$\sigma_s^2 = E[(\mu_{sj} - \mu_a)^2] \tag{2.7}$$

When the sample variance is measured with reference to two different samples, 'k' and 'l', we have

$$\begin{aligned}
\sigma_s^2 &= E[(\mu_{sk} - \mu_a)(\mu_{sl} - \mu_a)] \\
&= E[\frac{1}{V}\int_V (H_{ik} - \mu_a)dV.\frac{1}{V'}\int_{V'}(H_{il} - \mu_a)dV'] \\
&= \frac{1}{M}\sum^{M}\frac{1}{V^2}\int_V\int_{V'}(H_{ik} - \mu_a)(H_{il} - \mu_a)dV'dV
\end{aligned} \tag{2.8}$$

since $V' = V$.

Also, the correlation coefficient function between two points 'k' and 'l' is given by

$$\begin{aligned}
\rho(r) &= \frac{covariance(k,l)}{\sigma_k^2\sigma_l^2} \\
&= \frac{E[(H_{ik} - \mu_a)(H_{il} - \mu_a)]}{\sigma_a^2}
\end{aligned}$$

Therefore, we have the relationship,

$$E[(H_{ik} - \mu_a)(H_{il} - \mu_a)] = \rho(r)\sigma_a^2$$

Equation 2.8 can then be expressed as

$$\sigma_s^2 = \frac{\sigma_a^2}{V^2} \int_V \int_{V'} \rho(r) dV' dV \tag{2.9}$$

From this relationship, it is obvious that the sample variance is a function of the sample shape. As the shape changes, due to the different volumes, we get a different value for the sample variance. Hence, a function called as the sample shape function is used to make the model flexible to such changes in the sample shape.

Consider a spherical shell of radius 'r', with a thickness 'dr', centered at the corners of one of the samples, as shown in Figure 2.5. A function called as the volume fractional function is defined to describe the sample bounds. The volume fractional function $W^*(x, r)$, is the fraction of the volume of the shell described above, centered at a point 'x', that lies inside the sample. Figure 2.6 explains the method of calculation of the volume fraction function for a typical sample. The figure explains the method of calculation of the volume fractional function when the center of the shell lies on one of the faces of the sample or if the shell is completely inside the sample. However, in the calculation of the sample shape function the volume fractional function needs to be calculated for some shells whose centers lie inside the sample, but have portions outside the sample. This is illustrated by one such shell shown in Figure 2.7. This necessitates analytical calculation of such volumes.

Consider a shell of radius 'r', centered inside the sample, as shown in Figure 2.7. Let the sample extend by distances 'h_1', 'h_2' and 'h_3' in the three directions

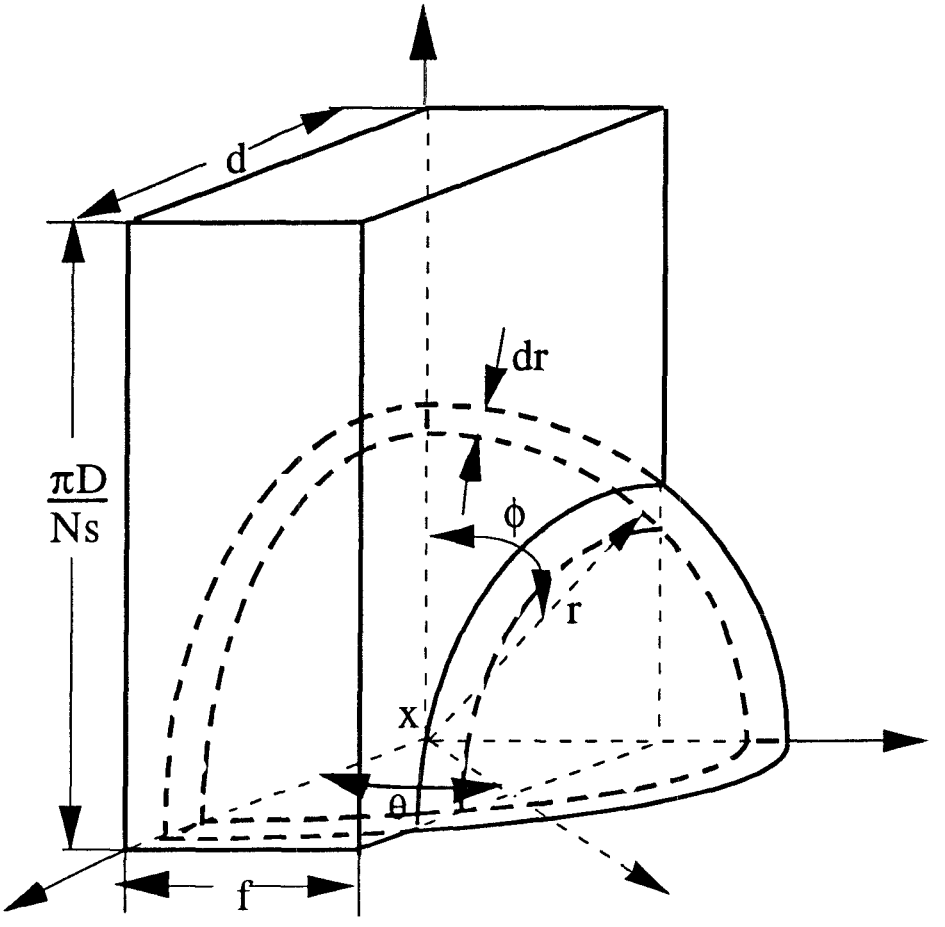

Figure 2.5: Illustration of volume fractional function

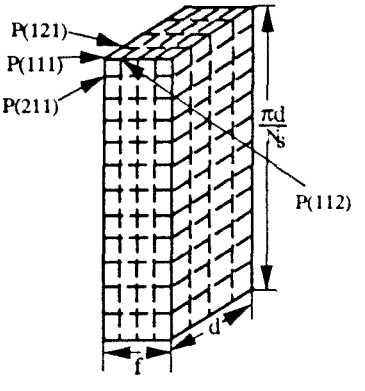

W*(x, r) for r = 1

@ P(111) W*(P(111), r = 1) = 1/8 * Δv
@ P(121) W*(P(121), r = 1) = 1/4 * Δv
@ P(122) W*(P(122), r = 1) = 1/2 * Δv

Figure 2.6: Calculation of volume fractional function by computer program

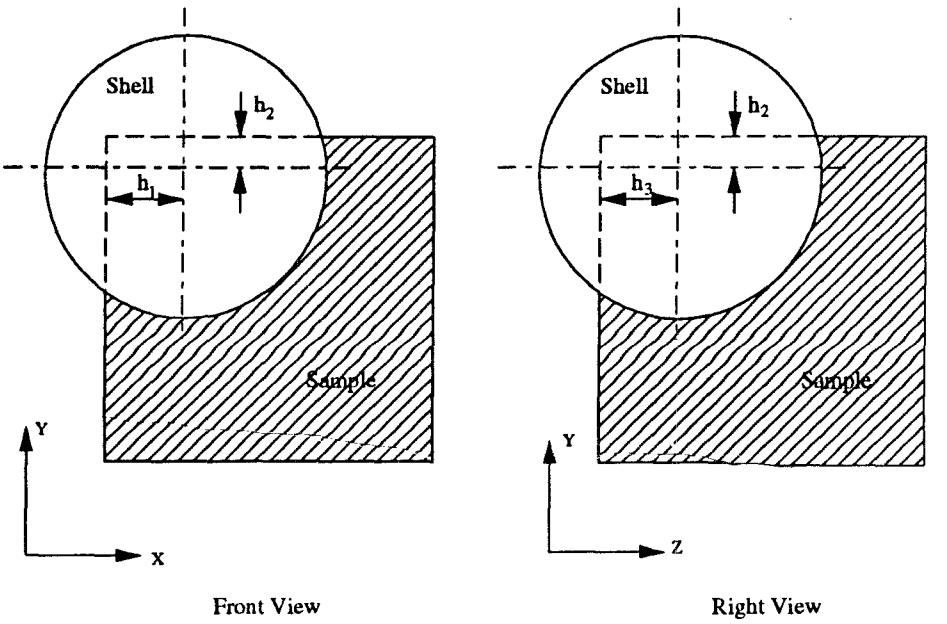

Figure 2.7: Calculation of volume of shell inside sample

marked x, y and z in the figure. In order to calculate the sample shape function, the volume of the shell inside the sample is needed. The volume of a part of a shell that is at a distance 'h_0' from the center, as shown in Figure 2.8 is derived here.

$$v = \int_{\theta_0}^{\frac{\pi}{2}} \pi x^2 dh \tag{2.10}$$

where, $\theta_0 = Tan^{-1}\frac{h_0}{\sqrt{r^2-h_0^2}}$. But,

$$\begin{aligned} x &= r * Cos\theta \\ x + dx &= r * Cos(\theta + d\theta) \\ h &= r * Sin\theta \\ h + dh &= r * Sin(\theta + d\theta) \end{aligned}$$

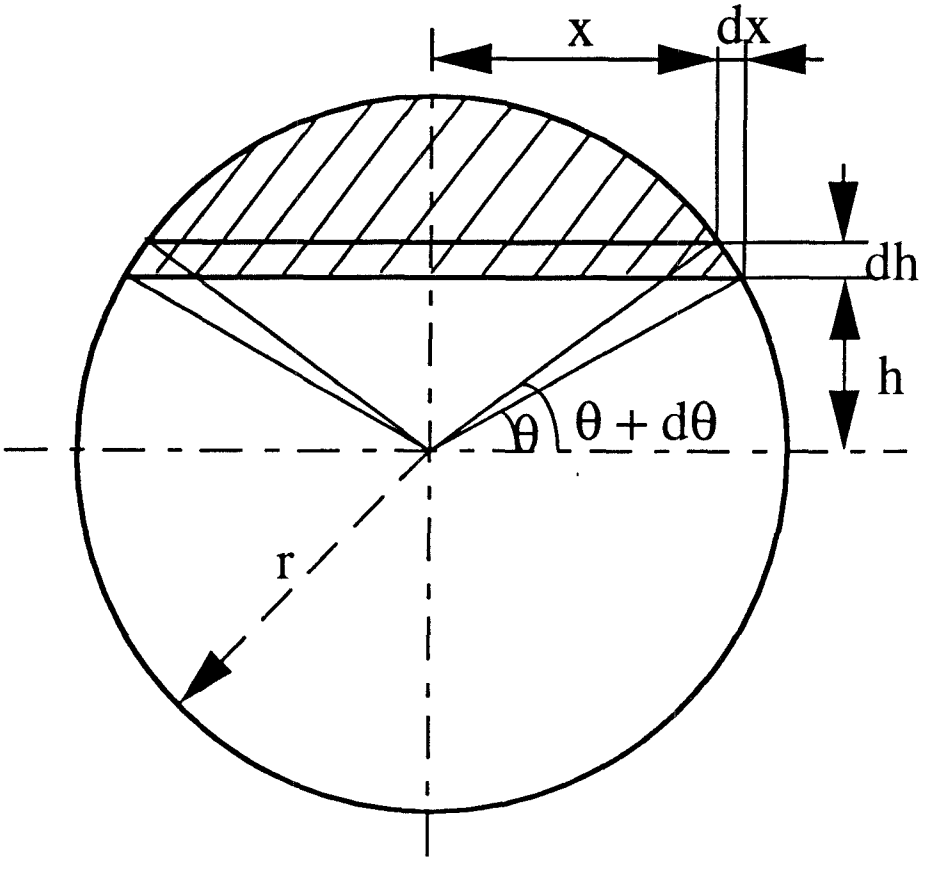

Figure 2.8: Calculation of volume of a part of a sphere

$$
\begin{aligned}
dh &= h + dh - h \\
&= r[Sin(\theta + d\theta) - Sin\theta] \\
&= r[Sin\theta Cos(d\theta) + Sin(d\theta)Cos\theta - Sin\theta]
\end{aligned}
$$

For small θ, $Cos(d\theta) \approx 1$ and $Sin(d\theta) \approx d\theta$. Thus,

$$
\begin{aligned}
dh &= r[Sin\theta + d\theta Cos\theta - Sin\theta] \\
&= rCos\theta.d\theta
\end{aligned}
$$

The volume of the part of the sphere is,

$$
\begin{aligned}
v &= \int_{\theta_0}^{\frac{\pi}{2}} Cos^3\theta.d\theta \\
&= \pi r^3[\frac{2}{3} - \frac{Sin3\theta_0}{12} - \frac{3Sin\theta_0}{4}]
\end{aligned} \tag{2.11}
$$

The volume fractional function for a shell that has a portion extending out of the sample in only one direction is given by

$$W^*(x,r) = V - v \tag{2.12}$$

where V is the volume of the shell and is given by $V = \frac{4}{3}\pi r^3$.

However, if the shell extends in more that one direction as explained earlier, the solution is more complex and involves a number of integrations. Solving these numerically on the computer would slow down the simulation significantly, as hundreds of thousands of such calculations are made in order to calculate the sample shape function. Therefore, an approximation for the volume of the shell inside the sample has been made. The approximate solution is given by

$$W^*(x,r) = V - v_1 - v_2[1 - \frac{1}{2}(1 - \frac{h_1}{r})^{2.2}]$$

$$-v_3[1-\frac{1}{2}(1-\frac{h_1}{r})^{2.2}-\frac{1}{2}(1-\frac{h_2}{r})^{2.2}$$
$$+\frac{1}{4}[1-(1-\frac{h_1}{r})^{2.2}](1-\frac{h_2}{r})^{2.2}] \qquad (2.13)$$

where v_i is given by Equation 2.11 , $\theta_{0i} = Tan^{-1}\frac{h_i}{\sqrt{r^2-h_{0i}^2}}$.

The equation calculates the volume of the shell by eliminating any common regions in the parts of the shell that lie outside the sample in any two or three directions. The exponent has been chosen based on empirical studies. The approximation has been found to be good and the results are very close to the actual values. Also, any small errors exist only in the cases where the shell extends out of the sample in more than one direction. This case occurs a very small percentage of times in the calculation of the sample shape function, at low values of 'r'. When the value of 'r' is large the sample shape function are near zero and hence the errors do not affect the sample shape function. Hence, the approximation is very useful and makes computation rapid.

Consider an element of the sample as shown in Figure 2.9. The volume of the element in spherical coordinates is given by

$$dv = (rSin\phi d\theta)(rd\phi)(dr) \qquad (2.14)$$

Thus, in spherical coordinates, the inner integral in Equation 2.9 can be expressed as

$$\int_{V'} \rho(r)dV' = \int_{\phi}\int_{\theta}\int_{r} \rho(r)r^2 Sin\phi dr d\theta d\phi$$

Since the original integral has limits within the volume of the sample, the integrals with respect to θ , r and ϕ also have to be specified, to limit points of

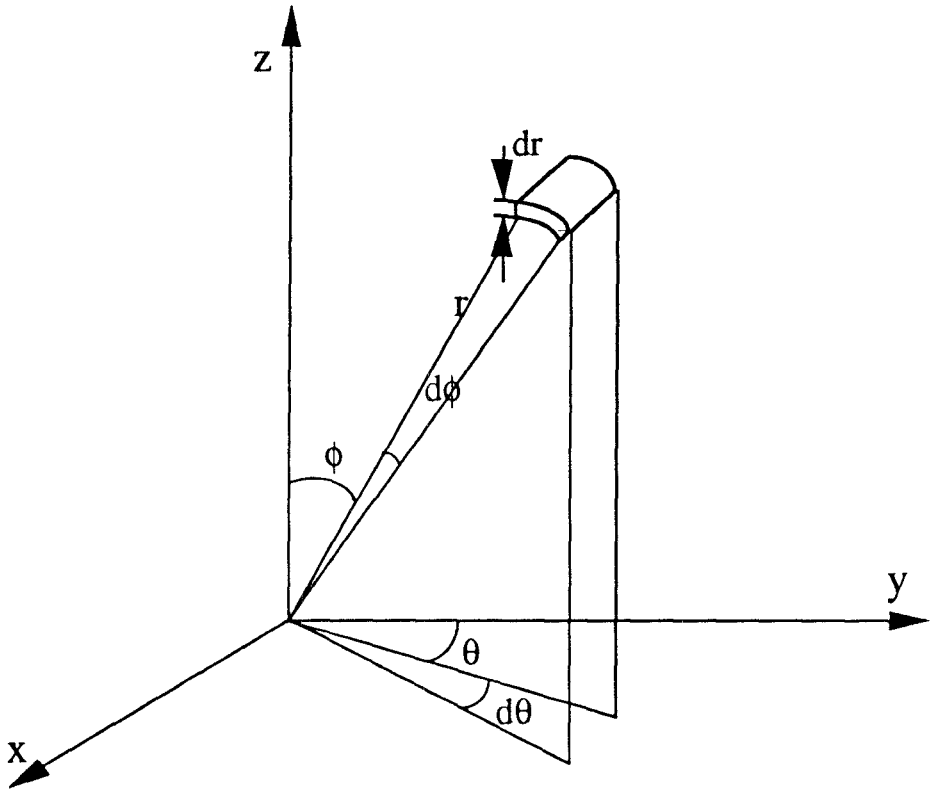

Figure 2.9: Element of sphere represented in spherical coordinates

analysis to be within the sample boundaries. It is important to note that 'r' only represents the distance between the volume increment dv' and the increment dv specified by the outer integral. If 'x' is the location of this incremental volume, $W^*(x,r)$, as described earlier, gives the volume fraction function. With the use of this function, the integrals with respect to θ and ϕ can be eliminated as they are a function of the radius 'r' and the location 'x' only. The inner integral can now be expressed as

$$\int_{V'} \rho(r) dV' = \int_{r=0}^{\infty} \rho(r) W^*(x,r) 4\pi r^2 dr \tag{2.15}$$

The upper limit of the integral being ∞ does not affect this integral, as any value for the function W^* with large 'r' will only be zero, as no volume of the shell is inside the sample. The sample variance can be expressed using this function as

$$\begin{aligned} \sigma_s^2 &= \frac{4\pi\sigma_a^2}{V^2} \int_V \int_{r=0}^{\infty} \rho(r) r^2 W^*(x,r) dr dV \\ &= \frac{4\pi\sigma_a^2}{V} \int_{r=0}^{\infty} \rho(r) r^2 \frac{1}{V} \int_V W^*(x,r) dv dr \end{aligned} \tag{2.16}$$

The order of integration has been changed and terms in the inner integral which depend only on 'r', have been grouped together. Defining W(r), the sample shape function as

$$W(r) = \frac{1}{V} \int_V W^*(x,r) dV \tag{2.17}$$

The expression for the sample variance reduces to

$$\sigma_s^2 = \frac{4\pi\sigma_a^2}{V} \int_{r=0}^{\infty} \rho(r) W(r) r^2 dr \tag{2.18}$$

The nature of the sample shape function is unique for a fixed sample shape. It can be evaluated by the help of numerical routines that calculate these volumes. The advantage of these kind of analysis is that the computer support system for the analysis and control of the machining process can easily calculate the sample variance for any different set of operating conditions used for the machining process.

An important requirement for the model is for it to be immune to different magnification factors so that the different correlation coefficient functions obtained due to different magnifications of the microstructure will not significantly alter the description of the microstructure. It is important here to note that the correlation coefficient function and the sample shape function are both varying with respect to the pixel dimensions of the digitized image. Hence, at different magnifications the pixels of the image represent different dimensions. With a change in the magnification, the correlation coefficient function changes. But this change is nullified by a corresponding opposite change in the sample shape function so as to yield a constant value of the sample variance. Thus this model is effective for any magnification of the microstructure. A detailed analysis to prove the immunity of the model to the magnification factor is presented in the chapter on results.

The sample mean and the sample variance together completely describe the nature of the samples that are removed by the cutting tool during the machining operation. Hence a model can be built that simulates the cutting operation with

the generation of random hardness representing the workpiece material. This variation is then converted to variations in the cutting forces and consequently into random vibration. This vibration is then related to the nature of the finished surface obtained. The mathematical model to bring about this transformation forms a very important part of this thesis work and is presented in the next chapter.

2.2 Markov Models

The microstructure of rolled steel bars exhibit a very different nature in terms of its size, shape and distribution along its longitudinal direction. This is primarily because of the nature of the material flow during the rolling process. The main effect of cold rolling, in terms of the microstructure, is elongation of the ferrite grains [20]. Figure 2.3 shows the nature of the microstructure in the longitudinal direction. The pearlite grains tend to get broken into fragments, groups of fragments being elongated in the rolling direction. A similar microstructure is present in most other multiphase steels and metal alloys.

The model to describe the nature of the microstructure distribution has to account for these kind of patterns observed. The sample variance model described earlier will not be an accurate model by itself, as this model does not take this longitudinal pattern into account. Hence, another model which uses the concept of Markov chains is used to characterize the microstructure.

The Markov chain model tries to establish the relationship between the samples adjacent to each other in the direction of feed. The transition of the cutting process from sample to sample, with the completion of the first cutting revolution of the workpiece is made to be a function of the structure of the adjacent sample in the feed direction.

Markov processes are stochastic processes which probabilistically describe the changes of states $(S_1, S_2, ..., S_N)$ of systems, with respect to time. At any particular time instant the change of state is said to occur between events $(q_1, q_2, ..., q_t)$. Discrete, first order, Markov chains have their probabilistic description truncated to just the current and the predecessor states i.e.

$$P[q_t = S_j \| q_{t-1} = S_i, q_{t-2} = S_k, ...] = P[q_t = S_j \| q_{t-1} = S_i] \tag{2.19}$$

Also, the type of probabilities considered here have their probabilities independent of time, thus being described by the state transition probabilities, p_{ij} of the form

$$p_{ij} = P[q_t = S_j \| q_{t-1} = S_i]; 1 \leq i, j, \leq N \tag{2.20}$$

where N is the number of states, $p_{ij} \geq 0$ and $\sum_{j=1}^{N} p_{ij} = 1$. Markov processes are similar to Markov chains except that the state space is not discrete [21].

Hidden Markov processes can be defined as double embedded stochastic processes with an underlying stochastic process that is not observable i.e. hidden, but can only be observed through another set of stochastic processes that produce the sequence of observations. The meaning of the hidden Markov process

becomes clearer as the explanation of the model's application is made to the machining process.

In the case of microstructure distribution the different states represent different regions of the distribution of the microhardness at different cross sections along the material's axis. If a set of samples are taken from each of any ten different cross sections of a rolled steel bar, it is very likely that the samples from each revolution have ten different means and variances of this microhardness. But from a statistical point of view they can very easily be grouped into distributions having a mean and variance very close to that of the group members, by the use of the test on means, as explained later in the chapter. These groups of microhardness represent the different states of the hidden Markov process. Thus, based on the probability of occurrence, the particular cross section being machined at any instant in time can be expected to be in one of these states. Also, the nature of the distribution of adjacent cross sections is determined probabilistically based on certain transition probabilities.

For a complete description of a hidden Markov process, five characteristics are necessary.

1. N, the number of possible states which correspond to the number of groups of microhardness distribution,
2. M, the number of distinct observation symbols per state, which is infinite in this case, as the microhardness within a state can be any number that falls in the normal distribution that characterizes the

state,

3. The state transition probability distribution $P = p_{ij}$,

4. Observation symbol probability distribution in each state. This probability is described in terms of a normal distribution of microhardness for each of the states,

5. The initial state distribution $\pi_i = P[q_1 = S_i]; 1 \leq i \leq N$, which in this case is the distribution as decided by the sample variance theory.

To apply this model to characterize the microhardness distribution all these parameters need to be determined.

The concept of Markov chains has been applied to the modeling of material microstructure in two different ways. The first model approaches the material only on the concept of Markov chains. The sample mean hardness distribution in the direction of feed after the first revolution of the workpiece is determined by the state transition probability. Thus, with the proper selection of states and the state transition matrix, the longitudinal pattern existing in the workpiece material is reconstructed. The second model assumes that the hardness distributions of each of the material's cross section falls into a small finite number of distributions which are represented by the states of the Markov process. The selection of a particular distribution for any revolution is governed by the state transition matrix. Given the distribution for the revolution, the mean hardness of the sample is based on the normal distribution. Thus the selection of the sam-

ple mean is based on the results of the two stochastic processes, hence a hidden Markov process. These two models are described in the following sections.

2.2.1 Markov Chain Model

In this model the description of the microstructure in the longitudinal direction is probabilistically related, directly, to the adjacent sample along the feed direction, i.e. in the previous revolution. There is just one normal distribution that forms the basis for sample mean hardness generation. This mean hardness distribution is obtained experimentally from image analysis of the sample sections in the transverse direction. However, this distribution is divided statistically into a finite number of regions that represent the states of the Markov chains. For example, if the distribution is divided into three divisions as shown in Figure 2.10, then the states of the Markov chain represent the hardness bands in the distribution. The state boundaries are decided based on statistical "tests on means" performed on the images of the longitudinal sections of the material. A detailed description of this statistical test is presented in the appendix.

The nature of the longitudinal trend in the distribution of the microstructure in the material can be easily accounted for by the proper selection of the state transition matrix for the system. The state transition matrix consists of the probabilities of the adjacent sample moving from one state to another. These probabilities can be got from pictures of the microstructure of the samples. The method of formulating the state transition matrix is explained later in the chap-

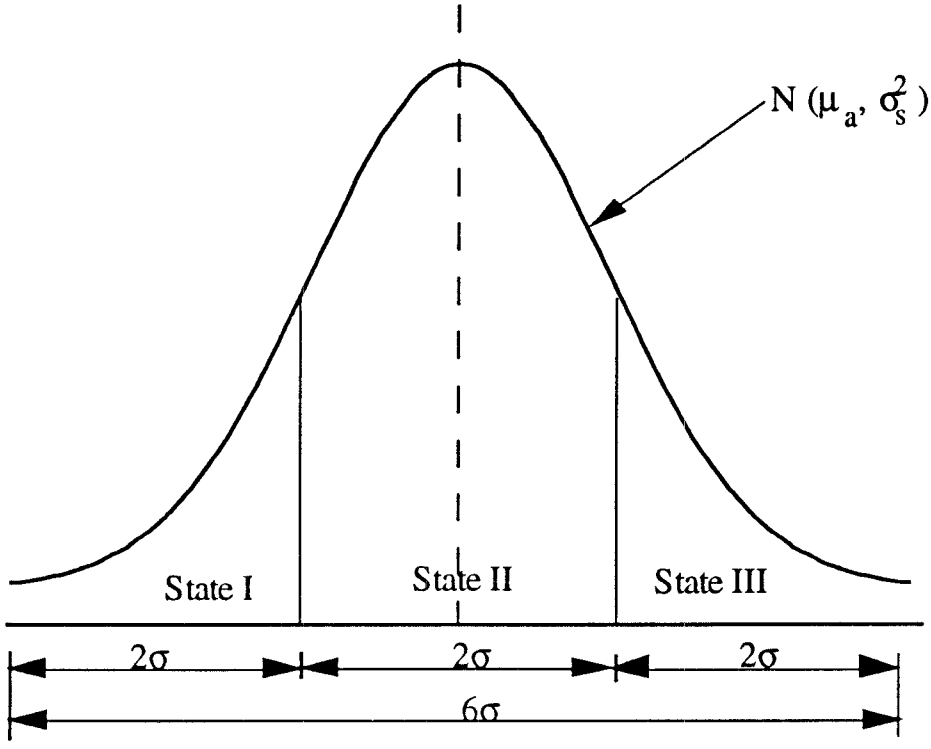

Figure 2.10: Selection of states of the Markov chain

ter.

2.2.2 Hidden Markov Model

This model, as explained earlier, is based on the concept that the distribution of the microstructure within a revolution is the same. Also, the number of such distributions is finite. This is very often the case in rolled multiphase metal bars which is the the type of material under study. For instance, the distribution of pearlite and ferrite in carbon steels usually fall into three to four normal distributions of the sample mean hardness, within a particular cross section. This is because of the fact that during the manufacture of rolled steel the concentration of microstructure is a result of a finite number of repeated, localized thermal or stress conditions present in the roll mills. Thus, when a rolled steel bar is sectioned and the microstructures analyzed, their sample mean hardness very often fall into three or four normal distributions, within statistically significant spreads. These distributions are represented as states of the model.

The nature of the sample hardness distribution for every revolution is dependent on the distribution in the previous revolution. The change in distribution is governed by the transition matrix for the hardness distributions.

The selection of these states is a statistical process. A number of tests of different hypotheses are made and their validity checked based on such concepts in statistics. Appendix A briefly covers these concepts on test of hypotheses [23, 24]. The number of images of the sample sections are taken from different

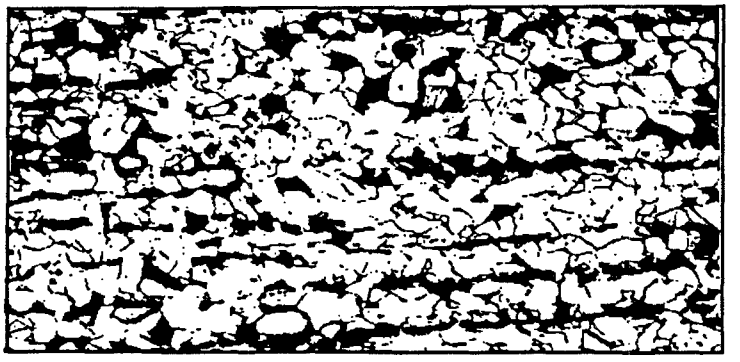

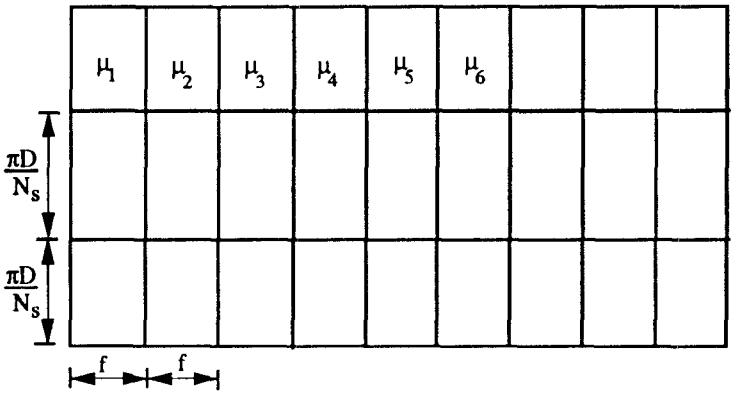

Figure 2.11: Division of the image into sections based on sample dimension

representative regions of the material. The images are divided into sections based on the dimensions of the sample as shown in Figure 2.11. The mean hardness of these sections and the variance of the hardness of these sections are calculated. These means are then compared against one another and checked for statistically significant differences. It is almost always found that these mean hardness fall into a finite number of distributions. It is these distributions that are represented as states explained earlier. Given the states, the probability of the samples assuming these distributions needs to be analyzed. This is quantified

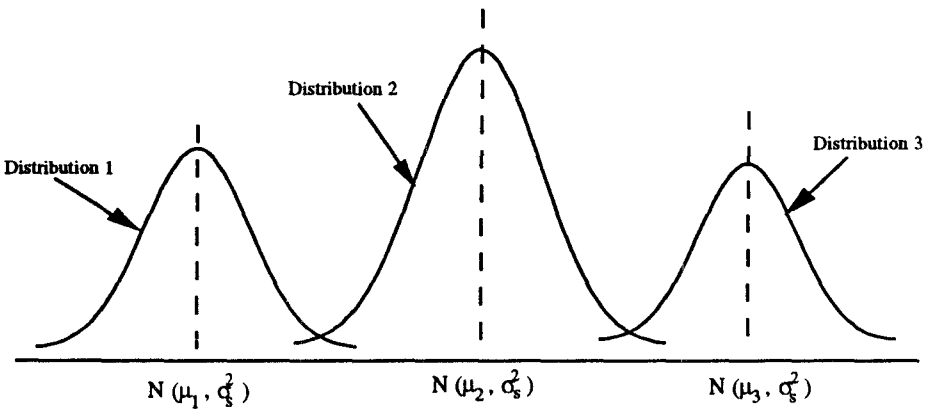

Figure 2.12: Nature of the different distributions in the Markov model

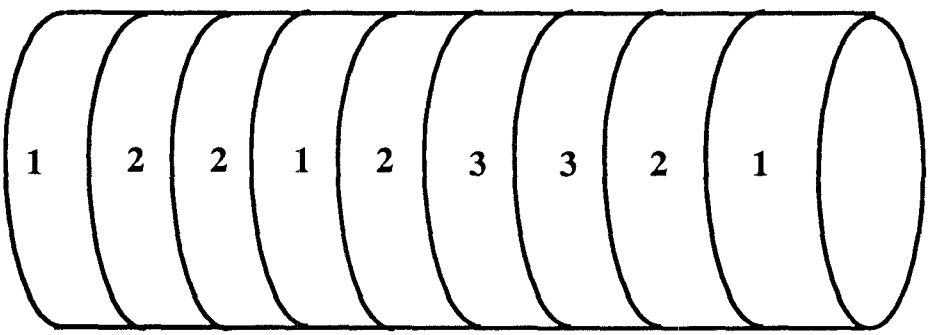

Figure 2.13: Assignment of distributions to cross sections of the material

by the state transition matrix. The formulation of the state transition matrix that exactly represents the nature of the sample hardness occurrences in the material is key to the success of this concept of a statistical model for the material microstructure.

The distributions, as seen from Figure 2.12, overlap each other for a small region with certain hardness values common to more than one distribution, within the given sigma-limits. This is because the variations in the conditions producing these different distributions during the material processing do not drastically vary. Also the chances of the sample mean hardness along adjacent

samples lying in the same part of the distributions, even if the distributions are different, are very high. This is analogous to the condition in the material description by the use of the Markov chains. Hence it would be very useful to use the strengths of that model to enhance the performance of the hidden Markov model. This can be done by the incorporation of the substates of the process. The substates of the process are the different regions of the normal distributions. Each of these distributions is divided on a similar basis into a equal, finite number of regions based on either the spreads or the areas enclosed, similar to the states of the Markov chain described earlier. The change of substates within distributions is again governed by another state transition matrix referred to as the transition matrix for the substates. An assumption is made here that the state transition for the distribution and transition matrix for the substates are mutually exclusive. This implies that the transition for substates between adjacent samples along the feed direction are independent of the transition of the states (distributions) between these revolutions. This assumption has been tested on the samples studied and holds good as is evident from the Figure 2.14. However, for materials where the distributions do not follow this pattern, a transition matrix for the substate calculated on individual basis for such distributions, needs to be used. The concept and structure of the hidden Markov model remains the same while the nature of the transition between the substates, which is critical for the success of the model to describe the stochastic process is greater in number, one for each distribution.

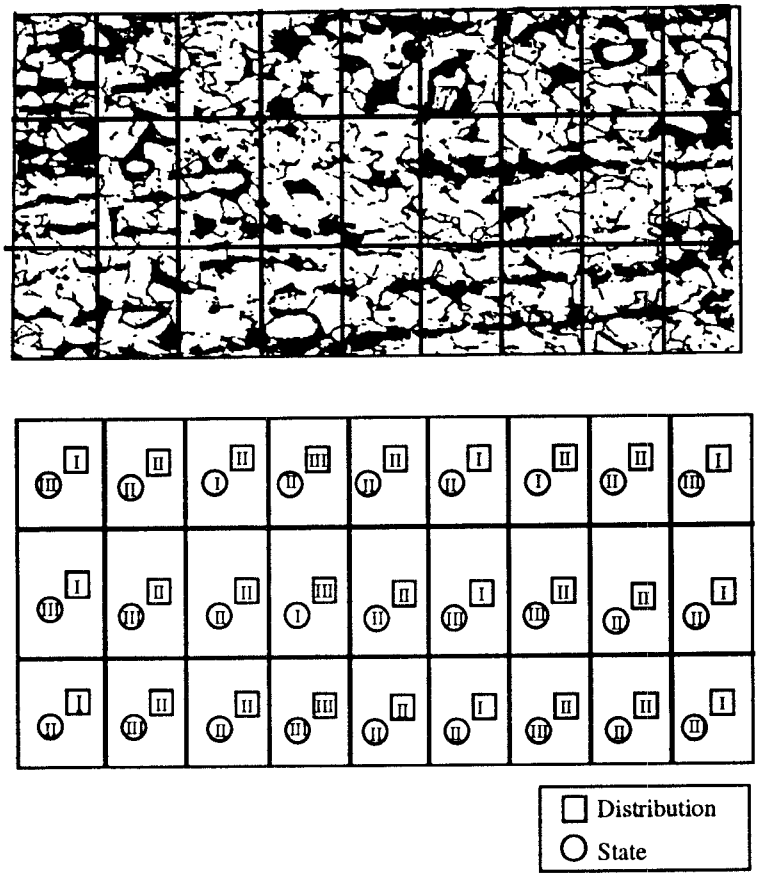

Figure 2.14: The state map showing distribution and state of the samples

Since the states, substates and events have been decided, the only parameter that is now required for the complete description of this model is the state transition matrix. The determination of the state transition matrix is done experimentally. Pictures of the microstructure in the longitudinal direction are divided into many sections, the dimension of each of these sections being decided by the dimensions of the sample as explained earlier. The mean hardness of these sections calculated on the basis of the microconstituents seen within the sections are grouped with respect to the distributions (states). The sample means and the states they fall into, for a representative section, are calculated. The representation of these sections into the different distribution or the state depending upon the nature of the model is referred to as the state map and is shown in Figure 2.14.

2.2.3 Formulation of State Transition Matrix

The state transition matrix consists of the probabilities of transition between the different states in the state space. The transition matrix is represented as $P = \{p_{ij}\}$ where

$$p_{ij} = P[q_t = S_j \| q_{t-1} = S_i] \tag{2.21}$$

$$1 \leq i, j \leq N$$

S_i and S_j being any two states in the state space, q_t and q_{t-1} are the events at times t and $(t-1)$ respectively and N is the total number of states constituting the state space [25]. These probabilities form the foundation on which the simulation

of the material microstructure is built. The formulation of the matrix is done from pictures of the material's microstructure in the longitudinal direction.

The transition probabilities exhibit the following two properties since they obey standard stochastic constraints.

$$\begin{aligned} p_{ij} &\geq 0 \\ \sum_{j=1}^{N} &= 1 \end{aligned} \tag{2.22}$$

In order to determine these probabilities the expected duration of the states need to be determined. The expected duration in a particular state is given by

$$\begin{aligned} E(d_i) &= \sum_{d=1}^{\infty} dP_i(d) \\ &= \sum_{d=1}^{\infty} d(p_{ii})^{d-1}(1-p_{ii}) \\ &= \frac{1}{1-p_{ii}} \end{aligned} \tag{2.23}$$

where $P_i(d)$ is the probability density function of duration 'd' in state 'i'. The transition probability p_{ii} can then be calculated as

$$p_{ii} = 1 - \frac{1}{E(d_i)} \tag{2.24}$$

The expected duration in the same state is obtained from the state representation (state map) of the image. The average duration of stay in a particular state $E(d_i)$ is given by

$$E(d_i) = \frac{\sum_{j=1}^{n} d_i(j)}{K_i} \tag{2.25}$$

where $d_i(j)$ is the duration of the state 'i' occuring at the j'th instance. K_i is the total number of occurrences of the state.

The determination of the probability of changing to a different state from a given state is made in a slightly different way. For a two state model the determination of this probability is straight forward and is given by

$$p_{ij}\|_{i\neq j} = 1 - p_{ii}$$

However, very often, the number of states present are more than two and so further analyses need to be made. The images are again analyzed for instances of the transition between any two different states from the state representation of the image. If d_{ij} is the number of instances of transition from state 'i' to 'j' obtained from the state representation of the microstructure, the transition probability is given by

$$p_{ij}\|_{i\neq j} = \frac{d_{ij}}{\sum_{j=1}^{K_i} d_{ij}} \tag{2.26}$$

The steel specimens used in this thesis showed significant longitudinal trends. Hence the probability of transition between non-neighboring states was found to be almost zero. But, since the patterns did not yield exact zero values for transition probabilities between non-neighboring states, these small probabilities have been considered in the model in order to accurately represent the material distribution.

Chapter 3

Surface Generation Modeling

Integration of the sample variance theory and the hidden Markov method forms a very effective way of characterizing the microstructure of the workpiece material. As explained in the earlier chapters, the variation of the hardness of the microstructure and thus the samples cause a variation of the cutting force which is the source of vibration to the tool. Thus, before any prediction of the nature of the machined surface is made, based on the nature of the material, a realistic model is necessary to describe the dynamic nature of the force and the vibration of tool structure during the cutting process. The first part of this chapter explains the model used to describe the dynamics of the tool structure. Once the description of the dynamic structure is made and the nature of the tool response understood, the response of the tool needs to be translated to its effects on the nature of the surface generated. The second part of this chapter is devoted to the characterization of the generated surface and the method of calculation of

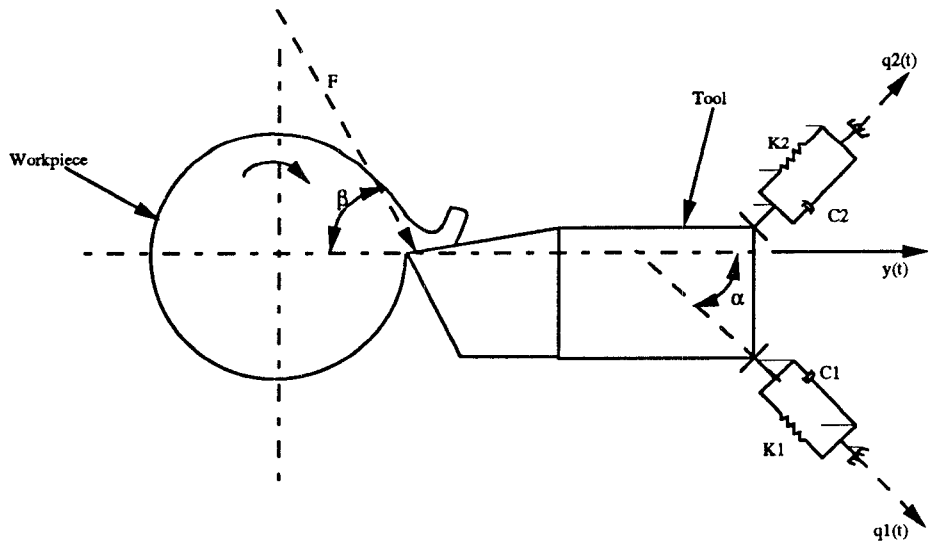

Figure 3.1: Dynamic model of the tool structure

the surface finish parameters that quantify the quality of the generated surface.

3.1 Modeling of Cutting Process

The tool structure used for turning can be modeled as a two-degree of freedom lumped mass - spring - damper system as shown in Figure 3.1 [2]. Such a model was originally proposed by Merritt for the study of chatter in machine tools. The model has since been widely used by many other researchers for different machine tool structures. The model has also been used by Zhang and Kapoor [13] to describe the dynamics of the boring machine system. The nature of the tool vibration due to the random excitation caused by the hardness variation was also studied by them successfully. It is important to note that these models are based on the assumption that the rigidity of the workpiece is very high and

thus any vibration of the workpiece is very low and can be neglected. The only vibration is caused due to the vibration of the tool post, which almost always is the weakest member in the machine tool. Before any further discussion is made on the modeling of the cutting force and the nature of the tool structure, the nature of the forces present during metal cutting needs to be completely understood. The following section is a brief description of the cutting force and its components.

3.1.1 Cutting Force

Cutting forces play a very significant role in metal cutting. It is specially important here in this study of the effect of the material microstructure on surface finish. It is the variation of the forces caused by the different microhardness of the samples that induce random vibration in the tool and hence affect surface finish. Hence a detailed analysis of the cutting force relations are made here.

Orthogonal cutting, which assumes forces in two directions is assumed for the turning process. The direction of rotation in this type of cutting is such that the cutting direction is perpendicular to the cutting edge. Although this is not the exact situation when turning of the outer surface of a cylinder, this is fairly accurate. Looking at the continuous chip as an isolated free body, Merchant [1] established several cutting force relationships by resolving the resultant cutting force (F_r) into three force systems. Figure 3.2 is the Merchant's cutting force diagram which shows the three force systems [18].

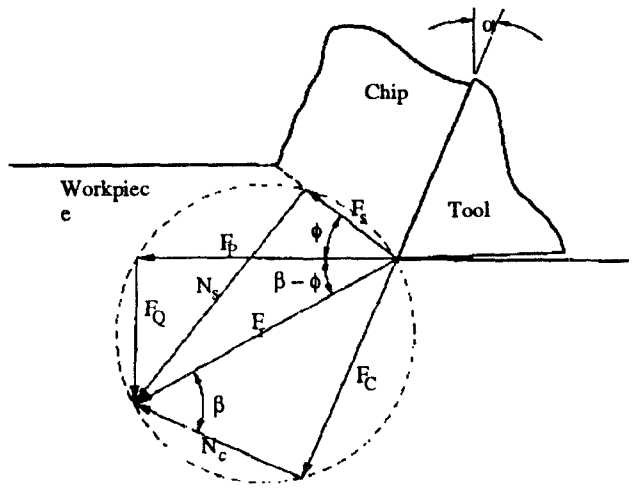

Figure 3.2: Merchant's composite cutting force diagram

The three systems comprise of the following:

1. The main cutting force (F_P), in the direction of the cutting velocity (tangential to the workpiece in the case of turning) and the force component normal to it in the direction of feed called the feed force (F_Q);
2. The frictional force (F_C) acts along the face of the tool and the normal component (N_C);
3. The shearing force (F_S), acting in the shear plane and the compressive force (N_S) normal to it, together comprise the third force system.

The relationship between the three force systems can be expressed in terms of the shear angle, the rake angle and the angle of the resultant force as is shown

in the diagram. The force system that is analyzed in this thesis is the first one. The other two force systems can be expressed as a function of these two forces and the three angles - rake angle (α), shear angle (ϕ) and the friction angle (β) [18]. The two forces F_P and F_Q can be determined experimentally by the use of dynamometers as explained later in the thesis.

From the Merchant's diagram a very popular relationship between the cutting area and the cutting force can be derived. An important term called the unit cutting force is very often used in cutting force relations. The unit cutting force (K_a), is an established constant that relates the cutting area ($b * t$) with the cutting force F_C.

$$F_C = K_a * w * a \tag{3.1}$$

where 'w' is the width of cut and 'a' the thickness of cut, measured in the direction normal to the cutting direction.

As can be seen from Equation 3.1, from a static cutting point of view the cutting force is a constant and is proportional to the uncut chip thickness. This, however, is inadequate to describe the nature of the cutting force in reality. The cutting force varies continually due to the dynamic nature of the machine - workpiece structure. There is often a lot of vibration and the thickness of the workpiece cut is constantly varying, thus making the cutting force fluctuate. It is, hence, necessary to model the dynamics of the tool - workpiece structure. It is assumed that the workpiece is large and properly supported and hence rigid. Thus the cause of the vibration is only due to the nature of the tool structure.

The cutting force generated can be modeled as comprising of three components. They are the components due to the nominal chip load, regenerative chip load and the random excitation due the hardness variation. These three components are described separately and then integrated to yield the overall system dynamical equations.

3.1.2 Nominal Chip Load

As explained earlier, the cutting force from a static point of view, referred to as the nominal chip load, is directly proportional to the ideal cutting area. It can also be expressed in terms of the feed (f) and the depth of cut (d) as

$$\begin{aligned} F_P &= K_a * w * a \\ &= K_a * f * d \end{aligned} \tag{3.2}$$

Defining K_c, a constant called as cutting stiffness, as $K_c = K_a * w$ we have the equation for the cutting force as $F_P = K_c * a$. However, 'a' is not a constant and is dynamically varying about a value, called the uncut chip thickness, U_0.

The system response is in the form of tool displacement $y(t)$, at any time 't', in the direction normal to the cutting velocity. Considering this, the uncut chip thickness is a function of time and can be expressed as $U(t) = U_0 - y(t)$. It is now necessary to describe the model to explain the nature of y(t).

Assuming that the machine tool model is a second order system, if $q_1(t)$ and $q_2(t)$ are the two principal modes (mutually perpendicular) that describe the tool

displacement, then the cutting force can be decomposed as follows:

$$\begin{aligned} m\ddot{q}_1(t) + c_1\dot{q}_1(t) + k_1 q_1(t) &= K_c[U_0 - y(t)]Cos(\alpha - \beta) \\ m\ddot{q}_2(t) + c_2\dot{q}_2(t) + k_2 q_2(t) &= K_c[U_0 - y(t)]Sin(\alpha - \beta) \end{aligned} \tag{3.3}$$

The effective tool displacement $y(t)$ is given by

$$y(t) = q_1(t)Cos\alpha + q_2(t)Sin\alpha \tag{3.4}$$

3.1.3 Regenerative Chip Load

The dynamic variation of the tool position in the radial direction causes the uncut chip thickness to fluctuate about the ideal position. The movement of the tool away from this position causes a lump to be left on the workpiece, while a movement towards the workpiece causes a decrease in the uncut chip thickness. Since in most machining processes the cutting edge overlaps regions already cut partially, this causes the uncut chip thickness to vary a revolution or 'T' seconds later. Hence, to describe the turning process accurately, this has to be accounted for. An overlap factor, μ , is used to account for this effect [2]. The overlap factor defines the fraction of the previous cut that overlaps the present cut. It has a value 1 for plunge cutting, while it is 0 for thread cutting. But for most practical cases of surface turning it is between these two bounds. The effect of the overlapping load due to tool displacement in the previous revolution is referred to as the regenerative chip load.

Accounting for this, the uncut chip thickness is given by

$$U(t) = U_0(t) - y(t) + \mu y(t - T) \tag{3.5}$$

where $T = \frac{1}{N}$, N is the r.p.m. of the rotating workpiece. Thus,

$$U(s) = U_0(s) - y(s) + \mu e^{-st} y(s) \tag{3.6}$$

The displacement of the tool from the nominal depth of cut is modeled as a primary negative feedback. The effect of the residual uncut chip thickness from the previous revolution, referred to as regenerative feedback, has to be represented by a time delay feedback. Modeling of the structure in this form makes the system nonlinear. In order to linearize the system, the feedback is instead treated as a separate input along with the nominal chip load, U_0.

$$y_{res} = \mu * y(t - T) \tag{3.7}$$

3.1.4 Random Excitation

It is obvious that the cutting force is in some form proportional to the hardness of the material being cut. When a tool is cutting a hard material the induced force is much larger than that when cutting a soft material. When a perfectly homogeneous material is being machined the deflection caused by the constant cutting force remains more or less constant. But when the material is non-homogeneous, due to the impulsive variation of the cutting force when cutting microstructures (or samples) of different hardness, a vibration is set up in the

tool post structure. It is very important to model this source of vibration to explain the nature of the machined surface. Since the material's microstructure is grouped into samples, the variation of the cutting force is in effect a function of the sample mean hardness variation. Also, the mean hardness variation is a random variable. Hence the nature of the vibration caused by the excitation source is also random.

Meyer in 1908 [27] studied the effect of strain hardening of materials being cut on the cutting force generated and came up with what is popularly called as the Meyer exponent. This exponent has since widely been used in developing relations between cutting force and hardness and tensile strength of materials. Kronenberg [3] researched further into this topic and arrived at some concrete relationships between cutting force and hardness values. He found that the cutting force constant C_p was a function of the Brinell's hardness of the material. He introduced another constant called as the "exponent of Brinell's hardness" (t_h) which explains the relationship between the cutting force constants of materials of different hardness. The relationship between the cutting forces F_1 and F_2 while cutting materials of hardness BHN_1 and BHN_2 is given by

$$F_2 = (\frac{BHN_1}{BHN_2})^{t_h} * F_1 \tag{3.8}$$

As explained earlier in the sample variance description of the material, the cutting tool is assumed to be cutting different samples at discrete intervals of time. Since the mean hardness of the sample (μ_s) vary about the mean (μ_a), the cutting force also varies about an equilibrium value which is the cutting force

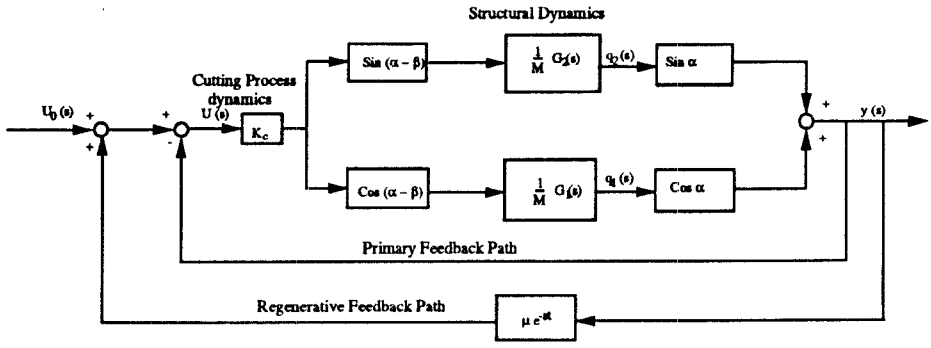

Figure 3.3: Block diagram of dynamical model of cutting process by Merritt

value while cutting a sample with hardness (μ_a). In order to account for this random variation in the equation for cutting force, the variation level is calculated for the force about the equilibrium value. For a tool operating at the nominal cutting depth, the contribution due to the hardness variation is given by

$$F_h = K_a w a[(\frac{\mu_s}{\mu_a})^{t_h} - 1] \tag{3.9}$$

The value of the exponent of Brinell's hardness for carbon steels is about 0.45 [3].

The complete description of the cutting force, including all the three components is given by

$$F = K_a * w[(a - y(t)) + y_{res} + a * ((\frac{\mu_s}{\mu_a})^{t_h} - 1)] \tag{3.10}$$

The system can be expressed in the block diagram form as shown in the Figure 3.3 and 3.4. Figure 3.3 is the block diagram of the system used by Merritt [2], while Figure 3.4 is the modified block diagram incorporating the random excitation.

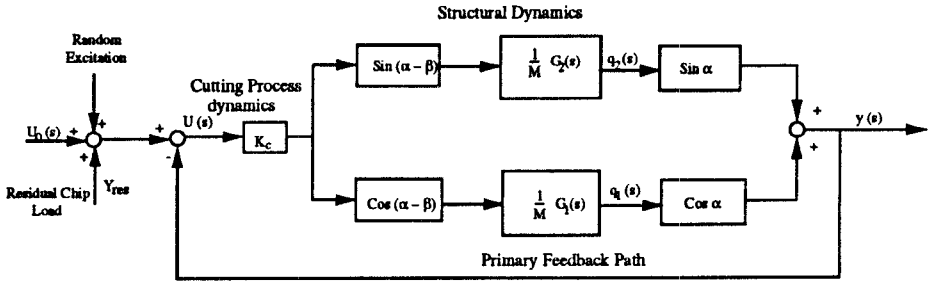

Figure 3.4: Modified block diagram to incorporate random excitation

The dynamical equation description of the system represented by Equations 3.3 and 3.4 are modified to incorporate the effects of residual chip load and the random variations in the cutting force. The modified dynamical equations are given by

$$\begin{aligned} m\ddot{q}_1 + c_1\dot{q}_1 + kq_1 &= [K_a w[a - y(t) + y_{res}] + K_a wa[(\frac{\mu_s}{\mu_a})^{t_h} - 1]]Cos\alpha \\ m\ddot{q}_2 + c_1\dot{q}_2 + kq_2 &= [K_a w[a - y(t) + y_{res}] + K_a wa[(\frac{\mu_s}{\mu_a})^{t_h} - 1]]Sin\alpha \\ y(t) &= q_1 Cos\alpha + q_2 Sin\alpha \end{aligned} \tag{3.11}$$

These equations can be represented in the state space form as follows:

$$\begin{aligned} x_1(t) &= q_1(t) \\ x_2(t) &= \dot{q}_1(t) \\ x_3(t) &= q_2(t) \\ x_4(t) &= \dot{q}_2(t) \end{aligned} \tag{3.12}$$

Differentiating and expressing in a matrix form,

$$\begin{aligned} \dot{X} &= AX + BU \\ y &= CX \end{aligned} \tag{3.13}$$

where

$$A = \begin{pmatrix} 0 & 1 & 0 & 0 \\ \frac{-(k_2+K_a w Cos\alpha Cos(\alpha-\beta))}{m} & \frac{-c_1}{m} & \frac{-(K_a w Sin\alpha Cos(\alpha-\beta))}{m} & 0 \\ 0 & 0 & 0 & 1 \\ \frac{-(K_a w Cos\alpha Sin(\alpha-\beta))}{m} & 0 & \frac{-(k_2+K_a w Sin\alpha Sin(\alpha-\beta))}{m} & \frac{-c_2}{m} \end{pmatrix}$$

$$B = \begin{pmatrix} 0 \\ \frac{K_a w Cos(\alpha-\beta)}{m} \\ 0 \\ \frac{K_a w Sin(\alpha-\beta)}{m} \end{pmatrix}$$

$$C = \begin{pmatrix} Cos\alpha & 0 & Sin\alpha & 0 \end{pmatrix}$$

The effect of the random hardness variation on the cutting force is accounted for by associating it with the thickness of cut. The nominal uncut chip thickness 'a' is scaled by a factor equal to the hardness variation effect. This scaled thickness of cut in this thesis is referred to as the "equivalent uncut chip thickness", (U_e).

$$U_e = a(\frac{\mu_s}{\mu_a})^{t_h} \tag{3.14}$$

The system is treated as a single input system by combining the inputs due to the equivalent chip thickness and the residual chip thickness (y_{res}). The input U is therefore a 1 x 1 matrix. $U(t) = U_e + y_{res}$. In order to simplify the derivation of the equation of the response of the system (y), the equations are transformed into another state space by the transformation matrix P, such that $X = PQ$

where Q is the matrix of the transformed variables. The matrix P consists of the eigen vectors of the matrix A chosen such that the product $P^{-1}AP = J$, the Jordan form of A. If the eigen values of the matrix A have σ_1 and σ_2 as their real parts and ω_1 and ω_2 for their imaginary parts then the matrix J has the form

$$J = \begin{pmatrix} -\sigma_1 & \omega_1 & 0 & 0 \\ -\omega_1 & -\sigma_1 & 0 & 0 \\ 0 & 0 & -\sigma_2 & \omega_2 \\ 0 & 0 & -\omega_2 & -\sigma_2 \end{pmatrix}$$

Thus we have

$$\begin{aligned} \dot{Q} &= P^{-1}APQ + P^{-1}BU \\ &= JQ + B'U \\ y &= C'Q \end{aligned} \tag{3.15}$$

In the derivation of the solution to the set of equations given above, Q, is presented in appendix. The response along the two principal modes $q_1(t)$ and $q_2(t)$ which in the state space representation are $x_1(t)$ and $x_3(t)$ are obtained by transforming the variables into the original system as $X = P^{-1}Q$. With the knowledge of X, the tool response can be calculated as $y = CX$.

This completes the analyses of the dynamical machining system and the nature of the tool response to the different excitations. These responses need to be transformed into its effects on the resultant machined surface and analysis of the nature of the surface generated needs to be done for evaluating the accuracy

of the model and also for effective use of the model to predict the surface finish. The method of making this transformation is explained in the following section.

3.2 Evaluation of Surface Finish

The model described in the earlier section, covered in detail, the nature of the tool vibration in response to the different sources of excitation. The responses by themselves cannot be of any physical significance to a machinist. It has to be translated to its effects on the machined surface. This is done by the calculation of some popularly used surface parameters. These parameters will first be described here before the methodology of calculating them from the tool response is made.

3.2.1 Surface Texture

Surface texture refers to the fine irregularities (peaks and valleys) of a surface produced by the forming process [28]. The texture comprises of two components, roughness and waviness. The irregularities of the process that are a result of the dynamic motion of the tool comprise the roughness, where as the more widely spaced irregularities produced due to external sources of vibration in the machine tool are termed waviness.

Surface topography is a term that describes the overall resulting surface, comprising of the two surface texture components along with the errors of form and

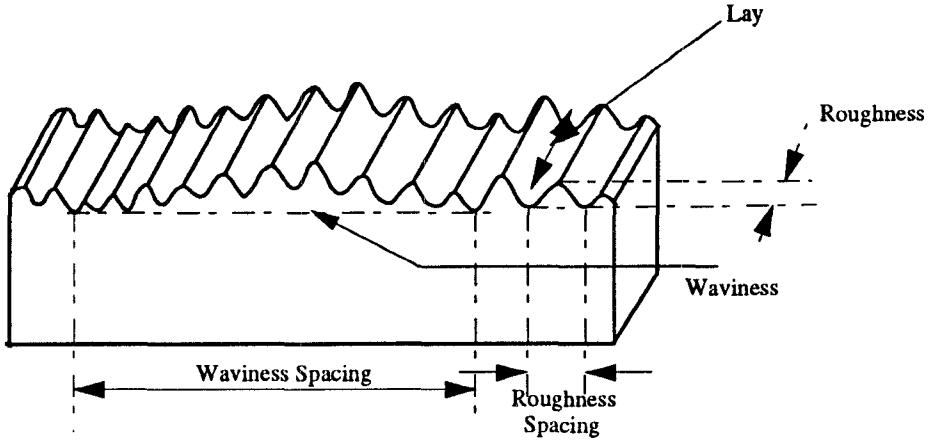

Figure 3.5: Surface characteristics

flaws on surfaces. Errors of form are long-period or noncyclic deviations in the surface profile which usually are a result of the errors in machine guideways or spindles or uneven wear in the machine. Flaws on the other hand are irregularities like cracks, pits and scratches that are discrete and occur rarely. Under ideal conditions the error of form and flaws do not occur. Hence, according to ANSI standard B46.1 only roughness and waviness are considered when a description of the surface finish is made for a machining process. Another term that is often used in the description of the surfaces is 'lay'. Lay is the term used to refer to the direction of the dominant pattern of texture of surfaces. In the case of turning of a cylindrical bar it is the circumferential direction of the bar. Figure 3.5 illustrates these terms. The set of parameters that are used for the evaluation of surfaces are referred to as the surface statistics. To completely describe the nature of surfaces produced by different manufacturing processes two types of descriptors are necessary - the surface parameters and surface statistical functions.

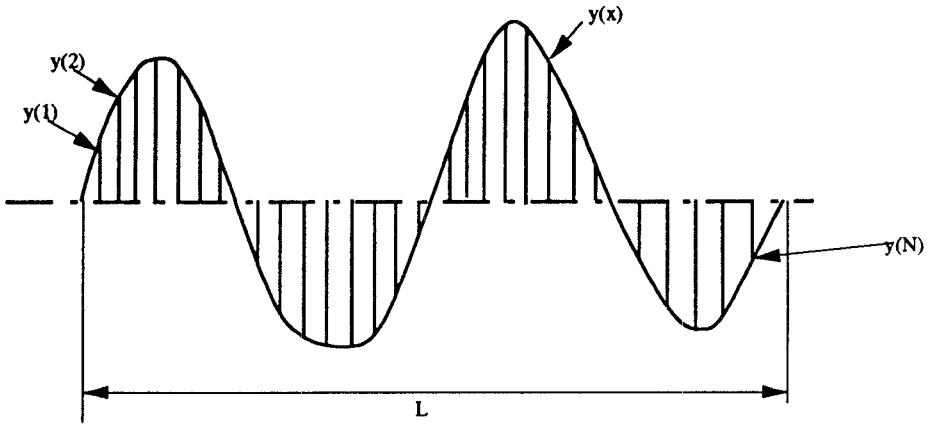

Figure 3.6: Method of calculation of (R_a) and RMS values

The surface parameters which comprise of height, wavelength and shape parameters quantify the surface statistics with a single number while surface statistical functions are functions that yield an array of information about the surface. Each of these surface parameters or functions are used for different applications. However, three important parameters evaluated for most applications are roughness average (R_a), rms roughness (R_q) and peak-to-valley. We limit our analysis of machined surfaces only with respect to these important parameters. Since the machining tests described later are conducted under controlled conditions, these parameters adequately describe the surface.

The roughness average (R_a) is the most widely used measure of surface finish. Figure 3.6 describes the method of calculation of R_a. It is given by the equation

$$R_a = \frac{1}{L}\int_0^L |y(x)|dx \tag{3.16}$$

or

$$R_a = \frac{1}{N}\sum_{i=1}^{N}|y_i| \tag{3.17}$$

where y_i is the i'th deviation from the mean line as shown in Figure 3.6.

The rms value of roughness is given by

$$R_q = [\frac{1}{L}\int_0^L y^2(x)dx]^{0.5} \tag{3.18}$$

or

$$R_q = [\frac{1}{N}\sum_{i=1}^{N} y_i^2]^{0.5} \tag{3.19}$$

3.2.2 Surface Generation and Evaluation

The surface generated in the presence of tool vibration, given the excitation model and the dynamical equations, is a function of the instantaneous location of the edge of the tool cutting edge, along the direction of vibration. The time history of the tool vibratory response, y(t), together with the geometrical shape of the tool tip, can be used effectively to generate the coordinates of the machined surface in the computer simulation. The surface generation is done on lines parallel to that of the boring machine model by Zhang and Kapoor [14]. The tool nose is assumed to be an arc of the circle with the radius being the tool nose radius. The tool moves in a spiral trajectory defined by the feed rate and the diameter of the workpiece. Also, due to the vibration of the tool, there is a movement of the tool to and away from the nominal depth of cut. These two motions are together required to generate the surface topography of the machined

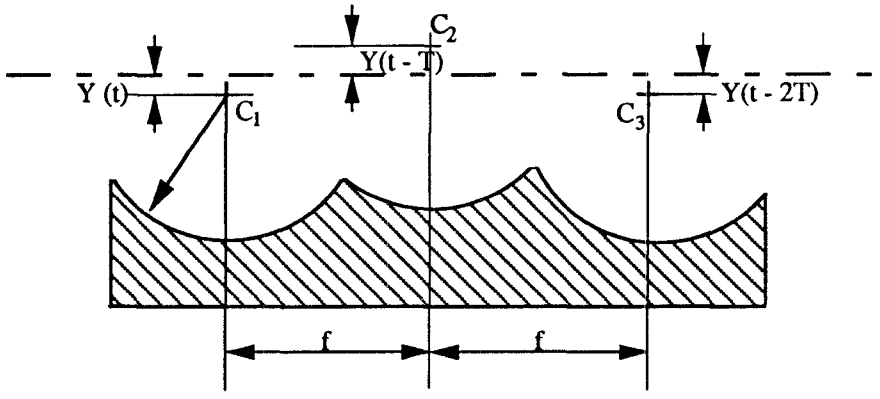

Figure 3.7: Geometrical representation of adjacent revolutions

surface.

The ideal surface generated is shown in Figure 5.14. It is necessary to keep track of the coordinates of the centers of the arcs representing the tool nose, at different instants in time. The coordinates of the set of points that describe the surface are calculated with respect to the center coordinates. The nature of the surface generated in the presence of chatter is shown in Figure 5.18. The centers of adjacent arcs described by the tool nose, taken along the same trace, in the direction of feed, are not at the same level with respect to their Z-coordinates. They are offset by a distance equal to the tool response y(t) at that instant in time. Correspondingly, the arcs are created as shown in Figure 3.7. It is necessary to find the points of intersection of two adjacent arcs in order to be able to exactly locate the peaks on the surfaces. The coordinates of the points of intersection of arcs with centers C_1 and C_2 respectively are given by the solution

to the two simultaneous equations

$$\begin{aligned}(C_{1x} - X)^2 + (C_{1z} - Z)^2 &= R^2 \\ (C_{2x} - X)^2 + (C_{2z} - Z)^2 &= R^2 \end{aligned} \tag{3.20}$$

The coordinates of the consecutive centers along the feed direction is given by, ($C_{1x} = 0.5f$, $C_{1z} = Y$) and ($C_{2x} = 1.5f$, $C_{2z} = Y(t+T)$), where 'T' is the time for one revolution of the workpiece and is given by $T = \frac{60}{N}$, 'N' being the spindle speed in r.p.m. It is important to note that the component of the response of the tool in the direction of depth of cut is the one that describes the nature of the surface. Thus the response $Y(t) = y(t)SinC_s$ as seen from Figure 3.8.

With the information of the time history of the tool response, the circumferential location of the tool nose and the points of intersection of all adjacent circles that represent the tool nose at different feeds along the surface of the workpiece is calculated. These points can then be used to create the three dimensional view of the generated surface as when opened up, so that the circumference lies along a plane. The purpose of the surface topography generation is purely for user perception of the nature of the surface. This can be easily understood by any user even without any understanding of the surface statistics.

The different surface parameters can then be calculated by the use of the equations presented earlier. Traces taken by the use of a profilometer or a Talysurf are simulated on the computer by calculating the parameters based on the coordinates of the points lying in the same direction along the feed.

The material description models together with the surface generation and

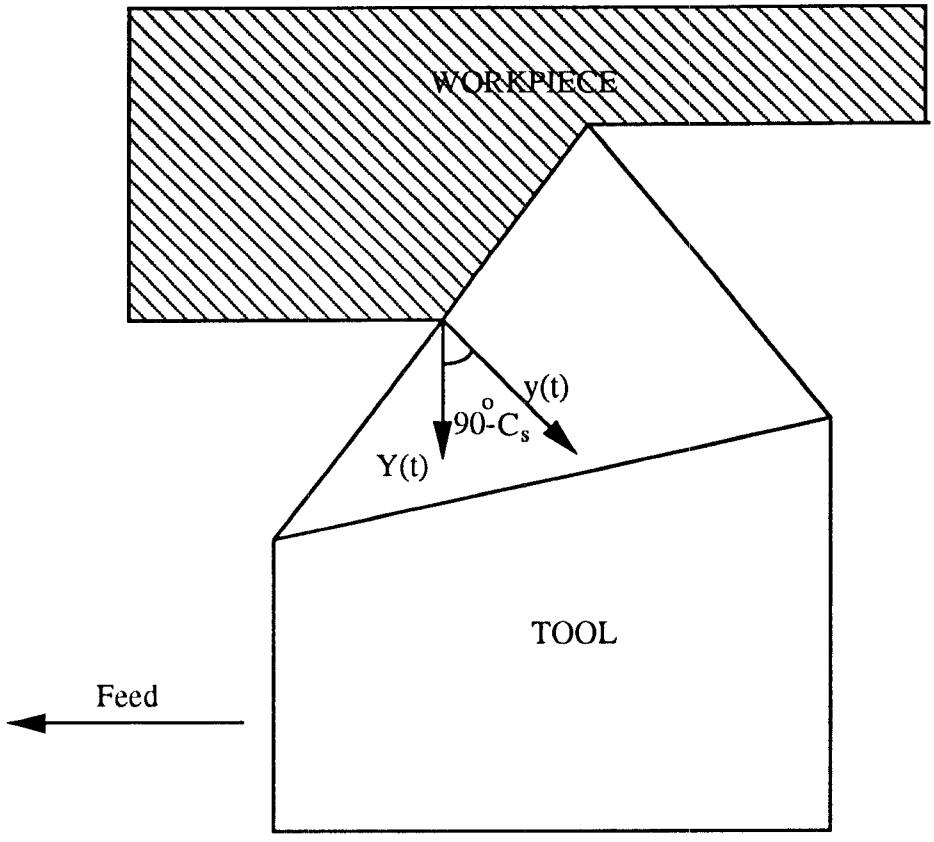

Figure 3.8: Calculation of effective tool response

evaluation models completely describe the approach taken to relate the material microstructure with the surface finish. These models have to be translated into computer jargon for the creation of a simulation package that can be used for cutting analysis. The nature of the simulation package and the working details are covered in the following chapter.

Chapter 4

Structure of Machining System Simulator

In order to test and derive meaningful results from the mathematical models developed, a systematic study needs to be done. This necessitates extensive simulation on computers for the different materials and cutting conditions. Moreover, one of the main objectives of the thesis work being carried out is to be able to use computers to simulate the machining operation under different cutting conditions, analyze material properties and hence, be able to use the simulator to select machining parameters for the best possible surface finish.

The computer simulation model is essentially built on the basis of the models described earlier in Chapter 3. The simulation package consists of three important modules. The first module is the image processing and analysis module which is capable of analyzing pictures of the microstructure and establishing the

material descriptive parameters like mean and variance of the population and distribution of the microstructure. It also forms the basis for the construction of the state transition matrices for the hidden Markov models. The second module is the tool vibratory response evaluation module. This model takes its input in the form of material descriptors, cutting conditions and other dynamical system parameters to arrive at the response of the tool for different excitations from the workpiece material. The output of this module is used by the third module which is the surface topography generation and surface evaluation module. This model evaluates the cutting performance under given conditions and offers quantitative measures for the system performance. It also has the capability of displaying the nature of the surface obtained graphically, to augment surface parameters as a means of evaluation of the machined surface, for the user. A comprehensive description of the three modules is presented later in the chapter.

The computer programs used for the simulation are created with the execution time in perspective. The main body of the simulation is coded in C-language. However, the popularly available math package "MATLAB" has been widely used too, for many math calculations and as a means of graphical display. Some other subroutines for some other mathematics have been invoked from IMSL, another popular math library. The alternative C-routines have also been included so as to make the simulator minimally dependent on software availability and thus portable. A comprehensive flow chart for the simulation is presented in Figure 4.1.

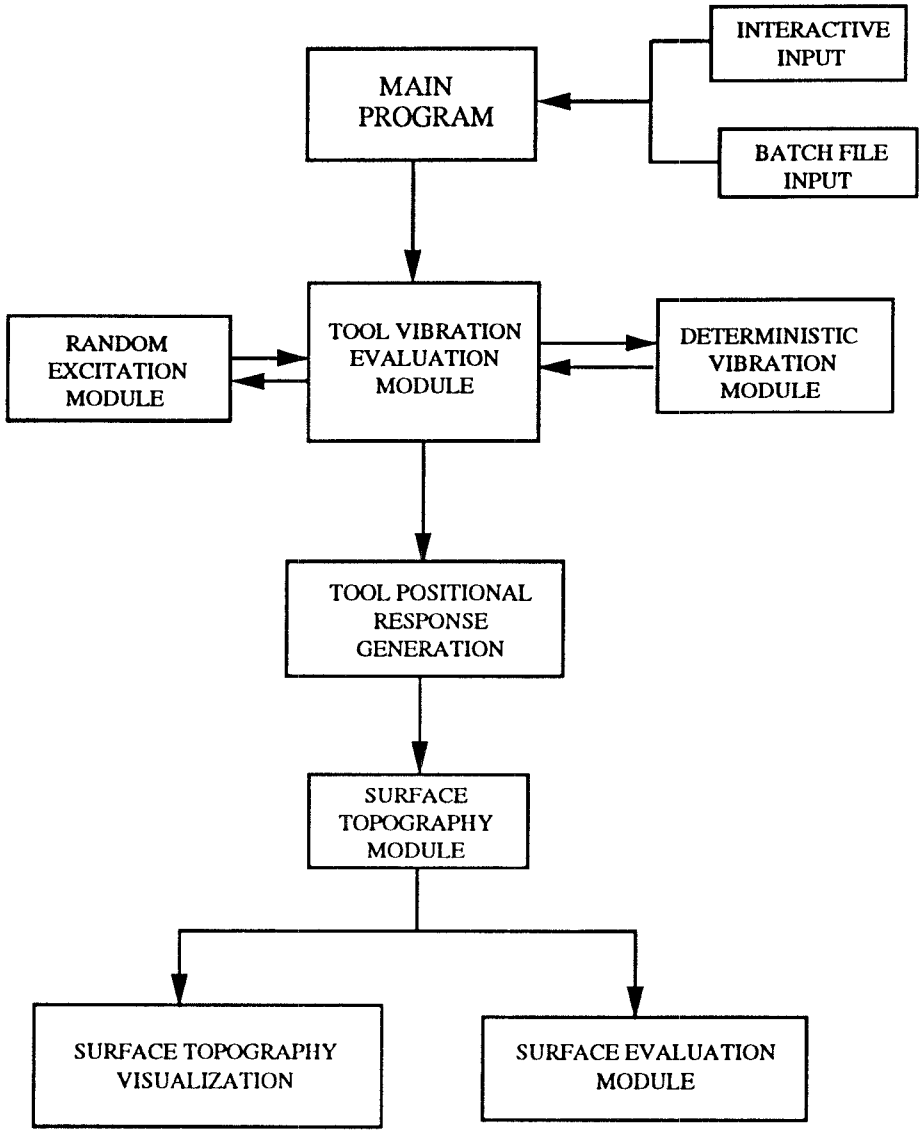

Figure 4.1: Flow chart for the computer simulation

4.1 Material Analysis Module

The microstructure of the material in analyzed with the help of pictures taken from the microscope. These images are scanned and digitized. The digitized images are then stored in the form of binary files in the computer. This is the only process in the simulation wherein the analysis cannot be made on-line. However, since the microstructure for a particular grade of the material manufactured under identical conditions is similar, these pictures taken from different sections of the material are representative of the whole material. The binary image files are then read by the image analysis programs to arrive at the mean and variance of the population. The sample variance calculation is then made based on these images and the models described in Chapter 2. The program then analyses the pictures of the material in the longitudinal direction to detect any existing trends. If such trends are present then the appropriate Markov model can be applied for the calculation of the different states and the state transition matrices. The output of this module then forms the input to the second module - the tool vibratory response evaluation module.

4.2 Tool Vibratory Response Evaluation Module

This module simulates the actual cutting process. The input to the module is in the form of cutting conditions, material descriptors and various system parameters. The model generates random numbers for the instantaneous material sample mean hardness based on the material description model chosen. The individual responses of the tool for the different excitations are calculated. The resultant response of the tool is obtained by the principle of superposition, since the system is linear. The tool response is in the form of the deviation from the ideal position (equilibrium or stable position). It is this deviation that is fed into the surface topography generation module for analysis of the generated surface. The tool vibratory response is calculated based on the dynamical system model described in Chapter 3. The three components of the cutting force - the nominal chip load, the regenerative chip load and the random excitation are all incorporated into the machining system model. Since the tool response is also based on the random excitation, the material analysis module communicates its output to the tool vibratory response module. Figure 4.2 is a combined flow chart for the tool vibratory response module and the material module.

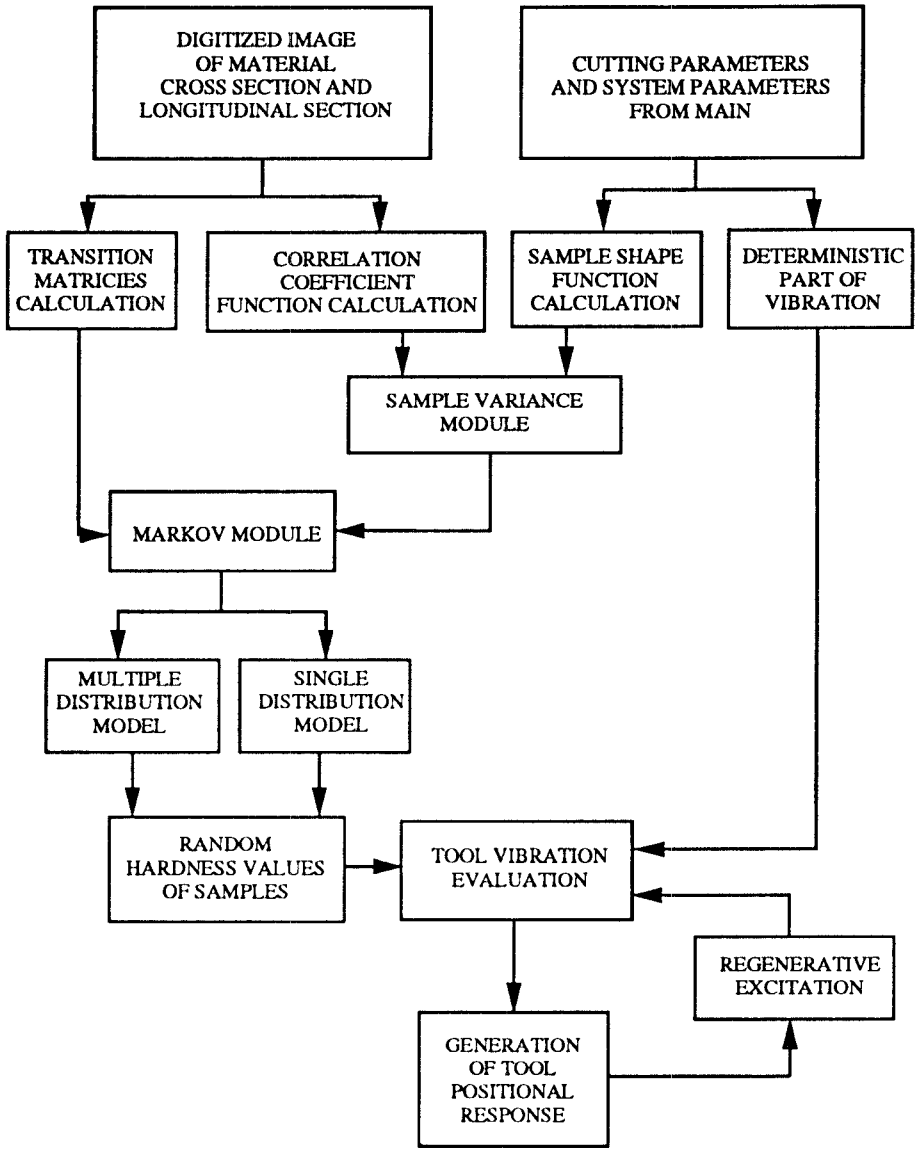

Figure 4.2: Flow chart for the tool vibration and material models

4.3 Surface Evaluation Module

This forms the most important module for the user as it is this model that communicates the nature of the machined surface to the user. One of the main objectives of the thesis is to be able to evaluate the machined surface based on the different cutting conditions and to use these results in the improvement of the machining process. Thus this model tries to evaluate the surface by the calculation of the different surface parameters and simultaneously generates a three dimensional view of the generated surface. The surface topography is done by the calculation of the different points that describe the surface with the knowledge of the tool's instantaneous location and the tool nose geometry. The graphics abilities of MATLAB are used here to display the surface. The surface parameters are the actual quantities used for the comparison of the different surfaces generated in this thesis, while the plots of the surfaces have been used for a visual perception of the nature of the surface and also to detect any possible flaws or irregularities that cannot be detected or directly described by the surface parameters. If any such deviations or flaws are detected then they can be easily noticed and any corrective measures can be immediately taken.

Chapter 5

Results and Discussion

This chapter presents the results of the detailed analyses done to validate the theoretical issues addressed in this thesis. The results of work done in order to analyze the nature of the material are presented in the first section. The second section presents results obtained from the simulator, to explain the importance of a few concepts that are critical to the material description model. The third section presents the results obtained from the simulator for the machining operation and compares them with those obtained from actual cutting tests. A detailed analysis of the nature of the cutting force variation during machining process is also presented.

5.1 Analysis of Material Microstructure

5.1.1 Imaging process of Material Microstructure

The nature of the random vibration that occurs during the machining process is dependent on the microstructural distribution and the microstructural hardness. The materials that formed the subjects of the study were chosen based on the variety of their microstructure. These materials chosen were in the form of rolled bars, as this is one of the popularly used forms of material on lathes. A number of cross sections of the bar were taken from different locations on the bar. They were cut into small pieces and mounted on specimen holders by the use of epoxy resins. These materials were then ground and polished to yield a perfectly flat surface. Figure 5.1 shows the polished specimens mounted on to plastic rings. These surfaces were then etched to remove the outer deformed layers that result from the grinding and polishing operations. This reveals the microstructure of the material. The sections were viewed under a microscope with a magnification of approximately 100X - 200X. The nature of the microstructure needs to be analyzed by the computer image analysis program to quantify the distribution in the form of a correlation coefficient function for the material. Hence these pictures were then digitized and fed as binary input files to the simulation. In order to get reliable values for the correlation coefficient function and to be assured of the consistency in the microstructural distribution, a number of such sections were analyzed from different regions of the bar. The analysis

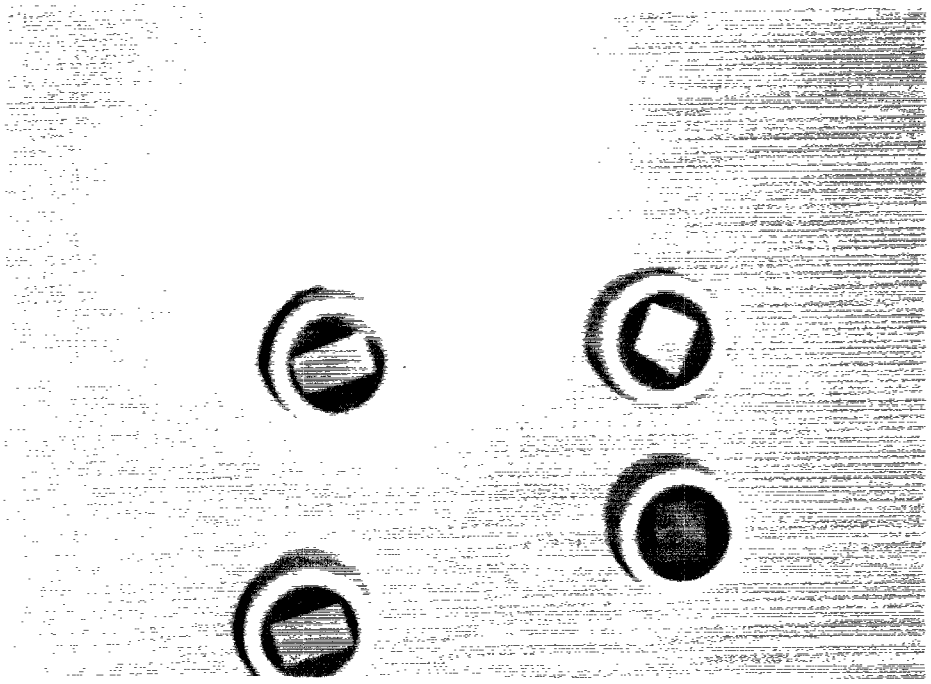

Figure 5.1: Material samples mounted on rings for microscopic analysis

also included a study of the sections in the longitudinal (rolled) direction, to identify the existence of any trends or consistent pattern. If such patterns exist then then they form the input to the Markov models, so that the description of the material microstructure is very close to the existing patterns.

5.1.2 Test for Microhardness

Another important part of the material microstructure study is the identification of the hardness of the microconstituents of the material. The description of the material variation, by itself, is worthless, if the hardness values of the microstructure is not identified. Thus, hardness tests were performed by the use of Vicker's microhardness tester.

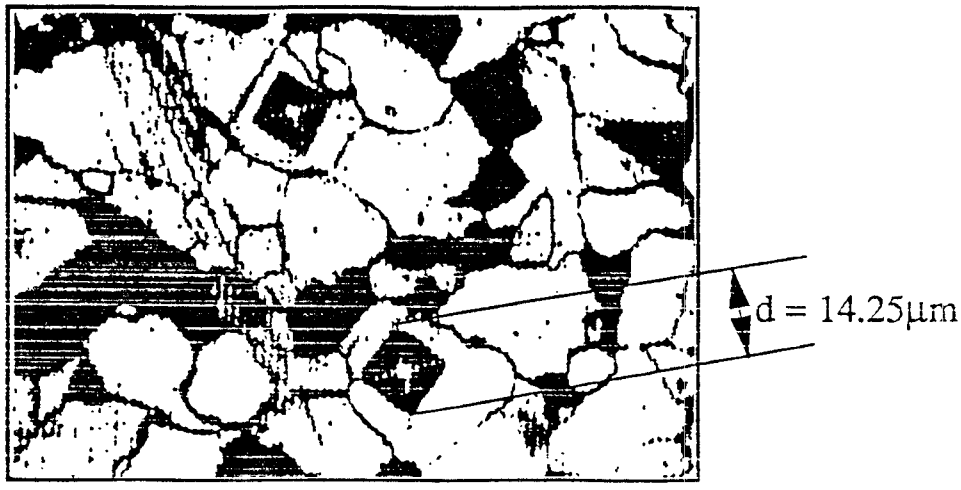

Figure 5.2: Indentation on microstructure from microhardness tester

The Vicker's hardness tester consists of a 136° diamond pyramid that is used to make the indentations on material. The hardness tester has facilities to view the microstructure and make indentations on only certain chosen grains. A very small load, which in the case of the steels was 10 grams, was used to make the indentations. The low load facilitates the making of indentations only on a local microconstituent, while not covering the other neighboring microconstituents. A picture of one such indentation is shown in Figure 5.2.

The length of the diagonals of the indentation made together with the load applied can be used to measure the material hardness by the use of the equation

$$HardnessVicker's = \frac{1.8544P}{d^2} \tag{5.1}$$

where P is the applied load in kilograms and d is the mean value of the diagonal of indentation in mm. A load of 10g was used for the microhardness tests. Since Brinell's hardness number (BHN) is used in this thesis, the Vicker's hardness number was converted to BHN using standard tables. Table 5.1 shows the hard-

Material	Phase	Mean Diagonal of Indentation (μm)	Hardness	
			HV	BHN
Steel (1018)	Ferrite	14.25	91.3	87
	Pearlite	10.5	168.2	161
Steel (4340)	Ferrite	13.5	101.75	96
	Pearlite	8.5	256.66	243
Aluminum		13.75	98	94

Table 5.1: Hardness values obtained from tests

ness values for the different phases obtained for the materials analyzed in this thesis.

The nature of the material microstructure distribution, its microhardness values together with the cutting condition, yield a value of sample variance for the material as described in Chapter 2.

5.2 Sample Variance Analyses

The following section presents results obtained from the simulator that address the nature of the variation in the sample variance as a function of different conditions in the machining operation. Although these results are not directly related to the surface finish obtained, they form the basis of the material description model, and hence have a very strong bearing on the nature of the excitation to the cutting tool.

5.2.1 Effect of Material Microstructure Distribution

An important area of focus of this research is the study of the effect of the different material microstructure on the tool random vibration. Hence, three different materials were used for the cutting tests. They are 6061 aluminum, 1018 low carbon steel and 4340 alloy steel. These materials were chosen as they exhibit different microstructures and are also commonly used on the shop floor. Figure 5.3 shows the digitized image of the cross section of these three materials. As can be seen from the figures, these three materials exhibit distinct microstructures. The correlation coefficient functions for two of these these three materials are also presented in Figure 5.4. The correlation coefficient function for aluminum is not presented as the microstructure is very much uniform. It is seen that 4340 steel has a higher value for the correlation coefficient function at low values of 'r'.

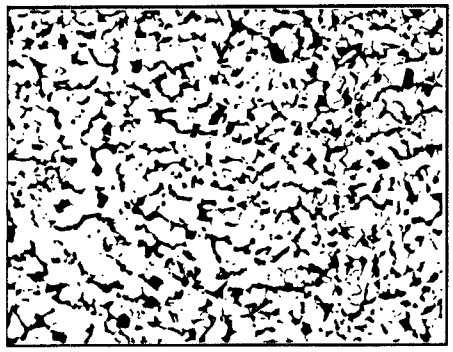

a) Cross-section of 1018 Carbon Steel

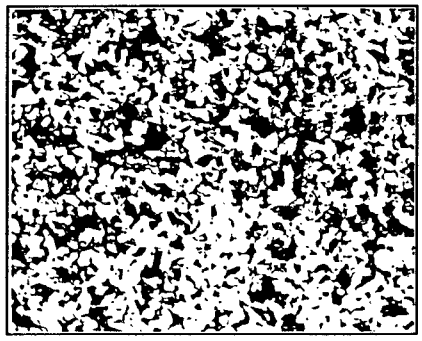

b) Cross-section of 4340 Alloy Steel

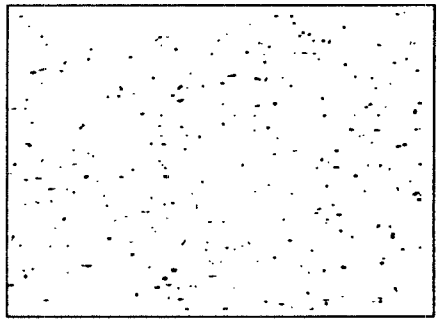

c) Cross-section of Aluminum

Figure 5.3: Microstructure of the three different materials analyzed

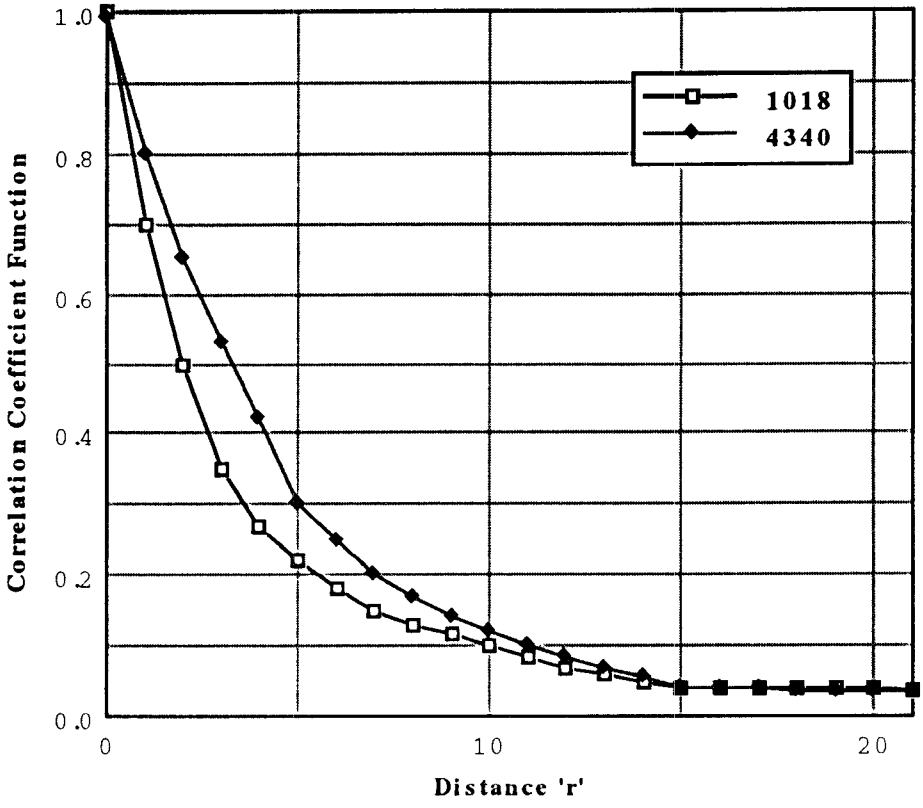

Figure 5.4: Correlation coefficient function for the steel samples

For any particular cutting conditions, these three materials exhibit three different sample variance. In fact, the aluminum sample should not actually have any sample variance associated with it, as it is homogeneous in its microconstituents. However, due to the presence of impurities and other extraneous conditions there are very small regions that make the microstructure discontinuous. Hence, it yields a very small value for the sample variance which can be neglected. The hardness of the microstructure varies for each of these samples and hence the sample variances need to be compared between materials with this in perspective. Since the cutting conditions for each of these tests are the same, they all have the same sample shape functions. Hence, the sample variance is a function of the population variance (σ_a^2) and the correlation coefficient functions only. The population variance is the dominant term of these two. It is important, here, to reiterate the physical significance of the Equation 2.14 which implies that the sample variance is a fraction of its population variance, with the fraction being determined by the size and distribution of the microstructure. By looking at the sample variance values obtained for the three different materials, it is evident that for the same cutting condition different materials exhibit different sample variances. The sample was found to have a higher value of its population variance. Hence, although the 4340 steel samples have a higher correlation coefficient function, it is seen that for all cutting conditions, the low carbon 1018 steel has the highest values of the sample variance. Aluminum does not yield any sample variance as the material is uniform in its microstructure. Consequently,

the random vibration is maximum in the 1018 steel, as is evident in the surface finish values obtained, which is presented later in the chapter.

5.2.2 Effect of Cutting Parameters

The most significant use of this model is in its capacity to predict random vibration for any set of cutting parameters. The different cutting parameters result in different sample shapes. The nature of the sample shape affects the nature of the sample shape function and hence yield different sample variances. In order to minimize the number of such analyses, the concept of three level factorial design has been adopted in this work for studying the effect of different parameters on the surface finish. A brief description of this tool in experimental design is presented in the appendix. The three most important parameters that are almost always the most common variables in a cutting process - the cutting speed, feed and the depth of cut have been used as the parameters of the factorial design. The eight set of parameters that have been used here are shown in Figure 5.5, which is a graphical representation of the factorial design.

Figures 5.6 , 5.7 and 5.8 illustrate the effects of changes in cutting conditions on the sample shape function. The values for the different cutting conditions chosen are some common practical values used on the shop floor. The figures indicate that the feed has the most significant effect on the sample shape function. This is because the feed is almost always the smallest of the three dimensions that describe the sample. Hence an increase in feed has the greatest impact in

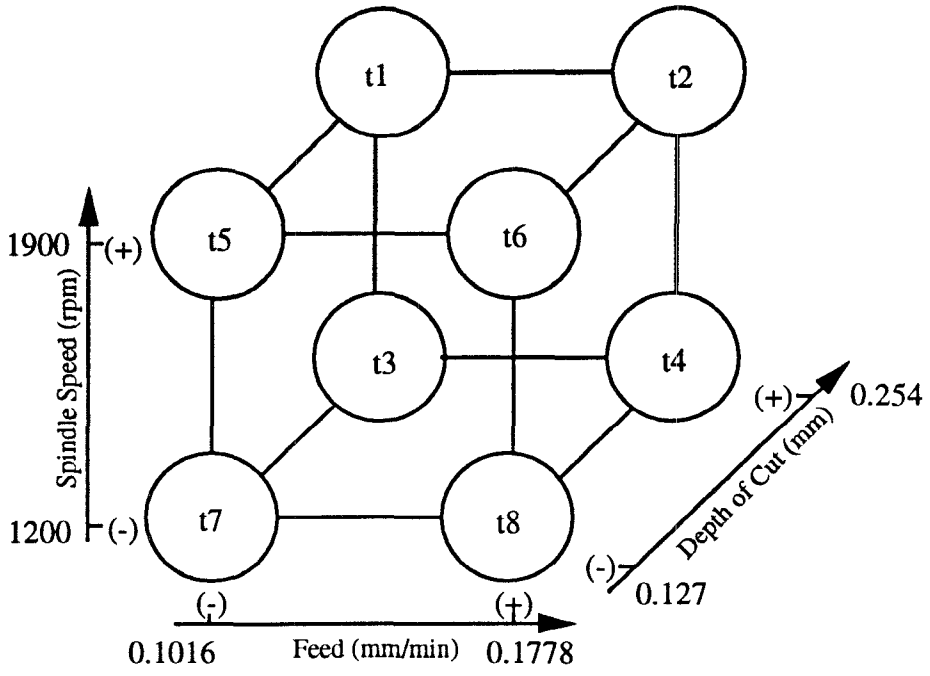

Figure 5.5: Graphical representation of factorial design

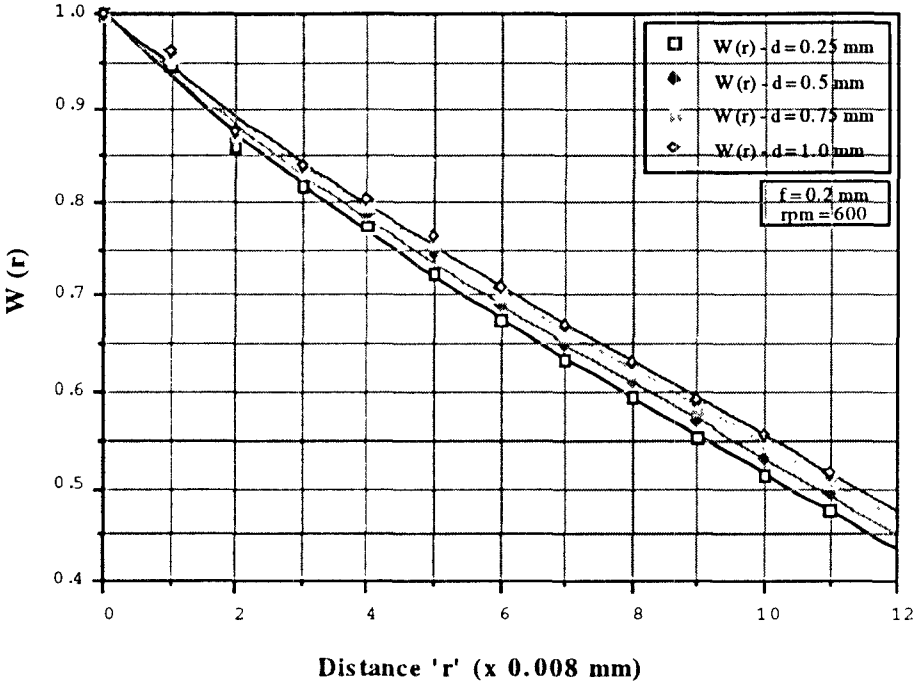

Figure 5.6: Sample shape functions for different depths of cut

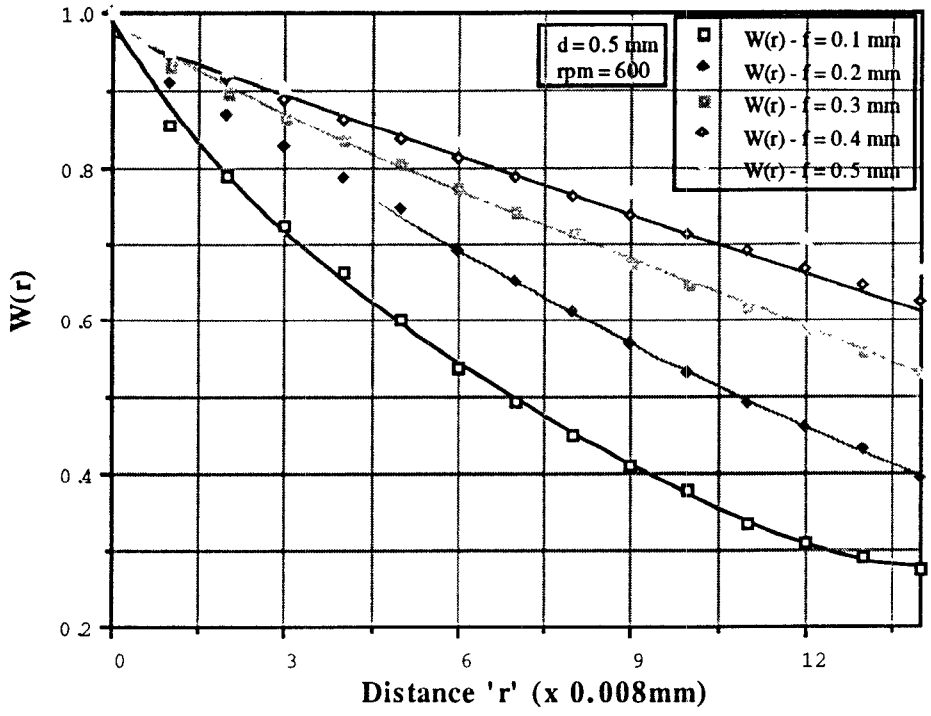

Figure 5.7: Sample shape functions for different feeds

increasing the volume of the sample lying in the shell of a much larger radius, as described in Chapter 2.

The practical significance of this observation is better understood when the effect of the variation of the sample shape function is observed on the sample variance. The sample variance values are a function of the population variance, the correlation coefficient function, the sample volume and the sample shape function. For a given material, the correlation coefficient function and the population variance are constant. An increase in any of the cutting conditions increases the sample volume and the sample shape function. The increase in volume is much larger than that of the increase in the sample shape function. Hence, the sample variance decreases. However, the decrease in sample variance for a change in feed

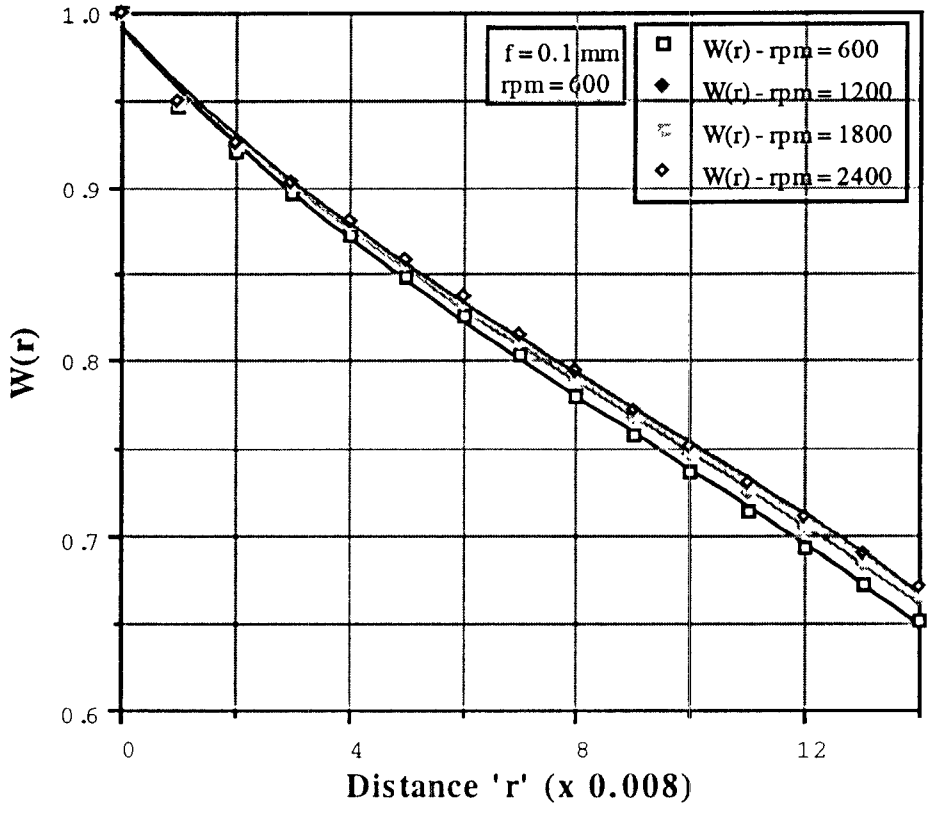

Figure 5.8: Sample shape functions for different spindle speeds

is the lowest, as the increase in the sample shape function is the greatest. This implies that for low feeds, the sample variance remains rather high and hence causes a high degree of random vibration.

The sample variance values for the cutting conditions investigated are shown in Figure 5.9. A pseudo-empirical model was developed based on the concepts of factorial design. It is presented in Equations 5.2 and 5.3.

For 4340 steel:

$$\begin{aligned} \sigma_s^2 &= 12.8313 - 2.1688x_1 - 3.2863x_2 - 2.6713x_3 + 0.7638x_1x_2 \\ &\quad +0.7013x_2x_3 + 0.7838x_1x_3 - 0.1238x_1x_2x_3 \end{aligned} \tag{5.2}$$

For 1018 steel:

$$\begin{aligned} \sigma_s^2 &= 20.77 - 3.2525x_1 - 5.44x_2 - 3.9x_3 + 0.7725x_1x_2 \\ &\quad +0.875x_2x_3 + 0.4425x_1x_3 - 0.0475x_1x_2x_3 \end{aligned} \tag{5.3}$$

where x_1,x_2 and x_3 represent the levels of feed, depth of cut and spindle speed chosen, respectively. They have values of -1 or $+1$ for the lower and higher levels of the cutting conditions respectively. The model is in agreement with the earlier discussion on the effects of cutting conditions on sample variance. It can be noticed that the role of random vibration is maximum for the condition where all these three cutting conditions are the lowest. The proof for this claim is presented in the form of a comparison of the surface indices for these materials machined under identical conditions, later in the chapter.

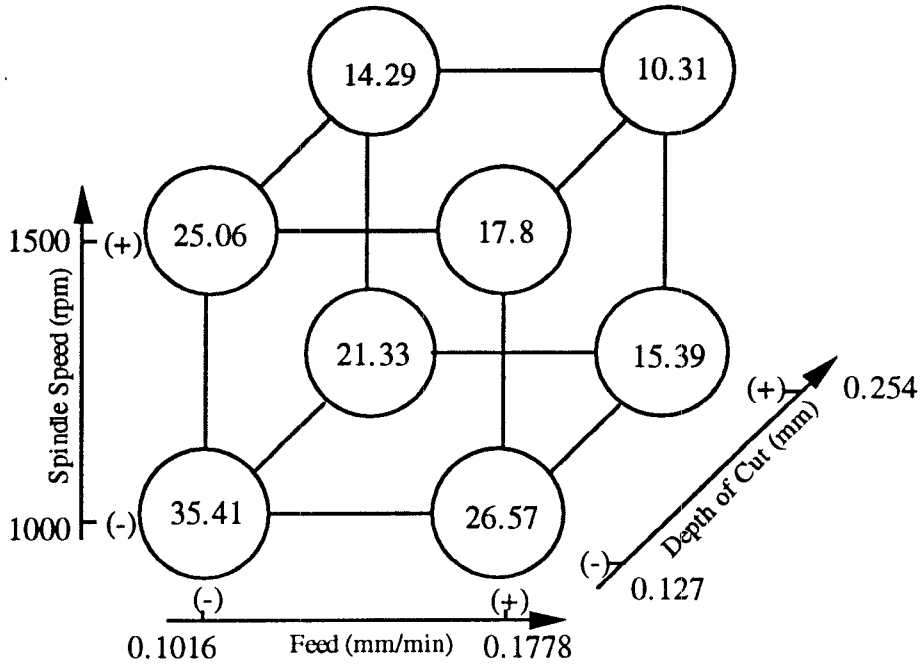

a) 1018 Carbon Steel

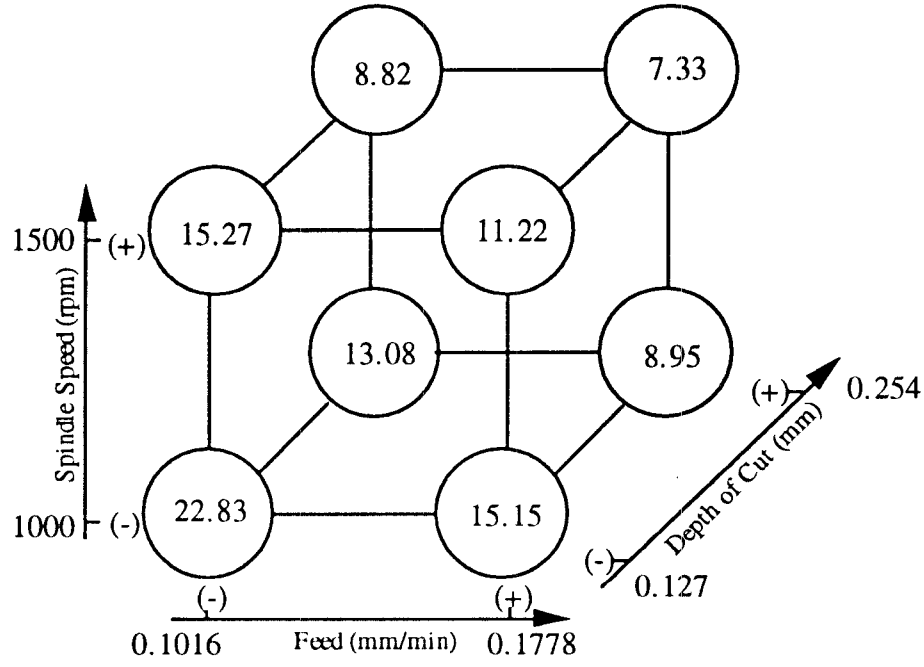

b) 4340 Alloy Steel Steel

Figure 5.9: Sample variance values for steel specimens

5.2.3 Effect of Magnification Factor

In order to derive meaningful results from any image analysis model, the model needs to be immune to the value of the magnification factor chosen. An analysis was, therefore, performed on a 1018 steel sample. A variation in the magnification factor only affects the correlation coefficient function. The correlation coefficient function obtained at three different magnification factors is presented in Figure 5.10. All the three magnification factors used yielded the same sample variance, for a given set of cutting conditions. Use of a larger factor yields larger correlation coefficient functions and sample shape functions, which is inversely proportional to the decrease in the pixel dimensional value. Consequently, Equation 2.14 averages out these variations to yield a constant value for the sample variance.

5.3 State Transition Matrix

The state transition matrices for the material were calculated as explained in Chapter 2. The matrix has to be calculated dynamically for each cutting condition as the sample size is a function of the cutting conditions. One such matrix calculated for the cutting condition-1 for 1018 steel is presented in Table 5.2.

The hidden Markov model has, in addition to the above state transition matrix, another state transition matrix for the assignment of distributions between revolutions, associated with it. The transition matrix obtained for the distribution for 1018 steel is presented in Table 5.3.

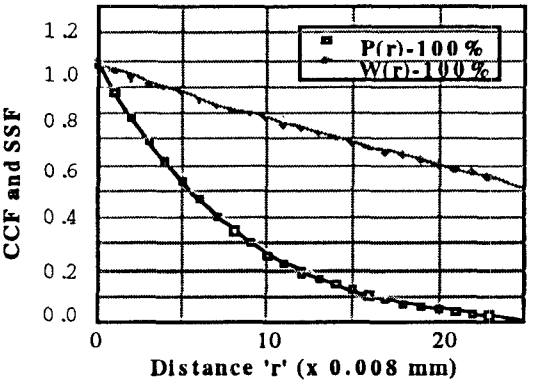

a) CCF and SSF plots for 100% Magnification

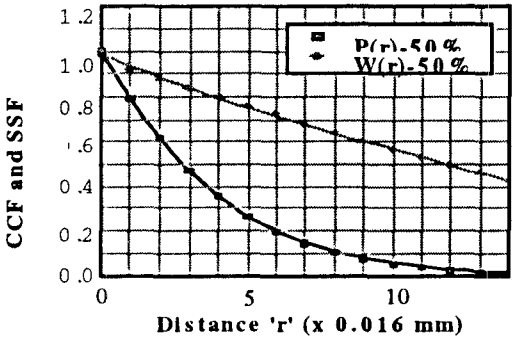

b) CCF and SSF plots for 50% Magnification

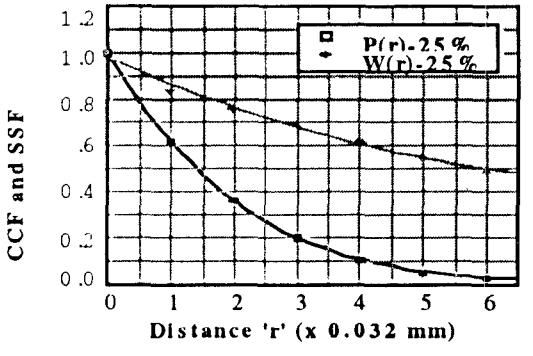

c) CCF and SSF plots for 25% Magnification

Figure 5.10: C.C.F for different magnification factors

	State		
	1	2	3
1	0.2828	0.6495	0.0677
2	0.1240	0.7209	0.1551
3	0.0556	0.6608	0.2836

Table 5.2: State transition matrix for cutting condition - 1

	Distribution			
	1	2	3	4
1	0.353	0.425	0.2	0.022
2	0.184	0.612	0.124	0.08
3	0.05	0.41	0.31	0.23
4	0	0.13	0.42	0.45

Table 5.3: State transition matrix for assignment of distribution

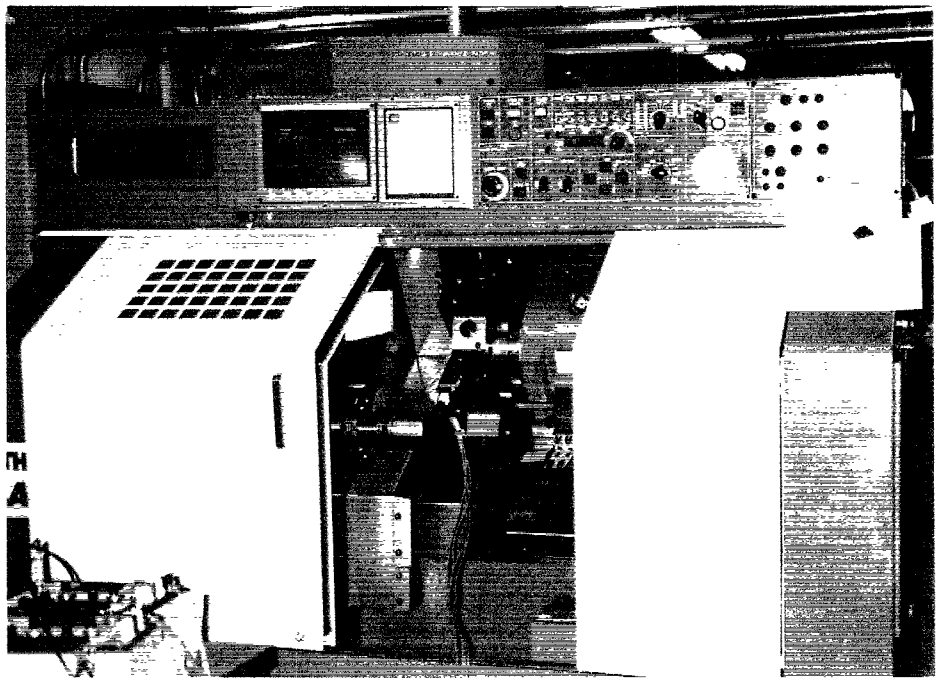

Figure 5.11: Experimental setup for cutting tests

5.4 Results from Cutting Tests

The validity and soundness of the models used can only be proved by the use of actual cutting data and information on surface characteristics. Hence a number of tests were performed on different materials having different microstructures. The three different materials chosen for the microstructural study were the ones used for the cutting tests. The cutting parameters used were also the same as those used in the computer simulations.

A Methods Slant Junior CNC lathe was used to perform the experiments. Figure 5.11 illustrates the set-up used for the cutting tests. The computer control on the lathe and the high accuracy reduces a lot of noise that can otherwise be

significantly present in an experiment. Some other factors that very often affect the surface finish in machining like tool wear and built-up-edge were to a large extent avoided in these experiments. Tool wear was not really a problem as a new insert was used for each of the tests. The short duration of the tests cannot cause any significant tool wear that can affect surface finish.

Built-up edge is a phenomenon that often affects the surface finish of machined parts. The adhesion of the material removed onto the rake face during machining is called as built up edge. It is subsequently removed from the tool abruptly when it reaches a large volume. This usually occurs during low cutting speeds. When the cutting speeds are high, the temperature in the interface between the tool rake face and the chip is also high and so the material removed is very plastic. Hence, this phenomenon does not occur. In order to avoid the effects of built up edge, high cutting speeds were used. The results obtained from the experiments, therefore, reflect almost only the true effects of the three cutting conditions chosen.

The simulator was used to simulate the machining operation under the different cutting conditions described in the factorial design. The effects of these parameters were then evaluated in terms of the tool vibration, nature of cutting forces generated and the surface generated. These results have to be compared with some experimental results before the model can be put to practical use.

The turning process has been simulated with each of these sets of cutting parameters on a particular material and the surfaces generated evaluated. The

different statistical models described in Chapter 2 have all been tested on the same set of conditions, to compare the performance of the models.

The material descriptive values obtained for the different cutting conditions shown in the factorial design model (Figure 5.6) were used as inputs to the random excitation models for all the three materials. The Roughness Average (R_a) values so obtained are compared with the experimental values. The measurement of the surface parameters for the machined surface was performed at National Institute for Standards and Technology. A Talysurf complete with a data acquisition system was used to take traces and obtain these surface parameters. An optical profilometer was also used for the measurement of some of the surfaces. Figure 5.12 is a picture of the Talysurf arrangement and Figure 5.13 shows the optical profilometer used. The traces obtained from the profilometers for 4340 steel are presented in Figure 5.14. The experimental Roughness Average (R_a) values are presented in Figure 5.15.

An empirical model was derived from the experimental data for each of the three materials machined. The models so formulated are presented here, after excluding insignificant factors based on the levels of standard error obtained from repetitive traces.

For aluminum:

$$\begin{aligned} R_a &= 0.9225 + 0.33x_1 - 0.03x_2 - 0.02x_3 \\ &\quad +0.11x_1x_2 + 0.02x_2x_3 \end{aligned} \tag{5.4}$$

Figure 5.12: Talysurf used for surface measurements

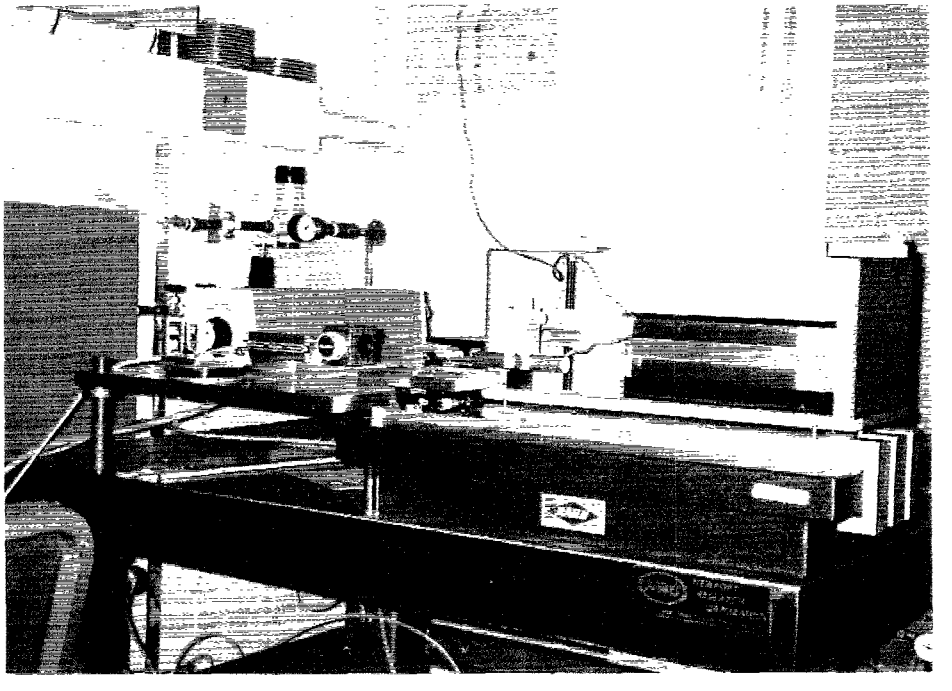

Figure 5.13: Optical profilometer used for two-dimensional traces

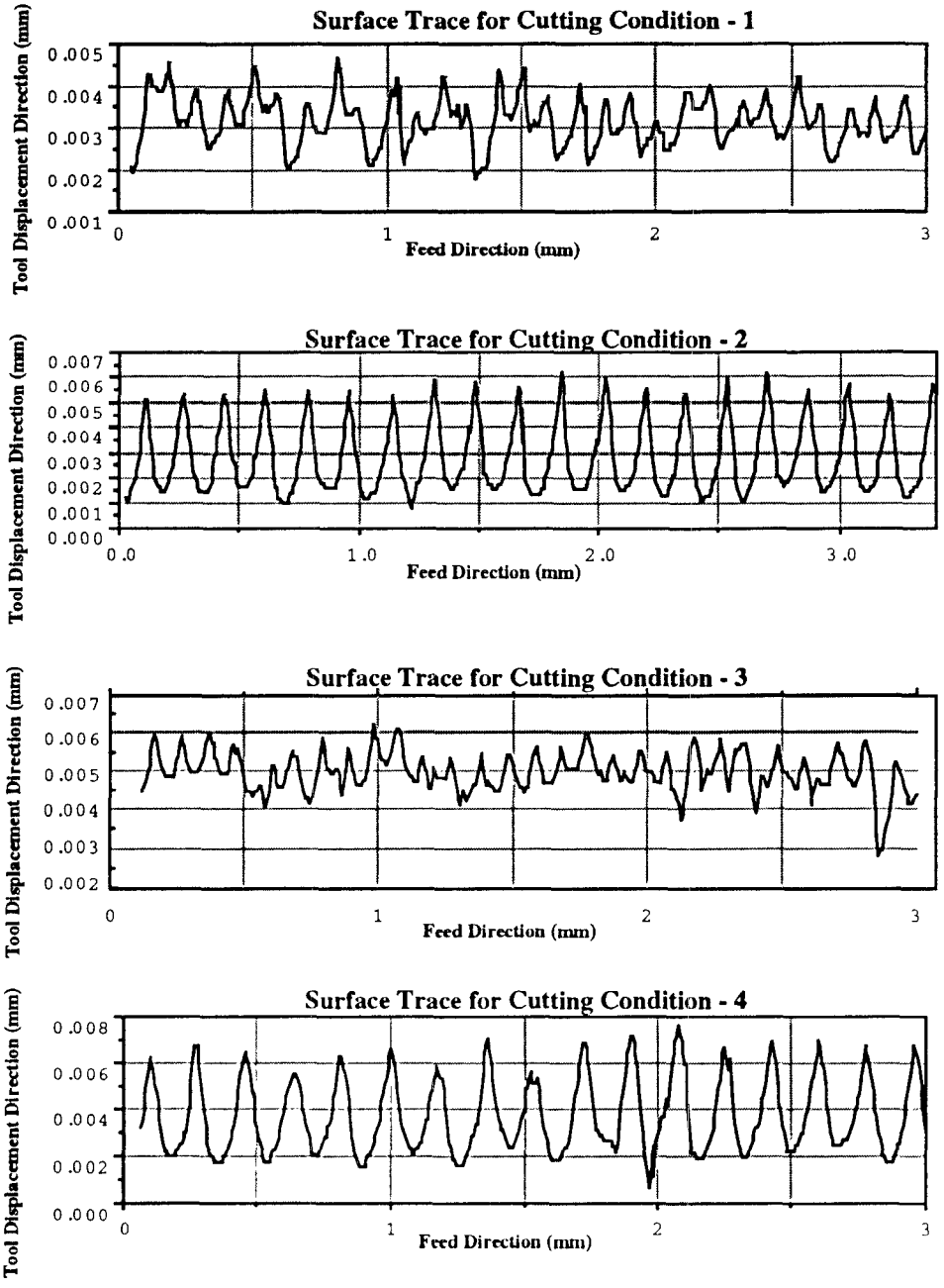

Figure 5.14: Traces obtained from optical profilometer

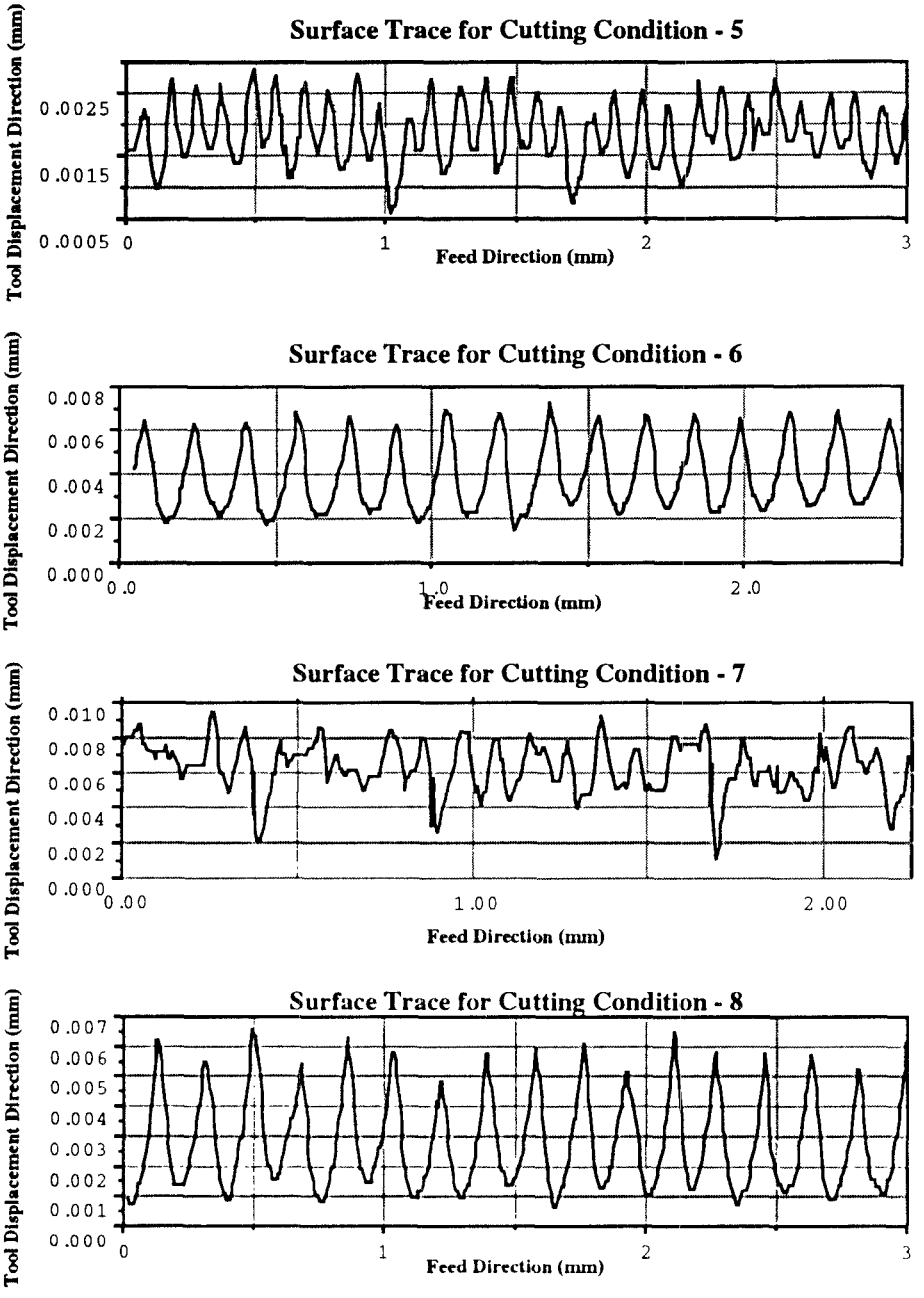

Figure 5.14 (cont'd): Traces obtained from optical profilometer

For 1018 steel:

$$R_a = 1.44875 + 0.4338x_1 - 0.0313x_2 + 0.02125x_3$$

For 4340 steel:

$$\begin{aligned} R_a &= 1.0825 + 0.2925x_1 - 0.08x_2 + 0.085x_1x_2 \\ &\quad +0.1275x_2x_3 + 0.17x_1x_3 - 0.1275x_1x_2x_3 \end{aligned} \tag{5.5}$$

where x_1,x_2 and x_3 represent the levels of feed, depth of cut and spindle speed chosen, respectively.

It is evident from the empirical models that an increase in the feed increases the R_a value. This trend is in agreement with the Equation 5.7 for the ideal R_a value obtained from the geometric motion of the tool [3].

$$R_a = \frac{32f^2}{R}\mu m, \tag{5.6}$$

where 'f' is the feed in mm/rev and 'R', the tool nose radius in mm. However, the effect of feed on the surface roughness is not completely accounted for by the geometric motion. As the feed decreases, the value of the sample variance increases, as explained earlier. Hence, the random vibration increases and so does the roughness average. But this increase in R_a value is overcome by a much larger decrease in R_a, due to the geometric motion of the tool. Hence, the coefficient for the feed is positive. It is important to note that the effect of material microstructure on tool vibration is more pronounced for lower feeds.

Increase in depth of cut or spindle speed decreases the sample variance, as shown earlier in Figures 5.6, 5.7 and 5.9. Hence, the random vibration and

consequently the R_a value decreases. The empirical model for 4340 steel is in agreement with this hypothesis as it shows significant negative coefficients for these two cutting conditions. The model shows high interactions. However, in the case of 1018 steel, the effect of increased spindle speed is in increasing the R_a value, although marginally. The explanation offered by the material microstructure models is not complete. Since the coefficient is very low, it is not in complete violation of the models. The effect of depth of cut is in agreement with the excitation model used.

Tables 5.4, 5.5 and 5.6 show the comparison of the experimental and simulated values for the three different materials analyzed. A pseudo-empirical model is developed for the simulated R_a values and is presented here. For aluminum:

$$\begin{aligned} R_a &= 0.8563 + 0.4013x_1 + 0.0038x_2 + 0.00375x_3 + 0.00875x_1x_2 \\ &\quad -0.00375x_2x_3 - 0.00125x_1x_3 + 0.01125x_1x_2x_3 \end{aligned} \tag{5.8}$$

For 1018 steel:

$$\begin{aligned} R_a &= 1.455 + 0.39x_1 - 0.0625x_2 - 0.05x_3 + 0.0125x_1x_2 \\ &\quad +0.0075x_2x_3 + 0x_1x_3 + 0.0375x_1x_2x_3 \end{aligned} \tag{5.9}$$

For 4340 steel:

$$\begin{aligned} R_a &= 1.0025 - 0.425x_1 - 0.0425x_2 - 0.03x_3 - 0.005x_1x_2 \\ &\quad +0.01x_2x_3 - 0.0075x_1x_3 + 0.0075x_1x_2x_3 \end{aligned} \tag{5.10}$$

where x_1,x_2 and x_3 represent the levels of feed, depth of cut and spindle speed chosen, respectively. The results obtained from the simulator are in reasonable

Test Number	Measured Ra	Simulated Ra Values
t1	0.46	0.45
t2	1.32	1.26
t3	0.44	0.47
t4	1.34	1.28
t5	0.71	0.46
t6	1.12	1.29
t7	0.76	0.46
t8	1.23	1.26

Table 5.4: Comparison of experimental and simulated Ra values for aluminum

agreement for the steel specimens. The high R_a value obtained for cutting condition 7 for 4340 steel, however, is beyond the prediction from the simulator. The values obtained from simulation show similar trends in the surface finish obtained experimentally, with the variation in cutting conditions. The model for aluminum, which does not exhibit random vibration because of its microstructure, shows considerable deviation from the experimental values, especially at lower depths of cut. In order to interpret this phenomenon typical to aluminum, further work needs to be done to completely understand the workpiece material behavior during machining.

The dynamic system constants used in this thesis are estimates based on the

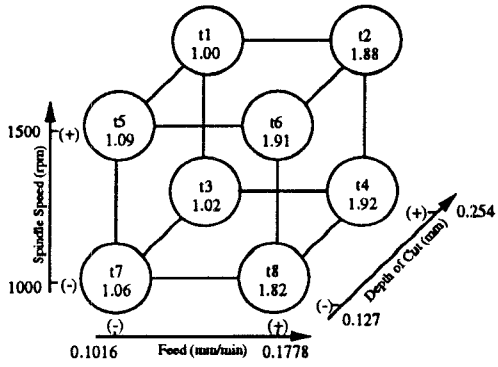

Experimental Ra values for 1018 alloy steel

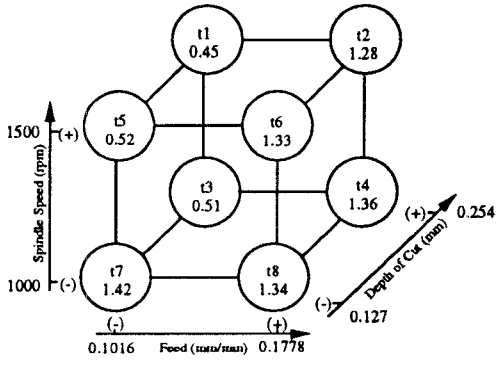

Experimental Ra values for 4340 alloy steel

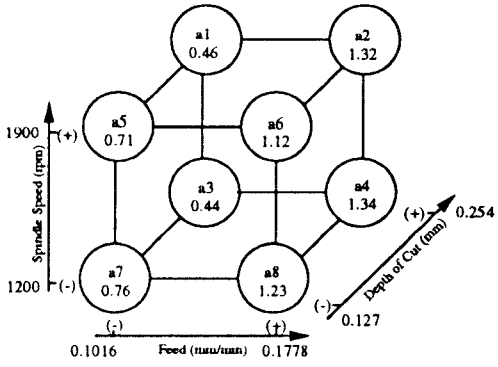

Experimental Ra values for aluminum

Figure 5.15: Experimental surface roughness (Ra) values

Test Number	Measured Ra	Ra from SV model
t1	0.45	0.52
t2	1.28	1.36
t3	0.51	0.56
t4	1.36	1.4
t5	0.52	0.59
t6	1.33	1.42
t7	1.42	0.64
t8	1.34	1.53

Table 5.5: Comparison of experimental and simulated Ra values for 4340 steel

Test Number	Measured Ra	Ra Value from SV model	Ra Value from Markov model (Single Dist.)	Ra Value from Markov model (Multiple Dist.)
t1	1.00	0.75	1.12	0.91
t2	1.88	1.48	1.93	1.79
t3	1.02	0.87	1.16	1.07
t4	1.92	1.56	1.99	1.80
t5	1.09	0.92	1.21	1.12
t6	1.91	1.64	2.04	1.80
t7	1.06	0.99	1.24	1.16
t8	1.82	1.71	2.06	1.99

Table 5.6: Comparison of experimental and simulated Ra values for 1018 steel

experimental work done in the measurement of forces during the machining operation. Table 5.7 shows the dynamical system constants used in the model. The values chosen were based on the experimental cutting force data. A power spectrum analysis of the cutting force data was performed and the power spectrum plotted, as shown in Figure 5.16. The two most significant frequencies of 100 Hz and 275 Hz correspond to the fundamental frequencies of the machine system. The values of 'K' and 'm' chosen were such that the frequencies of the machine system matched the true frequencies determined experimentally. This method was found to be quite effective as the values chosen were found to describe the system response in an accurate manner. The simulation software is very flexible as it allows for the easy changes of the system constants and hence can be widely

Dynamical stiffness in first principal mode, $K_1 = 4 \times 10^6$ N / m
Dynamical stiffness in second principal mode, $K_2 = 1.8 \times 10^6$ N / m
Damping constant in first principal mode, $C_1 = 141.42$ N . s / m
Damping constant in first principal mode, $C_2 = 75.68$ N . s / m
Equivalent Mass = 2 kg.
Angle between the first mode and the horizontal $\alpha = 60^\circ$
Angle between the resultant force and the horizontal $\beta = 45^\circ$

Table 5.7: Dynamic constants used in the model

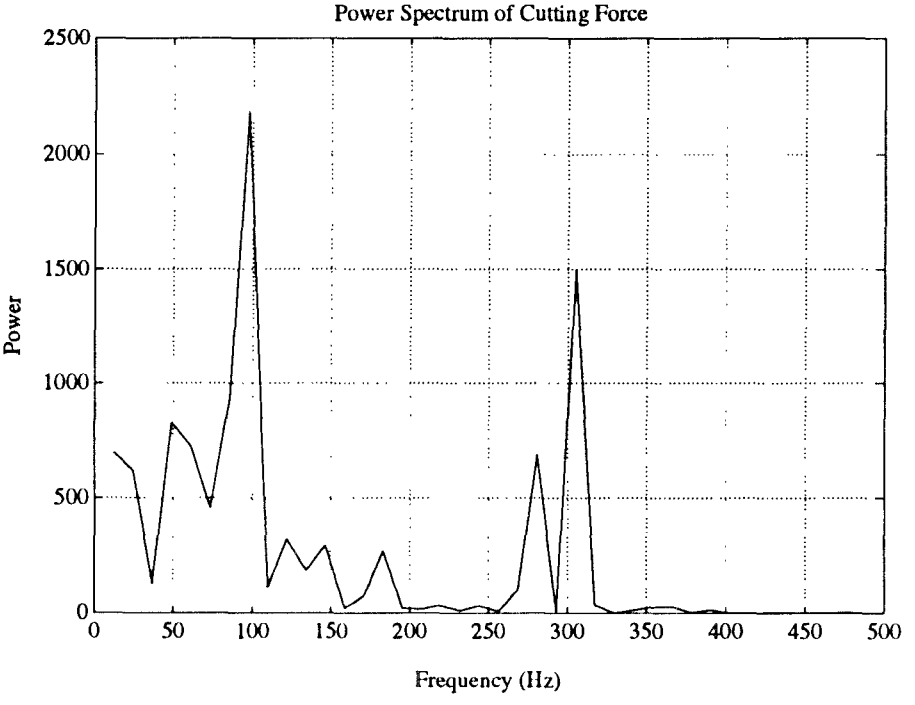

Figure 5.16: Power spectrum of the cutting force

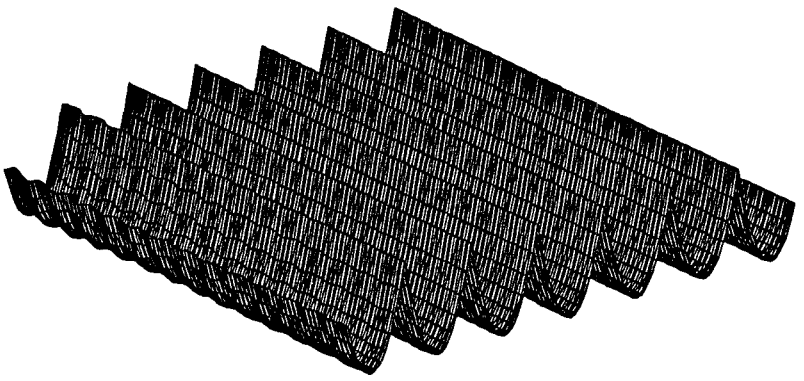

Figure 5.17: Ideal surface topography

used for any other machine systems which can be modeled on similar lines.

Figures 5.17 and 5.18 show simulated machined surfaces generated under ideal conditions and in the presence of random excitation, respectively. Comparisons of these surfaces were made with surfaces analyzed experimentally. In order to get a three dimensional profile of the machined surface a three-dimensional profilometer was used. Figure 5.19 is a picture of the profilometer. The profilometer is essentially a probe instrument with an indexing arrangement, fully integrated into a digital data acquisition system. Figure 5.20 shows the three-dimensional profile of the machined surface obtained experimentally. It was found that the simulation resulted in surfaces that very closely resembled the actual surfaces generated.

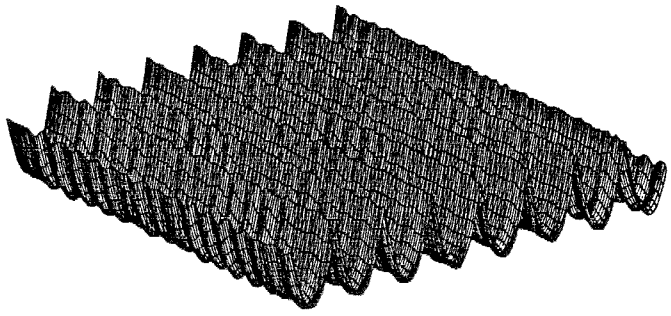

Figure 5.18: Surface topography in presence of random excitation

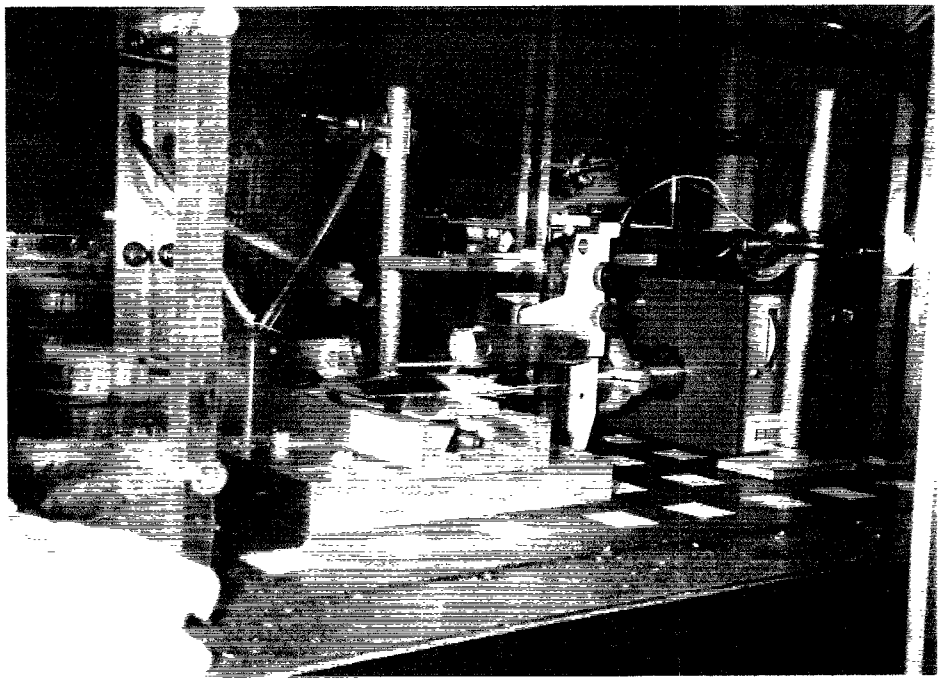

Figure 5.19: Three-dimensional profilometer

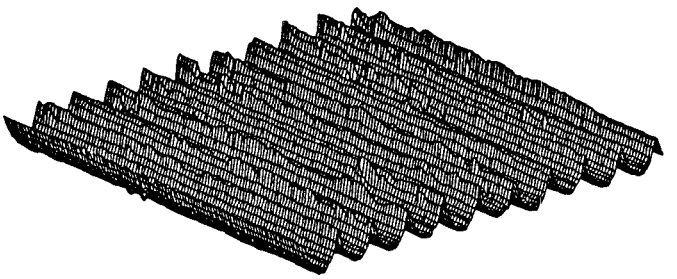

Figure 5.20: Surface topography of an experimental surface

The displacement of the cutting tool during the machining process is another measure of the nature of the machining process. It clearly illustrates the nature of the vibration occuring in the tool and hence explains the nature of surface generated. The effects of the different excitation models presented in Chapter 3 can be seen easily by analyzing the tool response. Figure 5.21 is the tool response obtained from the simulator in the absence of random vibration. The plot shows that after the effects of the initial excitation due to the entry of the tool into the workpiece dies out, the tool remains in an equilibrium position. This would result in the ideal Ra value for the workpiece. But as seen experimentally, the Ra value is very different from the ideal values. Figure 5.22 illustrates the nature of the tool response in the presence of random excitation. Figure 5.23 is an enlarged plot of the simulated tool response by the use of the sample variance excitation

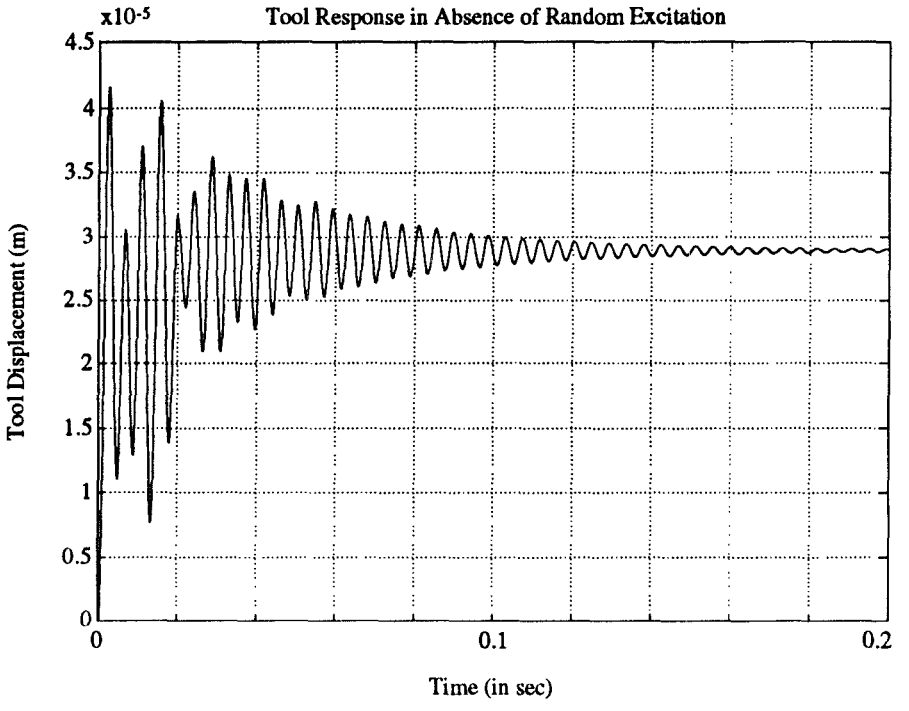

Figure 5.21: Tool response in absence of random excitation

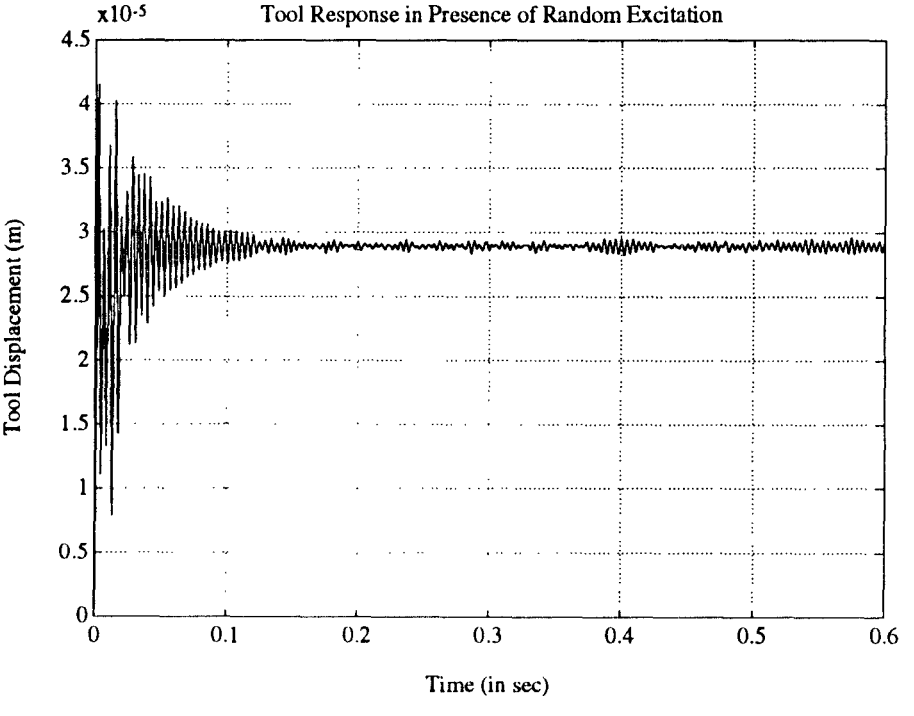

Figure 5.22: Tool response in presence of random excitation

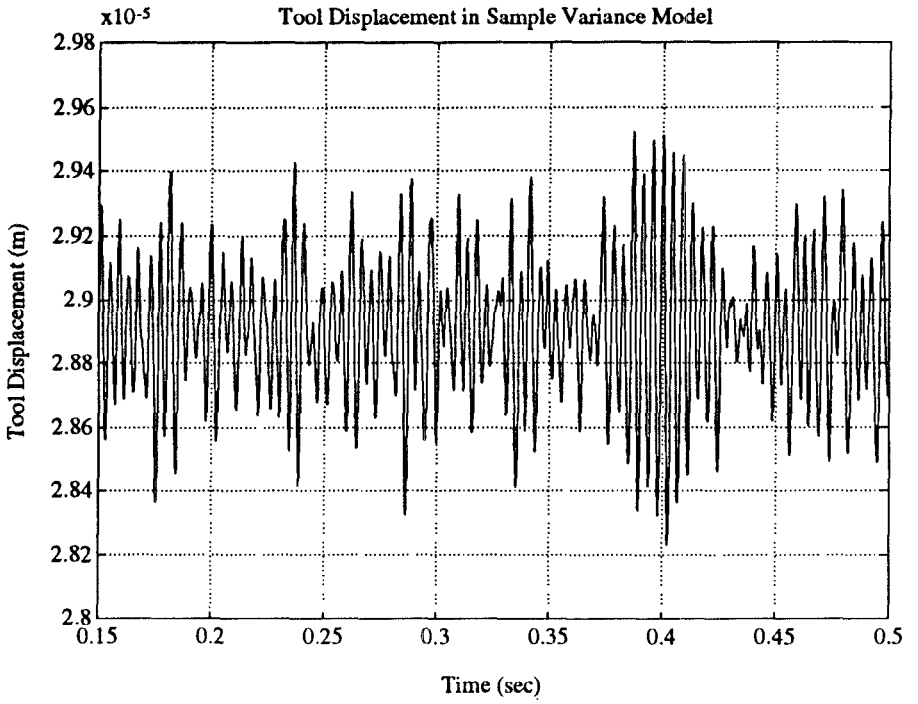

Figure 5.23: Tool response described by sample variance model

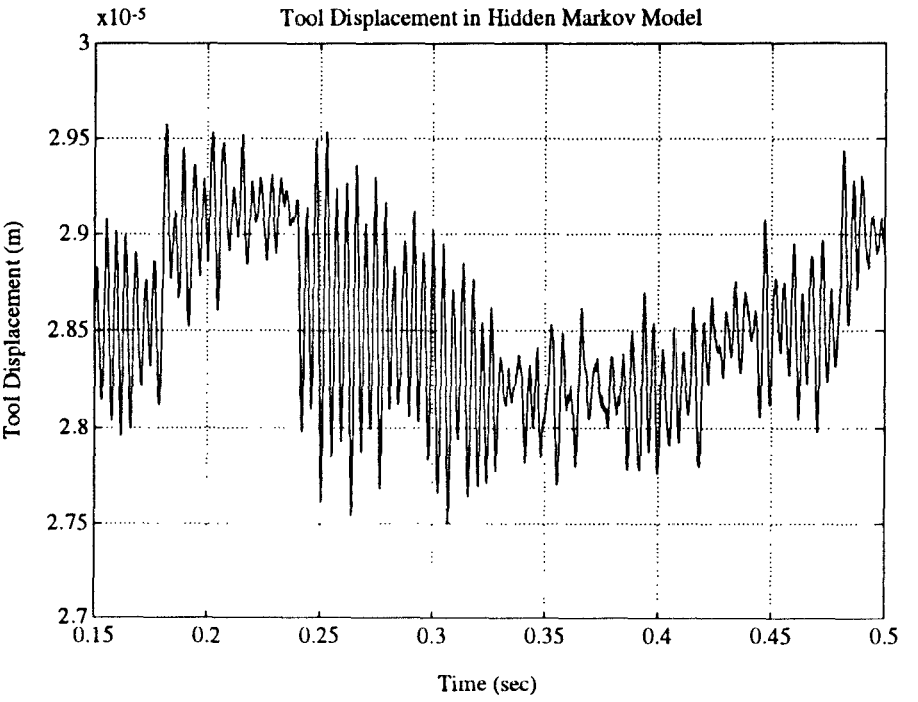

Figure 5.24: Tool response described by hidden Markov model

model after the response due to the initial excitation dies out. Figure 5.24 is a similar plot which was generated by the use of the hidden Markov model. It is very difficult to directly measure the displacement of the tool dynamically during the cutting process. The measurement of the response based on post-machining analyses of the workpiece is also very difficult, as the curvature of the workpiece together with the spiral path of the tool resulting from a combination of feed and rotation of the workpiece, makes it almost impossible for most profilometers to trace the tool path, without sophisticated fixtures. Hence in order to validate the excitation models, an analysis of the dynamic force signals during the machining process was adapted.

Cutting forces generated during the machining operation are perhaps the best indicators of the nature of the machining operation. It is, therefore, important to analyze the variation in forces in order to evaluate the effectiveness of the mathematical models used for the tool excitation.

The measurement of cutting forces essentially consists of a set-up comprising of three main components. They are the following:

- A sensor or transducer, in the form of a strain gage, that measures the cutting force, based on the deflection of the tool,
- An amplifier to magnify the signal,
- A digital data acquisition system.

The transducer for the force system consists of a set of strain gauges mounted

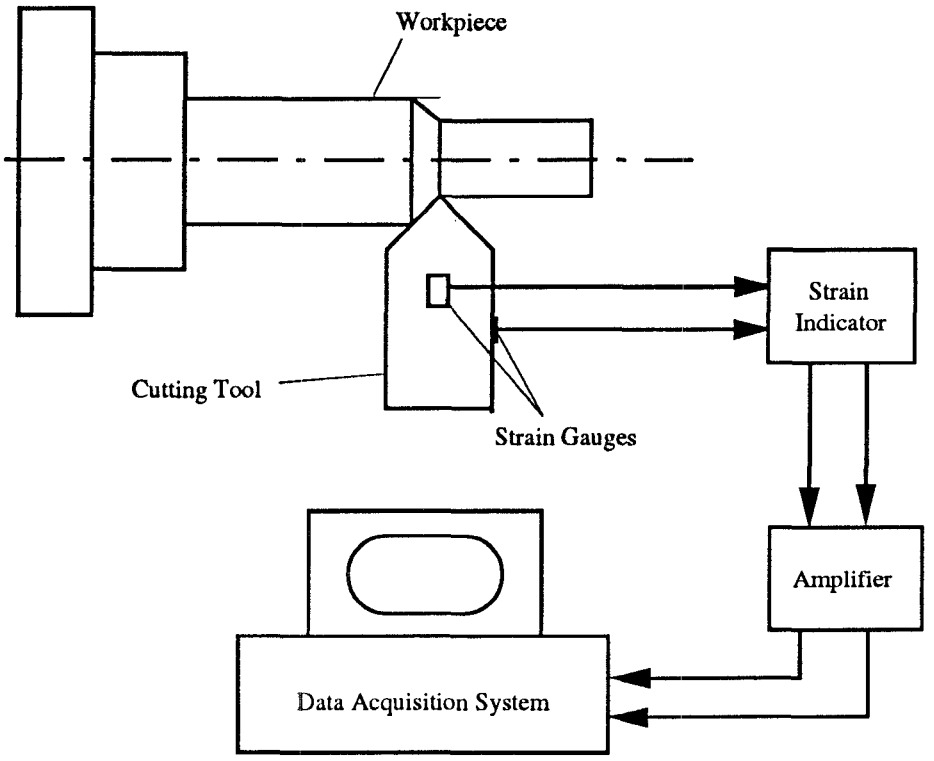

Figure 5.25: Schematic representation of force measurement system

on the tool holder. These strain gauges sense the deflection of the tool due to the force on the holder. These deflections are converted to measurable electric voltage signals through a bridge amplifier system. The measured voltage signals are amplified and sent to the digital data acquisition system. A calibration process establishes a relationship between the voltage signals and the cutting force components. Figure 5.25 is a schematic representation of the force measurement system. Figure 5.26 is a picture of the setup for the force measurement.

The strain gauges used are the CEA-06-062uw-350 type. They have excellent heat dissipation and a suitable gauge factor for the experiments. The strain gauges are mounted on the top - bottom and left - right regions of the tool

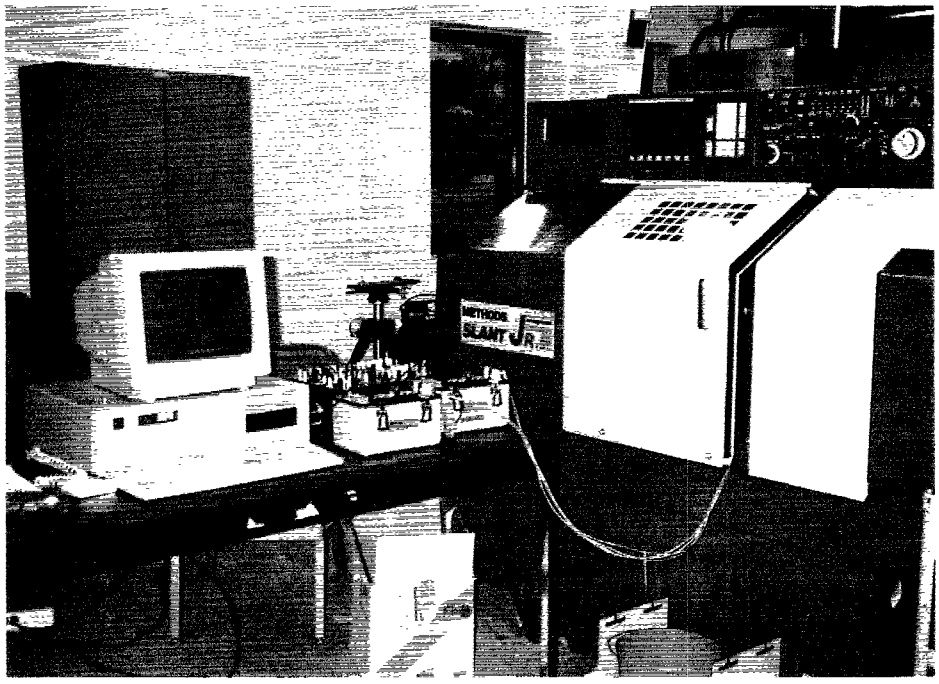

Figure 5.26: Experimental setup for measurement of cutting forces

holder. They are capable of measuring the two significant components of the cutting force - the tangential force (F_P) and the feed force (F_Q), as described in the system of forces in Chapter 2 and illustrated in Figure 3.2. A Wheatstone bridge is used in order to vary the resistance changes which the strain gages undergo when subjected to strains. The layout of the bridge circuit is as shown in Figure 5.27[17]. The voltage output of the bridge circuit, ΔE_{out}, due to the resistance changes of ΔR_1, ΔR_2, ΔR_3, and ΔR_4 is given by

$$\Delta E_{out} = E_{in} \frac{r}{(1+r)^2} \left(\frac{\Delta R_1}{R_1} - \frac{\Delta R_2}{R_2} + \frac{\Delta R_3}{R_3} - \frac{\Delta R_4}{R_4} \right)$$

where, E_{in} = bridge supply voltage and r = $\frac{R_2}{R_1}$. The term $(\frac{r}{(1+r)^2})$ is an index of the bridge circuit efficiency[29]. The maximum bridge circuit efficiency is

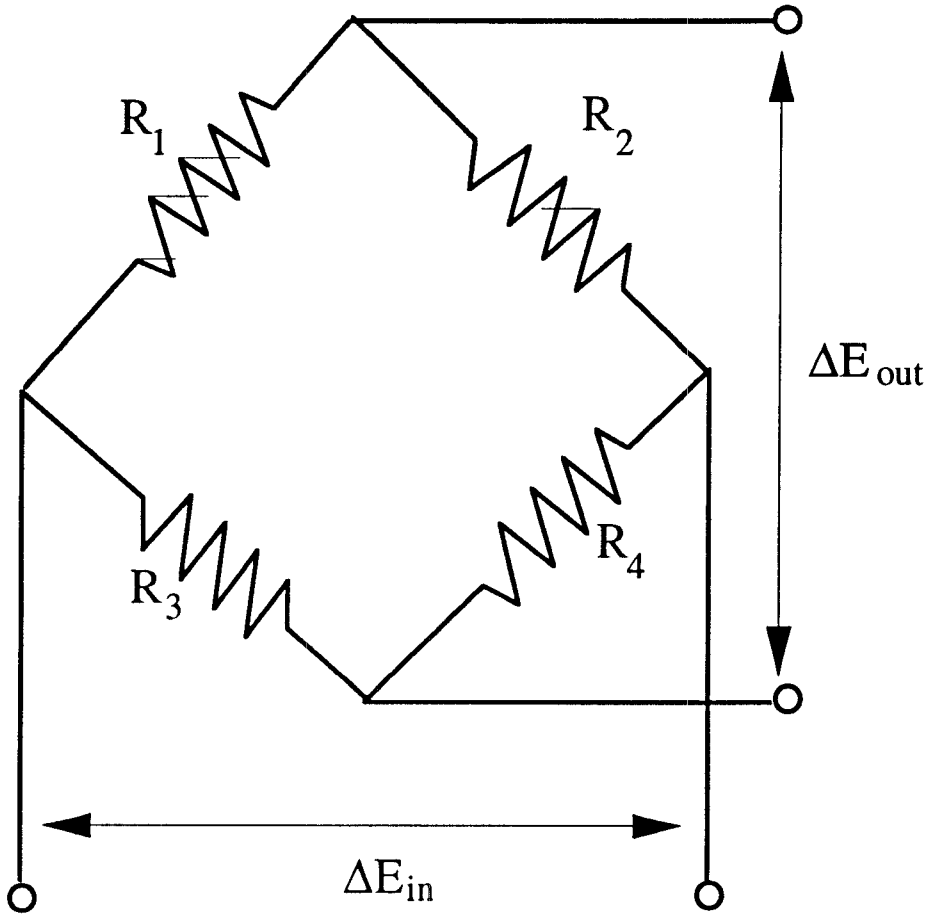

Figure 5.27: Schematic of a wheatstone bridge circuit

attained when $R_1 = R_2$, or r = 1.

The calibration of the strain gauges had been performed and the transformation matrix, for the conversion of the voltage signals to the cutting force, formulated. The transformation matrix, T_r, is defined as

$$[T_r] = \frac{Input}{Output} = \frac{V_{out}}{F}$$

or in the matrix form as

$$[T_r] = \begin{bmatrix} \frac{\Delta V_z}{\Delta F_z} & \frac{\Delta V_z}{\Delta F_x} \\ \\ \frac{\Delta V_x}{\Delta F_z} & \frac{\Delta V_x}{\Delta F_x} \end{bmatrix}$$

The force matrix is calculated for the voltage signals using the relation

$$[F] = (inv[T_r])[V]$$

After calculation of the transformation matrix the relationship is expressed as

$$\begin{bmatrix} F_z \\ \\ F_x \end{bmatrix} = \begin{bmatrix} 35.678 & 0 \\ \\ 0.4313 & 39.2153 \end{bmatrix} \begin{bmatrix} V_z \\ \\ V_x \end{bmatrix}$$

The tool with the cutting force measurement system described here, was used for the cutting tests. Tests were performed for the eight different cutting conditions shown in the factorial design and the voltage readings obtained from the strain gages recorded. These values were then converted to cutting force values in both the tangential and the feed directions, as explained earlier.

Figure 5.28 shows the plot obtained from one such force measurement, with respect to time. In order to validate the use of the different models, these forces were then compared with the forces generated by the simulator. Figure 5.29

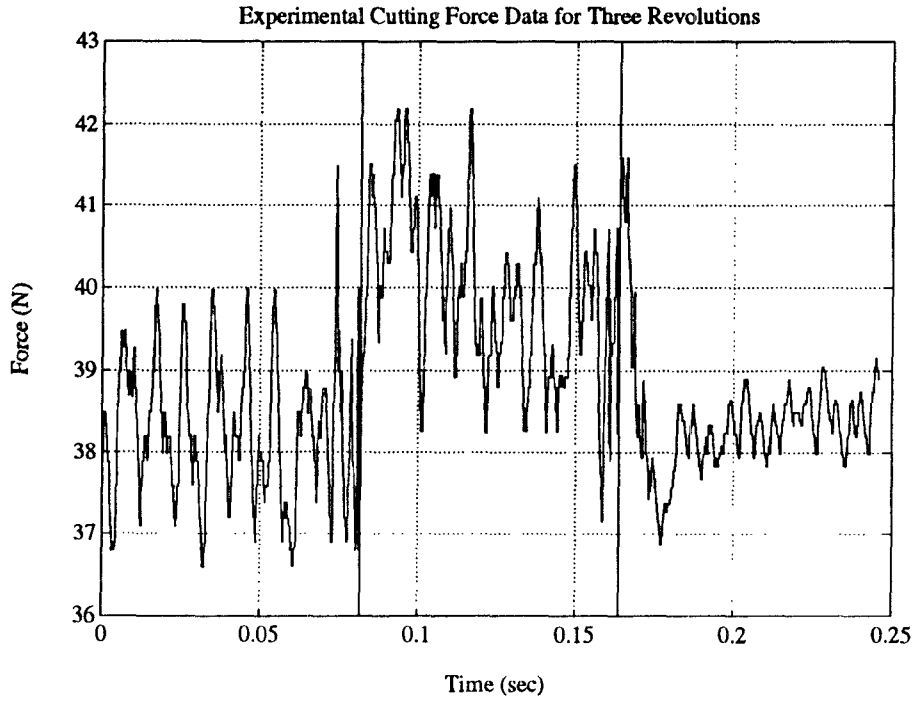

Figure 5.28: Force variation obtained experimentally

shows the force readings generated by the purely deterministic model. It is obvious that the deterministic model fails to account for the excitation present beyond the second and third revolutions of the workpiece, when both the responses due to the initial excitation and due to the regenerative excitation dies out. This strongly confirms the presence of the random excitation in the machining process.

The force values obtained for the sample variance model from the simulator are as presented in Figure 5.30. These can be compared with the experimental force values presented in Figure 5.28. It can be seen that the model is much more efficient than the purely deterministic model, as the nature of the random excitation has been fairly well simulated. However, the frequent change in the

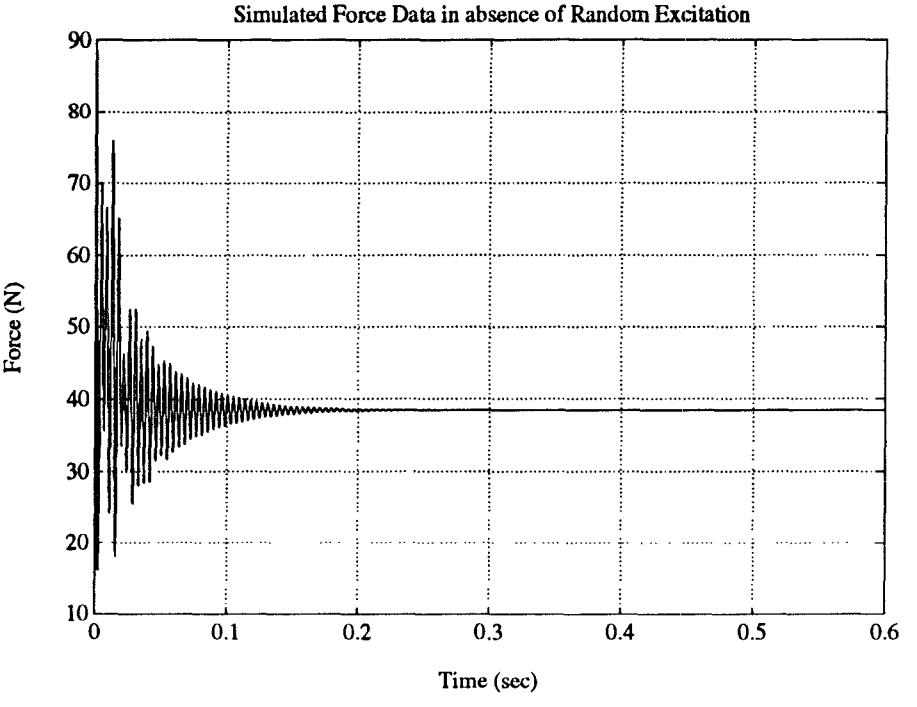

Figure 5.29: Cutting force described by the deterministic model

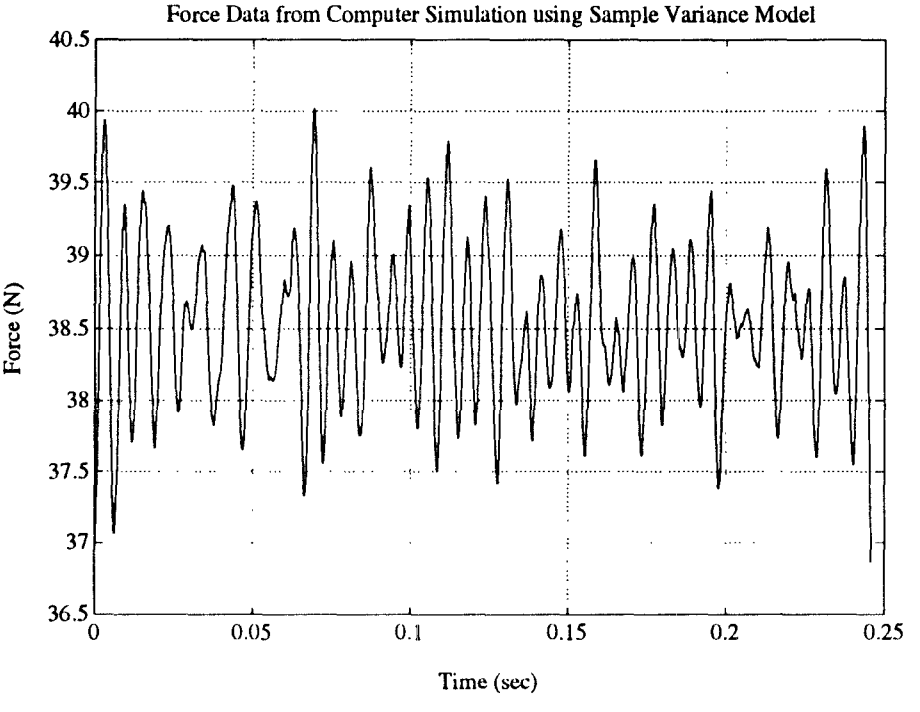

Figure 5.30: Cutting force described by sample variance model

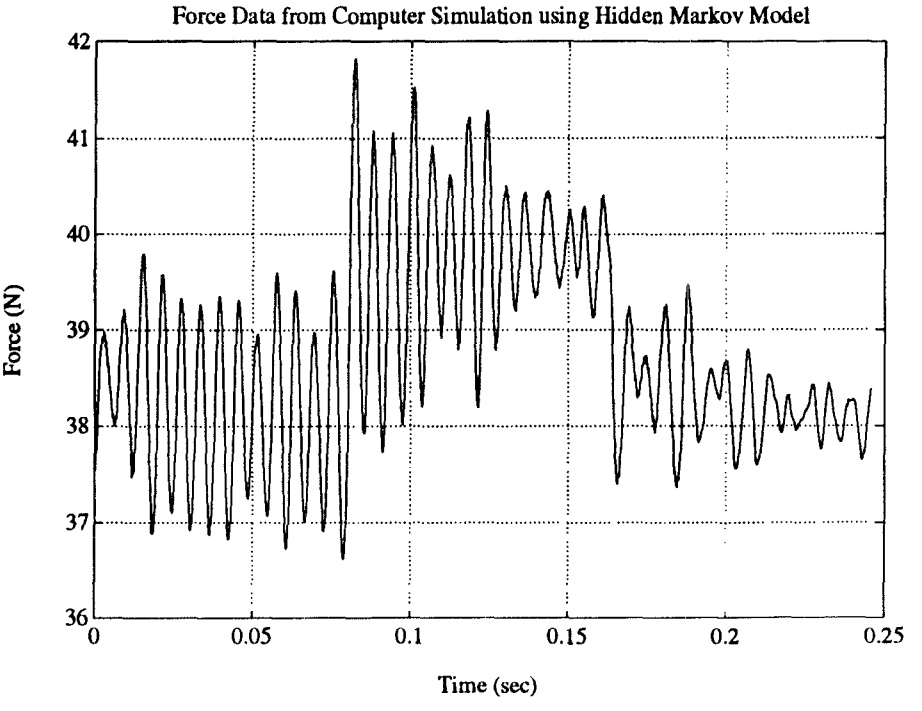

Figure 5.31: Cutting force described by the hidden Markov model

mean value of the forces between revolutions is not accounted for by this model. It is this phenomenon that justifies the use of the Markov models.

Figure 5.31 is the force variation for the same cutting process as obtained from the hidden Markov model. The change of the mean force level that is often observed in cutting processes is fairly well described. The change in the mean value is due to the hardness distribution in the steel bars. Although, the change in the hardness is not accurately a function of the number of revolutions, the hidden Markov model is indirectly able to simulate such variations by changing the mean value of the sample mean hardness, as described in Chapter 3. The similarity in the nature of the simulated and experimental force justifies the use of the excitation models.

Chapter 6

Conclusions and Recommendations

6.1 Conclusions

This section presents the important conclusions drawn from the thesis. The highlights of the different models and the nature of the results obtained from them are summarized.

This thesis represents an attempt at characterizing and modeling the effects of the material microstructure on the nature of the cutting process and hence, on the machined surface. Three statistical models have been used to quantify the micromechanical and metallurgical aspects of machining performance.

- The Sample Variance model has been used to describe the distribution of the material microstructure in adjacent regions (samples) of the material,

along the circumferential direction.

- The Markov chain model is used to describe the distribution of the microstructure in materials that exhibit strong longitudinal trends. The model quantifies the relationship between adjacent samples in the feed direction by the use of transition probabilities.

- The hidden Markov model quantifies the variation in the mean levels of the sample mean hardness at different locations along the cylindrical bar, by the assignment of different distributions to the different revolutions of the workpiece. The sample mean hardness is determined based on two transition matrices - the first determines the mean hardness for the revolution, while the second determines the relationship between adjacent samples in the direction of feed.

The estimation of the sample variance involves the calculation of the sample shape function which makes the sample variance relevant to the three machining parameters, i.e., feed, depth of cut, and spindle speed. An algorithm has been developed and implemented on a computer to estimate the sample variance based on a given set of cutting conditions.

The material microhardness distribution for the samples forms an important source of disturbance, which excites the machine tool structure during machining. A dynamical system model is developed and implemented on computer to simulate the tool motion under random excitation. A two degree of freedom model,

with second order dynamics in each of the two modes, is used. The tool response due to the excitation is translated into its effects on the surface produced.

A two-level factorial design approach has been used to evaluate the predictability of the simulator. Three different cutting conditions of feed, depth of cut and spindle speed have been used as variables in evaluating their effects on the machining performance. Three different materials - aluminum, 1018 steel and 4340 steel, with different nature of their microstructure have been used for the analyses. Empirical models have been developed to help interpret the results obtained.

The nature of the microstructure of aluminum is homogeneous and hence does not act as a source of random excitation during machining. The steel samples, however, exhibit non-homogeneity and act as a significant source of random vibration. The sample variance, which is directly related to the extent of random tool motion, was found to decrease with increase in any of the cutting conditions. The decrease caused by feed was found to be the least, indicating random vibration is significant when operating at low feeds. This effect of feed on surface finish is sometimes not observed due to the fact that the geometrical motion of the tool with small feeds leads to a better surface finish.

Finally, the cutting forces generated during the machining process are simulated and used to reinforce the validity of the different excitation models. Comparison of these simulated forces with the cutting forces measured during the machining tests justifies the use of the hidden Markov approach, which provides

a better prediction of machining performance, as evidenced in machining 1018 steel.

In summary, the contributions of the thesis are in improvising the sample variance model in order to make the model more receptive to changes in cutting conditions, development of a Markov model that accurately models the longitudinal trends together with the variations in the mean hardness levels of the material, experimental validation of the models used and the development of a comprehensive simulator that predicts surface quality, given any microstructure and material microstructure. The simulator is, thus, a tool that can be used to describe and analyze the nature of the tool response due to both the deterministic and the random excitations. Hence, it can be a very useful tool for a process engineer in predicting machining performance. If the simulator is linked to a database of the microstructure of popular engineering materials, it can also be very useful to a design engineer in the selection of materials based on their machinability.

6.2 Recommendations

A few recommendations for directions of future work are proposed in this section.

1. The material description models presented in this thesis have been applied only to the turning process. Material microstructure can also play a significant role in other machining processes, such as milling

and grinding. Application of the developed methodology to the other machining processes may provide a wide scope of application for the simulator.

2. Modern materials like ceramics and composites often display non-homogeneous distribution of their microstructure. This characteristic may pose difficulties in effectively machining these materials because of the presence of random excitation. By incorporating advanced analytical methods such as finite element method, into the developed model, we may gain a better understanding of the material removal mechanisms.

3. Making the simulator more user friendly and interactive, by the creation of an effective window-based interface can be an interesting direction of work. Creation of a database of sample shape functions for commonly used cutting conditions and microstructural images for widely used materials can make the simulator more efficient and rapid in its responses to any analysis.

4. The simulation package accounts for some of the most important factors affecting surface finish in machining. However, all analyses are done assuming an ideal condition in terms of tool wear. Tool wear can have very significant effects on the surface texture generated. The simulator needs to incorporate this effect to be considered as a complete tool for machining quality prediction.

Appendix A

Statistical Test on Means

The test on means is used in this thesis as a basis for decisions on the selection of states of the hidden Markov process. The states of the hidden Markov process represent different distributions representing different revolutions of the workpiece.

The test on means is a statistical tool used to compare the relationship between two means of different samples. The test of means has a null hypothesis (H_0) which states that the two means are equal within a confidence interval (α). The alternative hypothesis (H_1) states that the means are not the same [24]. Stated mathematically,

$$H_0 : \mu_1 = \mu_2$$

$$H_1 : \mu_1 \neq \mu_2$$

The objective of the test is to confirm or reject the null hypotheses. This is done by the use of a parameter 't' as explained here.

In the case of the two lots being compared having the same variance, the test parameter t_0 is given by

$$t_0 = \frac{\bar{y}_1 - \bar{y}_2}{S_p\sqrt{\frac{1}{n_1} + \frac{1}{n_2}}}$$

where $\bar{y}_1$ and $\bar{y}_2$ are the two means being computed from the two samples of size n_1 and n_2. S_p is the estimate of the variance and is given by

$$S_p^2 = \frac{(n_1 - 1)S_1^2 + (n_2 - 1)S_2^2}{n_1 + n_2 - 2}$$

S_1 and S_2 being the two individual sample variances. The decision of accepting or rejecting the null hypothesis is based on a comparison of t_0 with the value from the t-distribution for $n_1 + n_2 - 2$ degrees of freedom. Given a confidence interval (or significance level, α) the null hypothesis is rejected if $|t_0| > t_{\alpha/2,n_1+n_2-2}$ is the upper $\alpha/2$ percentage point of the t-distribution with $n_1 + n_2 - 2$ degrees of freedom.

If the two sample variances are different then the test parameter t_0 is given by

$$t_0 = \frac{\bar{y}_1 - \bar{y}_2}{\sqrt{\frac{S_1^2}{n_1} + \frac{S_2^2}{n_2}}}$$

The comparison of t_0 is made with 't' calculated on the basis of 'v' degrees of freedom, where 'v' is given by [23]

$$v = \frac{(\frac{S_1^2}{n_1} + \frac{S_2^2}{n_2})^2}{\frac{(\frac{S_1^2}{n_1})^2}{n_1+1} + \frac{(\frac{S_2^2}{n_2})^2}{n_2+1}} - 2$$

Appendix B

Derivation of Tool Vibratory Response

The solution to the set of dynamical Equations 3.16 can be got by transforming the equations into the frequency domain by taking the Laplace transform. Expanding the matrices and taking the Laplace transform we get

$$Q_1(s) = \frac{\sigma_1 B_1' + \omega_1 B_2'}{s^2 + 2\sigma_1 s + (\sigma_1^2 + \omega_1^2)} u(s) + \frac{B_1'}{s^2 + 2\sigma_1 s + (\sigma_1^2 + \omega_1^2)} [su(s) - u(0)]$$

$$Q_2(s) = \frac{1}{s(s+\sigma_1)} [\frac{K}{\omega_1^2} + \frac{B_1'\sigma_1}{\omega_1}] + \frac{1}{s^2 + 2\sigma_1 s + (\sigma_1^2 + \omega_1^2)} [-\frac{C_1}{\omega_1^2} - \frac{\sigma_1 B_1'}{\omega_1}] + \frac{1}{s(s^2 + 2\sigma_1 s + (\sigma_1^2 + \omega_1^2))} [-\frac{\sigma_1 K}{\omega_1^2} - \frac{B_1'(\sigma_1^2 + \omega_1^2)}{\omega_1}] + \frac{B_2'}{s(s+\sigma_1)}$$

$$Q_3(s) = \frac{\sigma_2 B_3' + \omega_2 B_4'}{s^2 + 2\sigma_2 s + (\sigma_2^2 + \omega_2^2)} u(s) + \frac{B_3'}{s^2 + 2\sigma_2 s + (\sigma_2^2 + \omega_2^2)} [su(s) - u(0)]$$

$$Q_4(s) = \frac{1}{s(s+\sigma_2)}[\frac{K'}{\omega_2^2} + \frac{B_3'\sigma_2}{\omega_2}] + \frac{1}{s^2+2\sigma_2 s+(\sigma_2^2+\omega_2^2)}[-\frac{C_1'}{\omega_2^2} - \frac{\sigma_2 B_3'}{\omega_2}] + \frac{1}{s(s^2+2\sigma_2 s+(\sigma_2^2+\omega_2^2))}[-\frac{\sigma_2 K}{\omega_2^2} - \frac{B_3'(\sigma_2^2+\omega_2^2)}{\omega_2}] + \frac{B_4'}{s(s+\sigma_2)} \quad \text{(B.1)}$$

where $K = -\omega_1(\sigma_1 B_1' + \omega_1 B_2')$ and $K' = -\omega_2(\sigma_2 B_3' + \omega_2 B_4')$.

Two assumptions are made here. The initial states of the system are assumed to be zero. All the inputs are assumed to be in the form of step inputs. These assumptions hold true for the machining system under consideration. Taking Laplace inverse of the the above equations, we get the solution to the tool motion in terms of the transformed variables, $\bar{Q}(t)$.

$$\begin{aligned}
Q_1(t) &= \frac{\sigma_1 B_1' + \omega_1 B_2'}{\sigma_1^2+\omega_1^2}[1 - \frac{\sqrt{\sigma_1^2+\omega_1^2}}{\omega_1}e^{-\sigma_1 t}Sin(\omega_1 t+\phi_1)] + \frac{B_1'}{\omega_1}e^{-\sigma_1 t}Sin\omega_1 t \\
Q_2(t) &= \frac{1}{\sigma_1}(K_1+B_2')(1-e^{-\sigma_1 t}) - \frac{K_1}{\omega_{n1}\sqrt{1-\zeta_1^2}}e^{-\zeta_1\omega_{n1}t}Sin(\omega_{n1}\sqrt{1-\zeta_1^2})t \\
&\quad \frac{K_2}{\omega_{n1}^2}[1 - \frac{1}{\sqrt{1-\zeta_1^2}}e^{-\zeta_1\omega_{n1}t}Sin(\omega_{n1}\sqrt{1-\zeta_1^2}t+\phi_1)] \\
Q_3(t) &= \frac{\sigma_2 B_3' + \omega_2 B_4'}{\sigma_2^2+\omega_2^2}[1 - \frac{\sqrt{\sigma_2^2+\omega_2^2}}{\omega_2}e^{-\sigma_2 t}Sin(\omega_2 t+\phi_2)] + \frac{B_3'}{\omega_2}e^{-\sigma_2 t}Sin\omega_2 t \\
Q_4(t) &= \frac{1}{\sigma_2}(K_1'+B_4')(1-e^{-\sigma_2 t}) - \frac{K_1'}{\omega_{n2}\sqrt{1-\zeta_2^2}}e^{-\zeta_2\omega_{n2}t}Sin(\omega_{n2}\sqrt{1-\zeta_2^2})t \\
&\quad \frac{K_2'}{\omega_{n2}^2}[1 - \frac{1}{\sqrt{1-\zeta_2^2}}e^{-\zeta_2\omega_{n2}t}Sin(\omega_{n2}\sqrt{1-\zeta_2^2}t+\phi_2)]
\end{aligned} \quad \text{(B.2)}$$

where

$$\phi_1 = Cos^{-1}\zeta_1$$

$$
\begin{aligned}
K_1 &= \frac{A}{\omega_1^2} + \frac{B_1'\sigma_1}{\omega_1} \\
K_2 &= \frac{-\sigma_1 A}{\omega_1^2} - \frac{B_1'(\sigma_1^2+\omega_1^2)}{\omega_1} \\
\zeta_1 &= -\frac{\sigma_1}{\sqrt{\sigma_1^2+\omega_1^2}} \\
\omega_{n1} &= \sigma_1^2+\omega_1^2
\end{aligned}
$$

and the other coefficients for Q_3 and Q_4 similarly defined.

Appendix C

Factorial Design of Experiments

The factorial design for experimentation is a concept that emerged as an offshoot of Taguchi quality methods. This design for performing experiments aims at minimizing the number of experiments to be performed for determining the effects of the different experimental factors on the outcomes of interest, usually the quality of the machined surface. The design selects a fixed number of levels (usually two) for each of a number of variables (factors) and then experiments with all possible combinations of these factors [24].

A two level factorial design is chosen for experimental work in this thesis. Three factors that are the most significant variables in any machining operation - the feed, the depth of cut and spindle speed are chosen as the factors to be analyzed. The two different levels for each of these factors are chosen. This yields a possible 2^3 combinations of the experimental factors that need to be analyzed. The two levels are represented by (-) and (+) signs in Table C.1. This can be

Experiment Number	FACTORS			Output (Surface Parameters)
	Feed (mm/rev)	Depth of Cut (mm)	Spindle Speed (rpm)	
1	-	-	-	y1
2	+	-	-	y2
3	-	+	-	y3
4	+	+	-	y4
5	-	-	+	y5
6	+	-	+	y6
7	-	+	+	y7
8	+	+	+	y8

Table C.1: Setup of factorial design

graphically represented by the vertices of a cube. Figure 5.5 shows this graphical representation. The effects of each of these factors can then be calculated as explained here. The effect of any factor, for example, the feed is the average change in the surface parameter value (the output) as the feed is changed from (-) level to (+) level. Thus, the effect of feed E_f is given by

$$\begin{aligned} E_f &= \frac{y_2 - y_1 + y_4 - y_3 + y_6 - y_5 + y_8 - y_7}{8} \\ &= \frac{-y_1 + y_2 - y_3 + y_4 - y_5 + y_6 - y_7 + y_8}{8} \end{aligned}$$

As can be seen from the above equation, the effects can be calculated based on the sign associated with the different levels in the table. The effects of depth

of cut and spindle speed are calculated in a similar way.

The two and three factor interactions can also be calculated by making similar calculations by assigning signs that result from the product of the signs of the factors representing the surface roughness for any particular cutting condition. These effects are then used to express the R_a value resulting from the use of different cutting conditions.

$$\begin{aligned} R_a &= Avg. + \sum_{i=1}^{3} \frac{E_i}{2} X_i + \frac{E_{12}}{2} X_1 X_2 \\ &\quad + \frac{E_{23}}{2} X_2 X_3 + \frac{E_{13}}{2} X_1 X_3 + \frac{E_{123}}{2} X_1 X_2 X_3 \end{aligned}$$

Bibliography

[1] Merchant, M. E., *"Mechanics of the Metal Cutting Process - Orthogonal Cutting and a type-2 Chip"*, Journal of Applied Physics, Vol. 16, No. 5, 1945, pp.267 - 275.

[2] Merritt, H. E., *"Theory of Self-Excited Machine Tool Chatter"*, Trans. ASME, Vol. 87, November 1965, pp.447 - 454.

[3] Kronenberg, M., *"Machining Science and Application"*, Pergamon Press Inc., 1966.

[4] Arnold, R. N., *"Mechanism of Tool Vibrations in Cutting Steel"*, Proc. I. Mech. E., Vol. 154, 1956.

[5] Tobias, S. A. and Fishwick, W., *"Theory of Regenerative Machine Tool Chatter"*, Engineering, London, Vol. 205, 1958.

[6] Tobias, S. A. and Fishwick, W., *"Chatter of Lathe Tools Under Ortogonal Cutting Conditions"*, Trans. ASME, 1958, pp. 1079.

[7] Tlusty, J., *"Die Berechnung des Rahmens der Werkzeugmaschine"*, Schwerindustrie der CSR, Heft. I, 1955.

[8] Tlusty, J. and Polacek, M. *"The Stability of Machine Tools Against Self-excited Vibrations in Machining"*, Prod. Engg. Research Conference, ASME, 1963.

[9] Danckwerts, P. V., *"The Definition and Measurement of some Characteristics of Mixtures"*, Applied Science and Research, Vol. 3, Section A, 1952, pp. 279 - 296.

[10] Scott, A. M. and Bridgewater, J., *"The Characterisation of Patchy Mixtures"*, Chemical Engineering and Science, Vol. 29, 1974, pp. 1789 - 1800.

[11] Tucker III, C. L., *"Sample Variance Measurement of Mixing"*, Chemical Engineering and Science, Vol. 36, No.11, 1981, pp. 1829 - 1839.

[12] Zhang, G. M., Kapoor, S. G., *"Dynamic Generation of Machined Surfaces, Part 1: Description of a Random Excitation System"*, Transactions of the ASME - Journal of Engineering for Industry, Vol. 113, May 1991, pp. 137 - 144.

[13] Zhang, G. M., Kapoor, S. G., *"Dynamic Generation of Machined Surfaces, Part 2: Construction of Surface Topography"*, Transac-

tions of the ASME - Journal of Engineering for Industry, Vol. 113, May 1991, pp. 145 - 153.

[14] Zhang, G. M., Kapoor, S. G., *"Dynamic Modelling and Analysis of the Boring Machine System"*, Transactions of the ASME, Journal for Engineering for Industry, Vol. 109, August 1987, pp. 219 - 226.

[15] Hwang, T. W. and Zhang, G. M., *"A Stochastic Modelling for the Characterisation of the Random Tool Motion During Machining"*, Systems Research Center, University of Maryland, Technical Report 92-57, 1992.

[16] Zhang, G. M. and Lin, Chein., *"A Hidden Markov Model Approach to the Study of Random Tool Motion During Machining"*, Sensors, Controls and Quality Issues in Manufacturing, ASME 1991, pp. 345.

[17] Zhang, G. M., *"Dynamic Modelling and Dynamic Analysis of the Boring Machining System"*, Ph. D. thesis, University of Illinois, Urbana - Champaign, 1986.

[18] Shaw M. C., *"Metal Cutting Principles"*, Oxford University Press, 1984.

[19] Sachs, L., *"Applied Statistics - a Handbook of Techniques"*, Springer Series in Statistics, 1982, pp. 406.

[20] Samuels, Leonard E., *"Optical Microscopy of Carbon Steels"*, American Society of Metals, 1980, pp.85.

[21] Karlin, Samuel and Taylor, Howard M., *"A First Course in Stochastic Processes"*, Second Edition, Academy Press, 1975.

[22] Karlin, Samuel and Taylor, Howard M., *"A Second Course in Stochastic Processes"*, Second Edition, Academy Press, 1975.

[23] Montgomery, Douglas C., *"Design and Analysis of Experiments"*, Second Edition, John Wiley and Sons Inc., 1976.

[24] Box, G. E., Hunter, W. G. and Hunter, J. S., *"Statistics for Experimenters"*, John Wiley and Sons Inc., 1978.

[25] Rabiner, L. R., *"A Tutorial on Hidden Markov Models and Selected Applications in Speech Recognition"*, Proc. of the IEEE, Vol. 77, No. 2, February, 1989, pp. 257 - 286.

[26] Rabiner, L. R. and Juang, B. H., *"An Introduction to Hidden Markov Models"*, IEEE ASSP Magazine, January 1986, pp. 4 - 16.

[27] Meyer, E., Z. Ver. Dtsch. Ing., Vol. 52, pp.645.

[28] Song, J. F. and Vorburger, T.V., *"Metals Handbook - Friction, Lubrication and Wear Technology"*, 10th Edition, Vol. 3, National Institute of Standards and Technology.

[29] Khanchustambham, R. G., *"A Neural Network Approach to On-line Monitoring of Machining Processes"*, M.S. thesis, University of Maryland, College Park, 1992.

[30] Walker, Helen M. and Lev, J., *"Statistical Inference"*, Holt, Rinehart and Winston, Inc., 1953.

[31] Boyer, Howard E., *"Hardness Testing"*, ASM International, 1987.